# PROCEEDINGS OF THE 5th INTERNATIONAL SCHOOL ON QUANTUM TECHNOLOGIES

QTS’22

Sochi 2022

CONTENTS

# Partial Key Leak Based Qubit-Optimized Quantum Grover Attack on Simplified-AES

Alexey Moiseevskiy

*Infotecs Scientific Research and Advanced Developments Centre, MSU Quantum Technology Centre, Moscow, Russia*
E-mail: `Aleksey.Moiseevsky@infotecs.ru`

**Abstract**

In this report I present a research of a quantum attack on the symmetric block cipher S-AES that allows to reduce required qubits number if part of the key is already known. Further research of this approach can provide pactical quantum computers application for cryptoanalysis in near future.

Quantum cryptanalysis is on of the most important possible applications of quantum computers. Quantum attack can reduce security exponentially for asymmetric ciphers like RSA using Shor's algorithm, and quadratically for symmetric cryptography like AES using Grover attack. Quadratic security loss means that for the same security level twice longer key will be required. This kind of potential applications is one of the major factors behind the last years quantum technologies industry growth [1].

The strongest limit that keeps classical cryptography secure for today is the number of qubits. For full attack on the $n$-bit key at least $n$ qubits are required to operate with the key. Talking about asymmetric cipher like RSA with a key length of 1024 or 2048 bits, it is unlikely that in the next 5 years there will be a quantum computer with a register size sufficient for a successful attack, even without taking into account that error correction will increase the required register size by several times. At the same time, for symmetric 128-bit AES, although the problem still remains, it no longer seems so critical, since quantum computer with 128 qubits already exists [2]. With qubit register available volume growth, it's possible, that experimental runs of the AES-128 quantum attack with basic error correction will become realistic by the end of the decade [3].

It is known that for a toy-model AES - the Simplified-AES algorithm with two rounds and 16 key bits, Grover's quantum attack can be implemented with only 32 qubits [4]. In this report I present an algorithm that allows to reduce this number by 6 qubits if the first or last 8 bits of the key are compromised. The key space is reduced by 8 qubits, corresponding to 8 known bits, but 2 extra qubits are required to extend irreversible transformation $X \bigoplus Sbox(X)$ and represent it as unitary. In addition to the obvious benefit of saving the quantum register requirements, this optimization allows to run S-AES attack simulation on hardware, that provides only 29 qubits in simulated register, which is common for 32-Gb graphic cards. Therefore, presented approach can be useful in modeling error mitigation methods for quantum cryptanalysis algorithms and further experimental runs on advanced NISQ devices with error correction.

## References

[1] National Security Memorandum on Promoting United States Leadership in Quantum Computing While Mitigating Risks to Vulnerable Cryptographic Systems, THE WHITE HOUSE (2022)

[2] Eagle's quantum performance progress, IBM, research.ibm.com/blog/eagle-quantum-processor-performance (2022)

[3] *Jaime Sevilla, C. Jess Riedel*, Forecasting timelines of quantum computing, arXiv:2009.05045v2 (2020)

[4] *K. B. Jang, G. J. Song, H. J. Kim and H. J. Seo*, Grover on Simplified AES. 2021 IEEE International Conference on Consumer Electronics-Asia (ICCE-Asia), pp. 1-4 (2021).

# Control of superconducting qubits by single flux quantum pulses

M. Bastrakova[1,2*], V.Vozhakov[3], N.V. Klenov[1−3], I.I. Soloviev[1−3], A.M. Satanin[4]

[1] *Lobachevsky State University of Nizhni Novgorod, Nizhny Novgorod, Russia*
[2] *Russian Quantum Center, Moscow, Russia*
[3] *Skobeltsyn Institute of Nuclear Physics, Lomonosov Moscow State University, Moscow, Russia*
[4] *Higher School of Economics, Russia National Research University, Moscow, Russia*
*E-mail: bastrakova@phys.unn.ru

**Abstract**

The implementation of single- and two-qubit gates in the registers of superconducting qubits using single flux quantum pulses propagating along Josephson transmission lines is proposed. The specifics of the control and the possibility of accelerating gates for flux and transmon qubits are discussed.

Superconducting circuits are one of the most promising candidates for large-scale quantum computers, as they can reliably implement strongly interacting artificial atoms (qubits) that have reduced susceptibility to environmental noise. Over the past couple of decades, various types of superconducting qubits have already been successfully produced, the classification of which is based on a comparison of the characteristic values of electrostatic and Josephson energies. The most common types of qubits are weakly anharmonic transmons, which formed the basis of noisy intermediate-scale quantum processors from companies such as IBM, Google, Rigetti, as well as flux qubits, which are the basic cells of the D-Wave quantum simulator.

At the same time, the development of controlled quantum dynamics devices raises a number of fundamentally new issues that have been actively discussed recently. One of the problems is related to the method of controlling and manipulating the states of quantum registers. Currently, microwave cavities are used for control and measurement, which involves the use of high-frequency modulated pulses with a frequency resonant relative to the distance between the qubit levels. The success of the microwave approach for various types of superconducting qubits is reflected in [1, 2], where it is stated that single-qubit operations can be carried out with fidelity 99.9%, while two-qubit gates are implemented with fidelity 99.64%. The decoherence time in qubits is on the order of hundreds of microseconds [1]. However, in the process of scaling, additional decoherentization channels arise and this time is greatly reduced. In this regard, the problem of accelerating the implementation of quantum gates is still relevant.

In this regard, an alternative control scheme for superconducting qubits is currently being actively developed, which is based on the idea of rapid excitation of a quantum system by using solitary single flux quantum (SFQ) pulses. Initially, the use of the element base of energy-efficient superconducting rapid single flux quantum (RSFQ) logic was developed to control classical superconducting registers. Recently, attempts have been made to adapt RSFQ variants to control quantum qubit registers [2]. This approach allows not only to implement single-qubit gates, but also to create entanglement states of pairs of qubits with the high-fidelity.

The main goal of this article is to develop new methods for implementing RSFQ circuits in a superconducting two–qubit register (a pair of weakly interacting qubits) for rapid implementation of quantum algorithms. We have considered the control principles for two types of qubits: flux and transmon. Due to the different specifics of the spectra of these qubits, we have developed approaches to control SFQ pulses to minimize the duration of gate operations while minimizing leakage.

We consider the effect of a small number of SFQ pulses propagating in transmitting Josephson lines to implement quantum operations and algorithms in two coupled flux qubits, which is schematically shown in Fig. 1a. It is based on the generation of Ramsey fringes due to unipolar subnanosecond control pulses [3]. The influence of the shape and duration of control pulse on the contrast of the interference pattern is revealed in the frame of Ramsey's paradigm. We also suggest a national engineering solution for creating the required subnanosecond control pulses with the desired shape and amplitude. We performed numerical simulation of the process of tomography of quantum entangled Bell states, and the simplest quantum algorithms (Deutsch–Jojsa and Grover search) on a two-qubit flux register using subnanosecond SFQ pulses ( 100 ps). An example of the calculation is shown in Fig. 1b and is described in detail in [3]. It is shown that the entangled states can be realized by several pulses, which is several tens of times faster

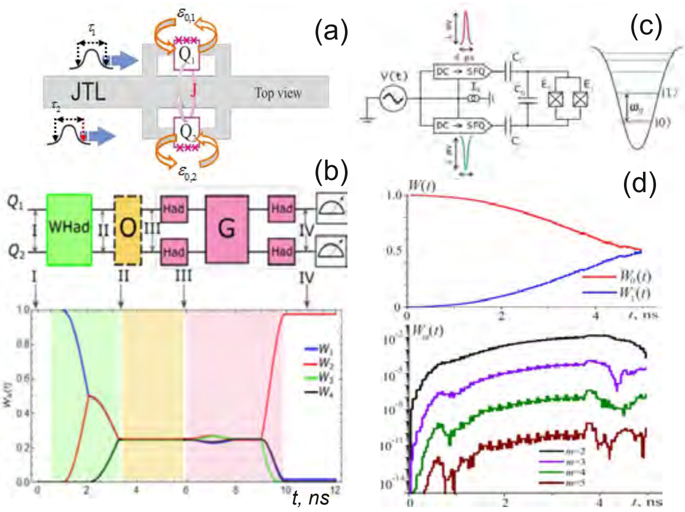

Figure 1: a) Control scheme for flux qubits by SFQ pulses; (b) an example of the implementation of Grover's algorithm, see for more details in [2]; (c) the scheme for controlling the transmon qubit by bipolar SFQ pulse sequence, and (d) the implementation of the operation $Y_{\pi/2}$, see for more details in [4].

than microwave technology based on extended modulated signals [1]. At the same time, the reliability of the creation of Bell states is 95-98%, and the execution of quantum algorithms is 93-98%.

In the case of a transmon register of qubits, the approach used to control streaming qubits by sub-nanosecond pulses is unacceptable. This is due to the weak anharmonicity of transmons and the resulting strong leakage from the computational subspace of states. We have proposed an original approach for fast control based on bipolar sequences of SFQ pulses, see the diagram in Fig. 1c. It is assumed that the acting unipolar pulses at the period of the natural frequency of the qubit have positive polarity, and at half of the period – negative polarity. As a result of numerical simulation, it is shown that it is possible to significantly reduce the time of typical operations (Fig. 1d for $Y_{\pi/2}$) while maintaining the accuracy of their execution. We introduce the bipolar SFQ pulse generator, doubling the allowable time range for effective application of the SFQ drive. We also develop a genetic optimization algorithm for finding bipolar SFQ control sequences that minimize qubit state leakage [4]. We show that the appropriate sequence can be found for arbitrary system parameters from the practical range. The proposed SFQ bipolar drive reduces a single qubit gate time by halve compared to nowadays unipolar SFQ technique, making it no slower than with microwave control while maintaining the gate fidelity over 99.99%.

Thus, we carry out a detailed analytical and numerical analysis on the implementation of quantum operations in superconducting registers by SFQ pulses based on flux and transmon qubits.

The work is supported by the Russian Science Foundation Grant (RSF) No. 22-72-10075.

# References

[1] *P. Krantz, M. Kjaergaard, F. Yan, T.P. Orlando, S. Gustavsson, W.D. Oliver*, A quantum engineer's guide to superconducting qubits. Applied Physics Reviews **6**, 021318 (2019).

[2] *V.A. Vozhakov, M.V. Bastrakova, N.V. Klenov, I.I. Soloviev, W.V. Pogosov, D.V. Babukhin, A.A. Zhukov, A.M. Satanin*, State control in superconducting quantum processors. Phys. Usp. **65**, 421 (2022).

[3] *M.V. Bastrakova, N.V. Klenov, V.I. Ruzhitskii, I.I. Solovyev, A.M. Satanin*, Sub-nanosecond operations on superconducting quantum register based on Ramsey patterns. Superconductor Science and Technology **35**, 055003 (2022).

[4] *V. Vozhakov, M. V. Bastrakova, N. V. Klenov, I. I. Soloviev, and A. M. Satanin*, Speeding up qubit control with bipolar single-flux-quantum pulse sequences. Submitted to Quantum Science and Technology (2022).

# Resource theory of quantum computation

**Anastasiia Poshevkina***, **Sergey Korolev**

*Saint-Petersburg State University, Saint-Petersburg, Russia*
*E-mail: st049468@student.spbu.ru

**Abstract**

In this work was developed the theory to evaluate the degree of non-Gaussianity of quantum states, which are the most important resource for constructing universal quantum computations in continuous variables.

The work is devoted to the research of continuous variables. The transformation states in continuous variables occurs in the infinite-dimensional Hilbert space, it is an important advantage over discrete variables, since it allows you to encode information much more capaciously.

When looking for a basis set of operators, it turns out that both Gaussian and non-Gaussian operations are necessary to construct universal quantum computation. However, there occurs a significant problem in experiments on the implementation of non-Gaussian operations. All known physical phenomena suitable for the role of non-Gaussian transformations turn out too weak to create effective computing. Therefore, non-Gaussian states and operators are the most important resources for the development of new quantum information technologies.

It is also known that some auxiliary non-Gaussian states, such as the cubic phase states, and the Gaussian protocol together can serve as a complete set, that is, sufficient to perform universal computation. However, the cubic phase states are difficult to realize, therefore it is important to understand exactly which other states would be enough.

As a result our research we obtained two criteria that allow us to estimate the degree of the non-Gaussianity of states: Wigner logarithmic negativity $W$ and quantum Non-Gaussianity $\delta$. There is no universal way to quantify a resource, since different functions are related with different tasks. They can be used to assess the feasibility of a transformation; in best case a complete set of criteria can provide necessary and sufficient conditions for transformations between resource states.

We use $W$ and $\delta$ to estimate the fullness of the resource in some paradigmatic significant examples of non-Gausian states, the results of that are presented in Fig.1 . Comparison of these two quantities is very useful for define properties of the considered state.

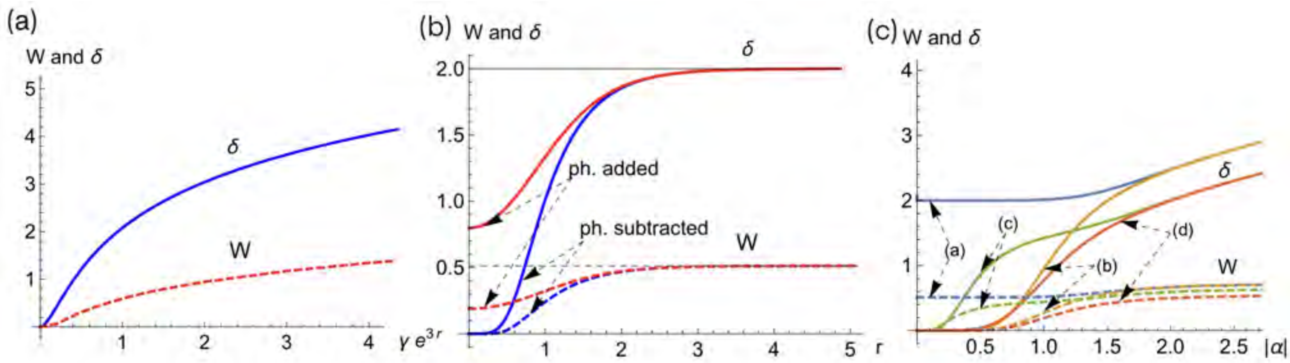


Figure 1: Quantum non-Gaussianity and Wigner logarithmic negativity of (a) pure cubic phase states, (b) photon subtracted/added states, (c) cat states for various parameter values.

Consideration of the states of Schrödinger's cat made it possible to observe fundamentally different behavior of the measures, indicating the design features of the two approaches. As we have seen, the Wigner logarithmic negativity tends to a finite value as the distance between the two Gaussian peaks of the Wigner function increases, while the non-Gaussian tends to infinity, since it is sensitive to this distance.

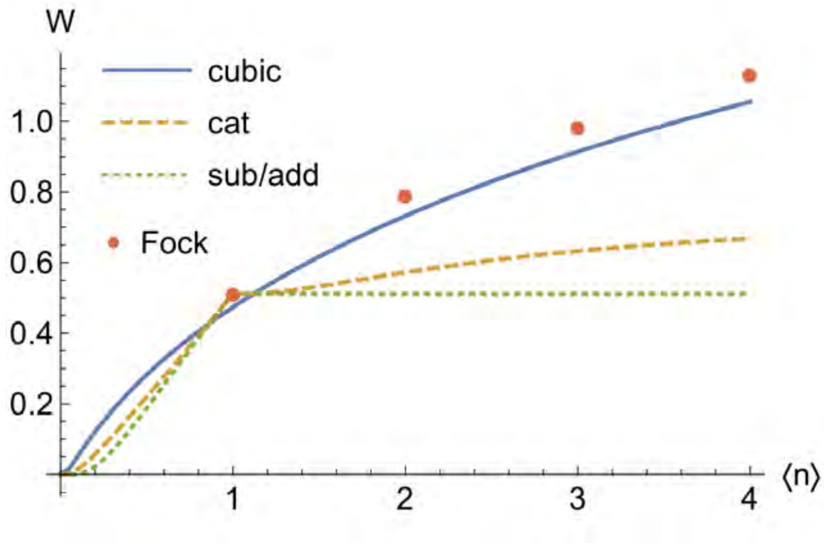


Figure 2: The maximum value of Wigner's logarithmic negativity $W(<\hat{n}>)$ for the considered classes of states

Next, we considered the behavior of Wigner's logarithmic negativity as a function of the average number of bosonic excitations $<\hat{n}>$ for each class of states, that makes it possible to compare the resource capacity of states relative to each other. The results are presented in Fig.2.

The Fock states are strongly non-Gaussian. The maximum value of the Wigner logarithmic negativity for the cubic phase state turns out to be very close to the Fock states. These classes of states claim to be the most resourceful, sufficient to form a complete set.

At the same time, the cat states and photon subtracted/added states turn out to be less resourceful, however, for $<\hat{n}>=1$, the maximum value of the function reaches the value for the Fock state 1, then there is a maximum resource.

However, since obtaining states with the addition/subtraction of a photon and Fock states is of a probabilistic nature, using them is inconvenient and greatly complicates the calculation.

Thus, in this work, we researched two measures of non-Gaussianity that can be used to assess the degree of suitability of the states for the implementation of universal quantum computation in continuous variables.

## References

[1] *Seth Loyd, Samuel Braunstein*, Quantum computation over continuous variables. Phys. Rev. Lett. **82**, 1784 (1998).

[2] *H. J. Kimble, John Preskill, Seth Lloyd, Al Despain*, Quantum Information and Computation. Volume 1 (2001).

[3] *M. Nilson, I. Chang*, Quantum Computation and Quantum Information. Publishing house "Mir" (2003).

# Quantum simulation of fermionic systems using hybrid digital-analog quantum computing approach

**Nikita Guseynov**[1,2], **Walter Pogosov**[1,3,4]

[1] *Dukhov Research Institute of Automatics (VNIIA), Moscow, Russia*
[2] *Moscow Institute of Physics and Technology, Dolgoprudny, Russia*
[3] *Institute for Theoretical and Applied Electrodynamics, Russian Academy of Sciences, Moscow, Russia*
[4] *HSE University, Moscow, Russia*
*E-mail: guseynovnm@my.msu.ru

**Abstract**

We consider a hybrid digital-analog quantum computing approach, which allows implementing any quantum algorithm without standard two-qubit gates. This approach is based on the always-on interaction between qubits, which can provide an alternative to such gates. We show how digital-analog approach can be applied to simulate the dynamics of fermionic systems, in particular, the Fermi-Hubbard model, using fermionic SWAP network and refocusing technique. We concentrate on the effects of connectivity topology, the spread of interaction constants as well as on errors of entangling operations. We find that an optimal connectivity topology of qubits for the digital-analog simulation of fermionic systems of arbitrary dimensionality is a chain for spinless fermions and a ladder for spin 1/2 particles. Such a simple connectivity topology makes digital-analog approach attractive for the simulation of quantum materials and molecules.

## Introduction

The ability of quantum computers to outperform classical supercomputers has recently been demonstrated for some special tasks. This regime of functioning of quantum computers corresponds to the so-called quantum supremacy [1–3]. Conventional quantum computers operate in accordance with the gate model of quantum computation which is based on a universal set of quantum gates. The minimal set of required gates [4] includes arbitrary single-qubit gates and two-qubit operations such as controlled-NOT (CNOT) or some equivalent gate. Such quantum devices are usually referred to as digital quantum computers. However, control of all relevant degrees of freedom becomes much more difficult when the system is scaled up. Quantum error correction codes [5] in combination with optimization protocols [6, 7] constitute a promising approach, but their effective implementation on modern quantum devices is challenging due to the relatively small number of qubits as well as existing gates errors. As a result of hardware imperfections, the Fermi-Hubbard model was simulated using digital quantum computers only for small systems with limited numbers of fermionic lattice sites [8]. Note that the main contribution to the gates error rate is due to the two-qubit gates. Thereby, it is interesting to consider alternative approaches, which are not based on the execution of the standard two-qubit gates.

One of the alternatives is associated with the idea of a hybrid digital-analog quantum computing [9–16]. In the simplest realization of such a strategy, single-qubit gates, as well as individual readouts of qubits, must be accessible similarly to the case of digital quantum devices, but instead of conventional two-qubit gates quantum entanglement is created using always-on native interaction of qubits. This requires a certain trade-off between the fidelities of single-qubit gates diminished by the always-on interaction between qubits and fidelities of entangling operations [12]. A more sophisticated approach is possible which requires switchable interaction between qubits that can be turned off during the execution of single-qubit gates. Particularly, we would like to mention a recent paper [16], which suggests a specialized superconducting circuit architecture for the digital-analog quantum computation and simulation.

## Results

This article pointed out that digital-analog quantum devices are prospective for the quantum simulation of fermionic models in different dimensions. The approach we proposed is based on the application of fermionic SWAP network [17] implemented through always-on interaction between qubits of the device.

The fermionic simulation gate [17] can be used to circumvent the non-locality problem of the Hamiltonian (1) under the Jordan-Wigner transformation. This gate is represented through the native interaction of qubits and single-qubit gates. We suggested using a refocusing technique when implementing a fermionic SWAP network to compensate for undesirable interactions between qubits at each simulation step. We argued that the digital-analog strategy is appropriate for the fermionic simulation since all qubits of the chip can be used uniformly in time, enabling it to perform multiple entangling operations simultaneously.

$$H = \sum_{n \neq m} T_{nm} a^\dagger_{n\uparrow} a_{m\uparrow} + \sum_{n \neq m} U_{nm} a^\dagger_{n\downarrow} a_{m\downarrow} + \sum_{n} V_n a^\dagger_{n\uparrow} a_{n\uparrow} a^\dagger_{n\downarrow} a_{n\downarrow}. \tag{1}$$

We concentrated mainly on the impact of the connectivity topology of the qubit network, its spread in interaction constants, and the effect of errors in entangling operations on the efficiency of quantum algorithm implementation. We found that an optimal topology for the digital-analog chip in the context of fermionic simulation is a one-dimensional chain for any dimensionality of the simulated model, in the case of spinless fermions, and a ladder, in the case of spin-1/2 fermions. In this case, the overhead associated with compensating undesired interactions between qubits is minimum. Such a simple connectivity topology makes it easier to probe our findings in experiments.

For optimal topology, the simulation of the single Trotter step of the evolution requires $\mathcal{O}(n)$ applications of multi-qubit gates, where $n$ is the qubit number. The method of refocusing has been extended to the case when there is a spread of interaction constants. It is shown that the circuit depth increases by a factor of $\mathcal{O}(n)$. We also found that errors associated with the inaccuracy in determining interaction constants lead to the weak quadratic growth of infidelity as a function of the deviation of the actual coupling constants from the assumed values, which is a positive fact in the view of the perspectives of the digital-analog approach. The effects of the depolarizing noise, phase damping and amplitude damping are more harmful since they lead to the linear decrease of fidelity as a function of error parameter both for digital-analog and digital strategies.

[1] A. P. Lund, M. J. Bremner, and T. C. Ralph, npj Quant. Inf. **3**, 1 (2017).
[2] H.-S. Zhong, H. Wang, Y.-H. Deng, M.-C. Chen, L.-C. Peng, Y.-H. Luo, J. Qin, D. Wu, X. Ding, Y. Hu, et al., Science **370**, 1460 (2020).
[3] R. Li, B. Wu, M. Ying, X. Sun, and G. Yang, IEEE Transactions on Parallel and Distributed Systems **31**, 805 (2019).
[4] F. Vatan and C. Williams, Phys. Rev. A **69**, 032315 (2004).
[5] S. J. Devitt, W. J. Munro, and K. Nemoto, Rep. Prog. Phys. **76**, 076001 (2013).
[6] A. Kandala, A. Mezzacapo, K. Temme, M. Takita, M. Brink, J. M. Chow, and J. M. Gambetta, Nature **549**, 242 (2017).
[7] C. Gidney, Quantum **2**, 74 (2018).
[8] F. Arute, K. Arya, R. Babbush, D. Bacon, J. C. Bardin, R. Barends, A. Bengtsson, S. Boixo, M. Broughton, B. B. Buckley, et al., arXiv:2010.07965 (2020).
[9] S. C. Benjamin and S. Bose, Phys. Rev. Lett. **90**, 247901 (2003), URL `https://link.aps.org/doi/10.1103/PhysRevLett.90.247901`.
[10] Y. Hu, Z.-W. Zhou, and G.-C. Guo, New J. Phys. **9**, 27 (2007), URL `https://doi.org/10.1088/1367-2630/9/2/027`.
[11] A. Parra-Rodriguez, P. Lougovski, L. Lamata, E. Solano, and M. Sanz, Phys. Rev. A **101**, 022305 (2020), URL `https://link.aps.org/doi/10.1103/PhysRevA.101.022305`.
[12] D. V. Babukhin, A. A. Zhukov, and W. V. Pogosov, Phys. Rev. A **101**, 052337 (2020).
[13] L. C. Céleri, D. Huerga, F. Albarrán-Arriagada, E. Solano, and M. Sanz, arXiv:2103.15689 (2021).
[14] A. Martin, L. Lamata, E. Solano, and M. Sanz, Phys. Rev. Research **2**, 013012 (2020), URL `https://link.aps.org/doi/10.1103/PhysRevResearch.2.013012`.
[15] D. Headley, T. Müller, A. Martin, E. Solano, M. Sanz, and F. K. Wilhelm (2020), URL `https://arxiv.org/abs/2002.12215`.
[16] J. Yu, J. C. Retamal, M. Sanz, E. Solano, and F. Albarrán-Arriagada (2021), URL `https://arxiv.org/abs/2103.15696`.
[17] I. D. Kivlichan, J. McClean, N. Wiebe, C. Gidney, A. Aspuru-Guzik, G. K.-L. Chan, and R. Babbush, Phys. Rev. Lett. **120**, 110501 (2018).

# Quantum error reduction with deep neural network applied at the post-processing stage

Andrey Zhukov[1*], Walter Pogosov[1,2,3]

[1]*Dukhov Research Institute of Automatics (VNIIA), Moscow, Russia*
[2]*Institute for Theoretical and Applied Electrodynamics, RAS, Moscow, Russia*
[3]*HSE University, Moscow, Russia*
*E-mail: `zugazoid@gmail.com`

**Abstract**

Deep neural networks (DNN) can be applied at the post-processing stage for the improvement of the results of quantum computations on noisy intermediate-scale quantum (NISQ) processors. Here, we propose a method based on this idea, which is most suitable for digital quantum simulation characterized by the periodic structure of quantum circuits consisting of Trotter steps. Two particular examples are considered that are the dynamics of the transverse-field Ising chain and XY spin chain, which were implemented on two real five-qubit IBM Q processors. A significant error reduction is demonstrated as a result of the DNN application that allows us to effectively increase quantum circuit depth in terms of Trotter steps.

Quantum information is a fast developing field that aims to utilize quantum properties, such as quantum interference and entanglement [1]. State-of-the-art quantum computers are already capable of solving many problems, which, however, are not of practical importance yet, because of relatively high quantum hardware error rates. Particularly, such processors can be useful for solving evolutionary problems. However, the simulation of the dynamics of such systems at long times requires a large number of Trotter decomposition steps of evolution operator. This leads to the fact that a large number of quantum gates are required for simulation, which means that the outcomes from the quantum computer become too noisy [2].

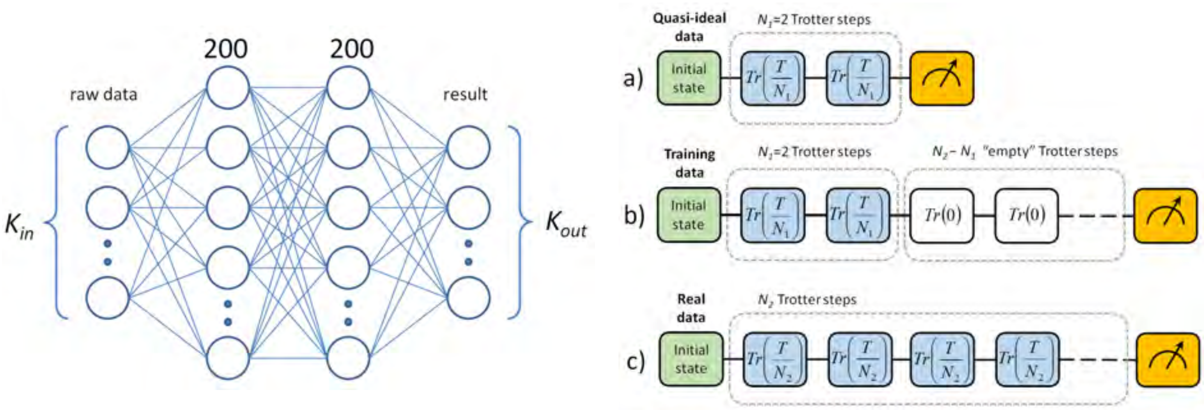


(1) (2)

Figure 1: (1) The feed-forward DNN architecture used in our problems for improving simulation results. (2) Schematic view of our approach. It consists of three steps: generation of quasi-ideal data with relatively shallow circuit (a); training the DNN – the data with artificially increased Trotter steps number are transformed towards quasi-ideal data (b); the trained DNN is applied to raw experimental data with the same Trotter step number as at the second stage (c).

An attempt to enhance capabilities of quantum devices, from one hand, and machine learning methods, from another hand, has led to the merger of these areas, which gave rise to a new discipline known as quantum machine learning (QML). For example, using deep machine learning in quantum tomography, it became possible to reduce errors in the preparation and measurement of quantum states [3].

In our work, we have proposed a method for the application of classical neural networks Fig. 1(1) for the improvement of the outcomes of noisy quantum computers at the post-processing stage. In contrast

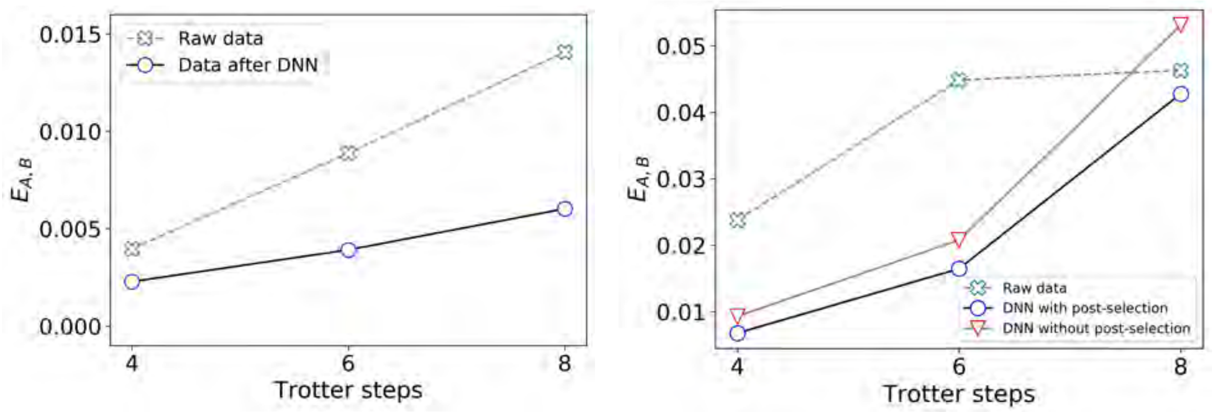


(1) (2)

Figure 2: Mean Square Error (MSE), between ideal simulation data for a given Trotter step number and experimental data from an IBM Athens 5-qubit quantum processor improved by the network (o-shape symbols and solid line) as well as raw data (x-shape symbols and dashed line) for (1) transverse-field Ising chain and (2) XY spin chain.

to other suggestions, using our approach, it is possible to get data for training a neural network without relying on a classical simulator or any other source of ideal data.

Our method is based on artificial increase of the quantum circuits depth on the training stage that can be done by incorporation of fictitious Trotter blocks formally equivalent to identity gates into the circuit (see Fig. 1(2)). Their role is to increase noise level due to the hardware imperfections while preserving the circuit's general structure and its relevant features. The network is trained to transform data obtained with such fictitious steps towards data obtained without them, that is, for rather shallow circuits, for which hardware errors are not critical. This idea seems to be more prospective for near-term generations of quantum computers with reduced gate errors, for which circuits at the training stage can already support large entanglement.

After being trained, the network can be applied to new data with the same Trotter step number, i.e., increased in the same way as at the training stage, but without fictitious Trotter steps. The amount of noise in this case is similar to that at the training stage. This trick allows for the effective increase of the Trotter number due to the post-processing, in the sense that errors become suppressed and results of simulations, which must have error rates below a given level, start to include data with larger Trotter step number.

We have demonstrated (see Fig. 2) the basic ingredients of our approach using two examples: digital quantum simulations of the dynamics of the transverse-field Ising chain(1) and XY chain(2). Deep neural network with simple architectures were used at the post-processing stage (Fig. 1(1)). For XY chain, an additional post-selection of the results at the training stage was applied by discarding a part of the data, which does not conserve the excitation number, as required by the Hamiltonian. The proof-of-principle results obtained on a real 5-qubit IBM Athens and Bogota quantum processors show that our method allows us to increase the number of Trotter steps while maintaining the same level of errors. The significant error reduction is the main result of our demonstration. A single neural network is able to improve the data for different initial conditions.

## References

[1] *R. Horodecki, P. Horodecki, M. Horodecki, and K. Horodecki*, Quantum entanglement. Rev. Mod. Phys. **81**, 865 (2009).

[2] *A.A. Zhukov, S.V. Remizov, W.V. Pogosov, and Yu.E. Lozovik*, Algorithmic simulation of far-from-equilibrium dynamics using quantum computer. Quant. Inf. Proc. **17**, 1 (2018).

[3] *A.M. Palmeri, A. Macarone, E. Kovlakov, F. Bianchi, D. Yudin, S. Straupe, J.D. Biamonte, and S. Kulik*, Experimental neural network enhanced quantum tomography. npj Quant. Inf. **6**, 1 (2020).

# Solving systems of linear equations on a quantum computer without ancilla postselection

Danila Babukhin[1*]

[1] *Dukhov Research Institute of Automatics (VNIIA), 127055 Moscow, Russia*
*E-mail: dv.babukhin@gmail.com

**Abstract**

Harrow-Hassidim-Lloyd algorithm (HHL) is a quantum algorithm, which allows solving a system of linear equation exponentially faster, using a quantum computer. However, this algorithm requires to postselect ancilla qubit measurement outcomes to provide a solution for the linear system, which makes this algorithm probabilistic. Here we show, that under certain conditions, the HHL algorithm can work without postselection of ancilla qubit, which makes the algorithm deterministic. We demonstrate this result explicitly on a simple input matrix example.

## Introduction

The HHL algorithm [1] is a quantum algorithm that provides a solution for a linear system with an exponential speed up. Since its invention, numerous applications of this algorithm to practical problems have been demonstrated: solving linear systems is used for differential equations, calculating scattering cross-sections, and building quantum machine learning algorithms. Progress in quantum computing devices in the last decades allowed conducting low-dimensional experiments, which investigate practical opportunities and caveats of the HHL algorithm.

The HHL algorithm requires postselection of an ancilla qubit in a quantum state $|1\rangle$ to produce a solution. Ancilla measurement in the $|1\rangle$ state has a non-unity probability, which leads to discarding part of the algorithm runs on a quantum processor. Consequently, discarding results leads to an increase in quantum processor running time. An amplitude amplification algorithm [2] is usually used after the HHL circuit to increase the probability of measuring ancilla in $|1\rangle$. This step requires $O(\kappa)$ repetitions of the amplitude amplification to make a success probability sufficiently high. Here $\kappa$ is a conditional number of the input matrix $A$, where $A$ represents a system of linear equations we want to solve. A running time of the HHL is $O(log(N)s^2\kappa^2/\epsilon)$[1], where one $\kappa$ comes from the amplitude amplification step. Although adding only a polynomial (in $\kappa$) complexity overhead, the amplitude amplification step increases algorithm running time and introduces gate errors into computation when the algorithm is running on a NISQ device [3]. Until fault-tolerant quantum computation is available, the postselection step decreases the efficiency of the HHL algorithm.

In this work, we demonstrate conditions for running the HHL algorithm without postselection of the ancilla qubit. This is possible for input matrices $A$ of linear equation systems and for measurement matrices $M$, which satisfy the commutator identity $[[M, A], A] = 0$. When this relation is satisfied, the algorithm produces quantum states for two ancilla measurement outcomes ($|0\rangle$ or $|1\rangle$), in which expectation values deviate from each other only by a constant. This connection of expectation values allows using both output states to obtain an expectation value of $M$ on the solution of the linear system. This reduction of postselection leads to the economy of $O(\kappa)$ operations of amplitude amplification, otherwise used to amplify the success probability of ancilla measurement.

## Results

To demonstrate the idea of the postselection-free HHL, we explicitly calculate a simple realization of the HHL algorithm, introduced in [4]. Here, the HHL algorithm is used to solve a system of 2 linear equations, represented by a matrix

$$A = \begin{pmatrix} 1.5 & 0.5 \\ 0.5 & 1.5 \end{pmatrix} \tag{1}$$

In Fig.1, we provide a quantum circuit of algorithm. In this example, for an observable $M = \begin{pmatrix} 0 & 1 \\ 1 & 0 \end{pmatrix} = X$

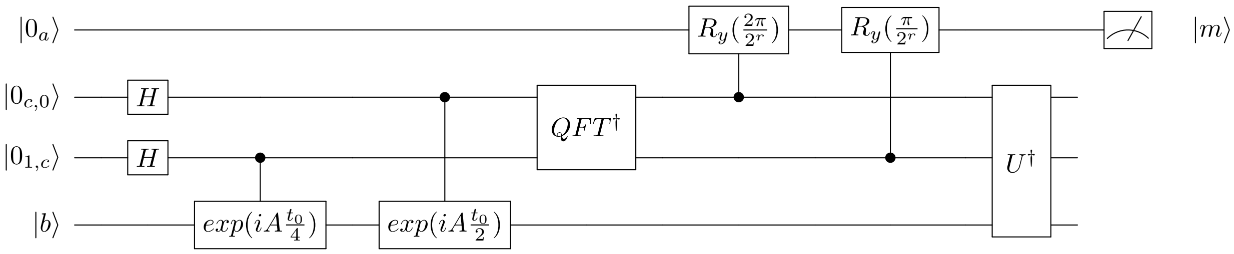


Figure 1: A quantum circuit implementing the HHL algorithm for a system of 2 linear equations for matrix (1)

a commutator with input matrix $A$ is $[M, A] = 0$, which is seen from decomposition $A = 1.5I + 0.5X$.

We run the algorithm for 100 random initial vectors $|b\rangle = \cos\frac{\theta}{2}|0\rangle + \sin\frac{\theta}{2}|1\rangle$ and obtained solution vectors $|x_0\rangle$ for ancilla measurement in state $|0\rangle$ and $|x_1\rangle$ for ancilla measurement in state $|1\rangle$. In Fig. 2 we provide expectation values $M_1 = \langle x_1| M |x_1\rangle$ and $\frac{1}{Pr(a=1)}(M_b - Pr(a=0)M_0)$, where $M_0 = \langle x_0| M |x_0\rangle$ and $M_b = \langle b| M |b\rangle$. We compared results with a classical solution for the system of linear equations $\vec{x}$, in particular, with a value $\vec{x}^T M\vec{x}$. From Fig.2, we see perfect coincidence with classical results and results obtained from the HHL algorithm outcomes for ancilla values 0 and 1.

As a result, we demonstrate that using both output states for two ancilla measurement outcomes can give a correct expectation value of $M$ with only slight postprocessing (subtracting a constant value). This extraction of correct expectation values is possible if a postselection-free condition is satisfied.

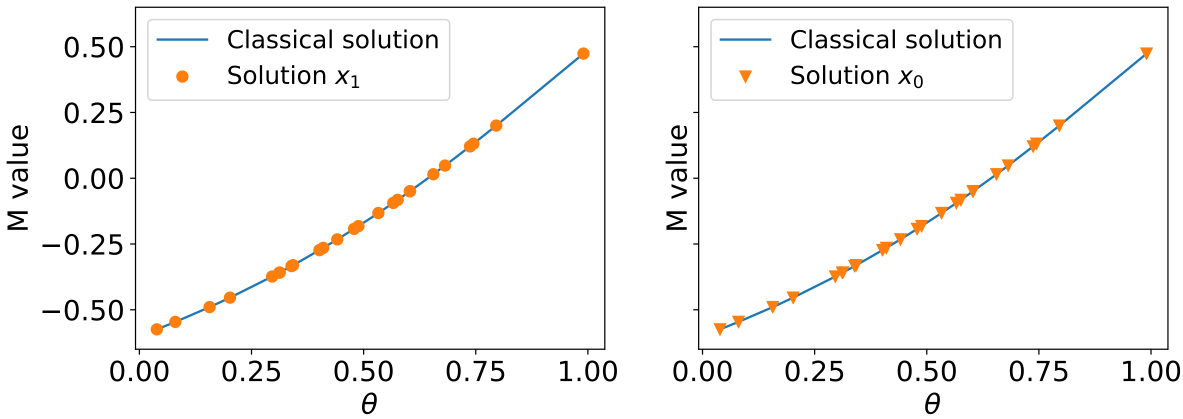


Figure 2: Expectation values of M on the HHL algorithm outcomes $|x_1\rangle$ (left plot), $|x_0\rangle$ (right plot), compared to $\vec{x}^T M\vec{x}$ value (blue solid curve), where $\vec{x}$ is a classical vector of the linear system solution. Classical solution values for different values of a parameter $\theta$ are connected with a curve to guide an eye.

# References

[1] *A. W. Harrow, A. Hassidim and S. Lloyd*, Quantum Algorithm for Linear Systems of Equations. Phys. Rev. Lett. **103**, 150502 (2009).

[2] *G. Brassard, P. Hoyer, M. Mosca and A. Tapp*, Quantum amplitude amplification and estimation. Quantum Computation and Quantum Information, Samuel J. Lomonaco, Jr. (editor), AMS Contemporary Mathematics, 305:53-74, 2002.

[3] *J. Preskill*, Quantum Computing in the NISQ era and beyond. Quantum **2**, 79 (2018).

[4] *Y. Cao and A. Daskin and S. Frankel and S. Kais*, Quantum circuit design for solving linear systems of equations. Molecular Physics 110, 1675 (2012).

# Study of single-photon detector blinding attack with modulated bright light

Daniil Bulavkin[1*], Kirill Bugai[1,2], Dmitriy Dvoretskiy[1,2]

[1] *SFB Laboratory, Ltd, Moscow, 127273, Russia*
[2] *Bauman Moscow State Technical University, 2nd Baumanskaya str. 5-1, Moscow, Russia 107005*
*E-mail: Daniil.Bulavkin@sfblaboratory.ru

**Abstract**

We present an experimental setup for blinding attack with modulated bright light with the opportunity of changing pulse width in the range of 5-20 ns at a 10 MHz repetition rate. Then we are comparing the conventional defense method via bias current analyses during CW and bright pulse blinding.

Quantum Key Distribution Systems (QKD) provide a secure exchange of information between legitimate users guaranteed by the laws of quantum mechanics. There are many attacks on the conventional components of QKD systems, and one of the most promising and dangerous for whole system security is the blinding attack of single-photon detectors [1]. When blinded, the single-photon detector is switched from Geiger mode to linear mode and, thus, ceases to be sensitive to single photons. This attack can allow the eavesdropper (Eve) to fully control the APD triggering and thereby impose his key [2].

An experimental setup for carrying out the blinding attack is shown in Fig. 1. Laser radiation passes through a polarizer and enters an amplitude modulator based on a Mach-Zehnder interferometer. The phase modulator is connected to a power supply, which brings it to the operating point corresponding to the minimum transmission of the modulator. A signal of a certain shape is fed to the high-frequency output of the modulator, which will set the shape of the optical signal going to the single-photon detector. Then the radiation hits the 90/10 beam splitter. From the 90% output, the radiation enters the wideband 20 GHz photodetector module, which monitors the signal shape. From the 10% output, the laser pulse goes to the attenuator, and from it to the single-photon detector. The single-photon detector is a commercially available device with software and electronics that allows monitoring the detector parameters such as counting rate, bias current, and temperature. The detector operates in gated mode and is synchronized using the signal generator with a frequency of 10MHz. We perform the blinding attack at different pulse widths using a signal generator and monitor the level of bias current. Then, we compare the bias current during CW and pulse single-photon detector blinding. Data depicted in Fig.2 clearly shows that blinding using modulated light causes the rising of the bias current less than CW blinding which proves that bright light pulses are more effective than CW blinding. However, increasing the bias current is enough to be detected if corresponding electronics components would be chosen.

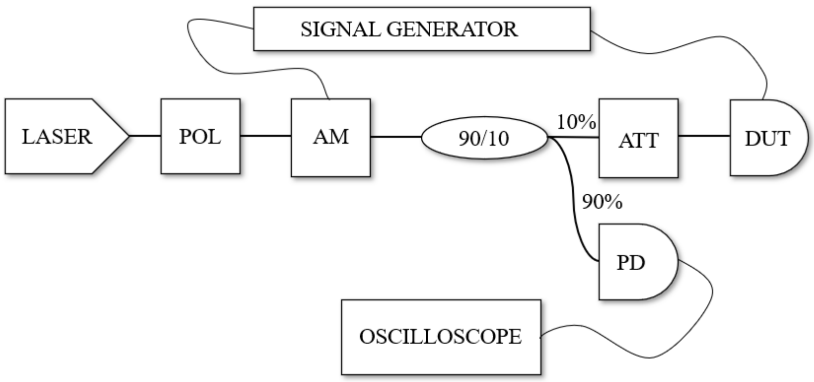


Figure 1: Experimental setup (LASER – 1550nm laser source, POL – polarizer, AM – amplitude modulator, 90/10 – 90/10 optical splitter, ATT – attenuator, PD – wideband photodetector module 20GHz, DUT – single-photon avalanche diode)

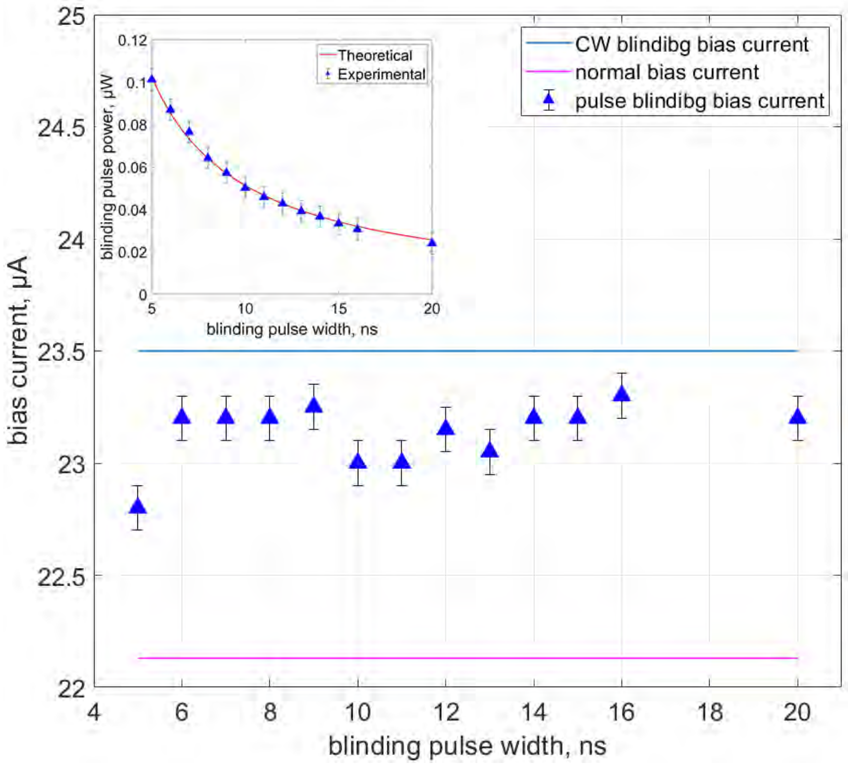


Figure 2: Bias current vs blinding pulse width during CW blinding and modulated blinding against bias current in normal condition of the SPAD. Inserted fig. – comparing of the experimental blinding pulse power dependence on pulse width vs theoretical fitted curve.

The inset of Fig.2 shows the experimental blinding pulse power dependence on pulse width fitted by the theoretical curve. The fitted curve has the form of the hyperbola, which proves that detector-blinding power depends mainly on the energy in the pulse.

## References

[1] *1. L. Lydersen, C. Wiechers, C. Wittmann, D. Elser, J. Skaar, and V. Makarov*, Nat. Photonics 4(10), 686–689 (2010).

[2] *2. V. Chistiakov, A. Huang, V. Egorov, and V. Makarov*, Opt. Express 27(22), 32253–32262 (2019).

# Experimental realization of quantum key distribution based on B92 protocol with strong reference pulses

**Polina Vinetskaya**[1,2*], **Konstantin Kravtsov**[1]

[1] *MSU Quantum Technology Centre, Moscow, Russia*
[2] *NRU Higher School of Economics, Moscow, Russia.*
*E-mail: polinvin@gmail.com

**Abstract**

The original setup of B92 with strong reference pulses QKD protocol is difficult to perform. In this work we suggest an alternative way to implement B92 protocol using polarization modes instead of temporal ones. Results obtained with the attenuated laser radiation and theoretical estimates indicate the possibility of using the scheme in practice.

Quantum key distribution is a method that allows two interlocutors Alice and Bob to generate a common random sequence of bits and guarantee its secrecy, using only communication channels open to intrusion. In theory, protocols involve the use of non-orthogonal two-dimensional quantum states, such as polarization of single photons, the source of which is difficult to implement in practice. Therefore, more practical attenuated laser pulses with an average number of photons per pulse $\mu \ll 1$ are used instead of single photons. Clearly, such states contain multi-photon components, that open up opportunities for various attacks, such as the PNS attack and the intercept-resend (I-R) attack [1]. One method of protection against these attacks is to add strong reference pulses (pulses of high intensity), which, due to their classical nature, signal the delivery of the quantum informational component. This method was proposed in the B92 protocol [2], but the protocol itself, as far as we know, was not implemented in its original form, since the temporal phase coding described in the article seems to be impossible to implement due to reflections from the channel components.

In this paper we study the possibility of implementing B92 QKD protocol with strong reference pulses by using a different encoding method – using polarization states for encoding information and extracting a reference signal. The work is devoted to the theoretical and experimental evaluation of the main parameters of the scheme and theoretical estimating their impact on secret key generation rate.

## Methods

Lithium niobate LiNbO3 crystals cut along the optical Z axis were used as polarization modulators (Fig.1). In the absence of an induced voltage, light propagates without changing polarization. If a voltage is applied to the uniaxial crystal, then due to the electro-optic effect, linearly vertically polarized light, when passing through it, becomes weakly elliptically polarized, acquiring a small horizontal component. After the second crystal, the effect will either double or disappear, depending on the combination of voltage signs that the interlocutors choose randomly. Thus, Bob can recover the value of the sent bit (the polarity of the voltage on Alice's crystal) only if the horizontal component is successfully detected. Therefore, it is possible to implement a key distribution protocol using a horizontal polarization signal to encode bits of information, and a vertical component as a reference "classical" signal. The main parameters of the scheme are the contrast (the ratio of the intensities of the horizontal component for constructive and destructive interference) and the ratio of the information and reference signals. Both parameters depend on the magnitude of the voltage applied to the crystals.

Measurements were carried out with a voltage switching frequency of 1 Hz for contrast analysis (Fig.2a). Similar measurements were also made of long blocks of a repeating signal at a frequency of 2 MHz (Fig.2, b).

Also, the dependence of the key generation rate on the scheme parameters was theoretically studied. Taking into account the measured contrast values and the error ratio in the channel, the influence of these parameters on the share of secret information and the key generation rate was estimated(Fig. 3).

## Results

For an 850 nm semiconductor laser with a pulse repetition frequency of 2 MHz, measurements were carried out with successive switching of 4 possible voltage configurations on the crystals at various values of the average number of photons in the information component prepared by the station "Alice". The average value of information and reference signals ratio was obtained (about $1 : 10^4$), as well as the maximum contrast of the information signal for a voltage of 30 V applied to crystals – about 18 units, which is consistent with the theoretical estimates. After proper alignment, it was possible to achieve the indistinguishability of the states corresponding to the constructive interference (for $++$ and $--$ voltage configurations as shown in Fig. 2). This, as well as the measured contrast values, allow us to conclude that the proposed scheme can be potentially used in practice.

For the measured parameters, the value of the average number of photons per pulse was found, at which the secret key generation rate is maximum: $\mu_{opt} = 0.1$, $r(\mu_{opt}) = 0.7$ KB/s (Fig. 3a).

The theoretical evaluation carried out showed that the contrast greatly affects the key generation rate (Fig. 3b). At the same time, the data obtained at a high switching frequency of voltages indicate a poorer contrast than the values used in the calculation. Currently, work is underway to improve the scheme performance at high rate modulation and study correlations with random switching of the voltage configuration on the crystals.

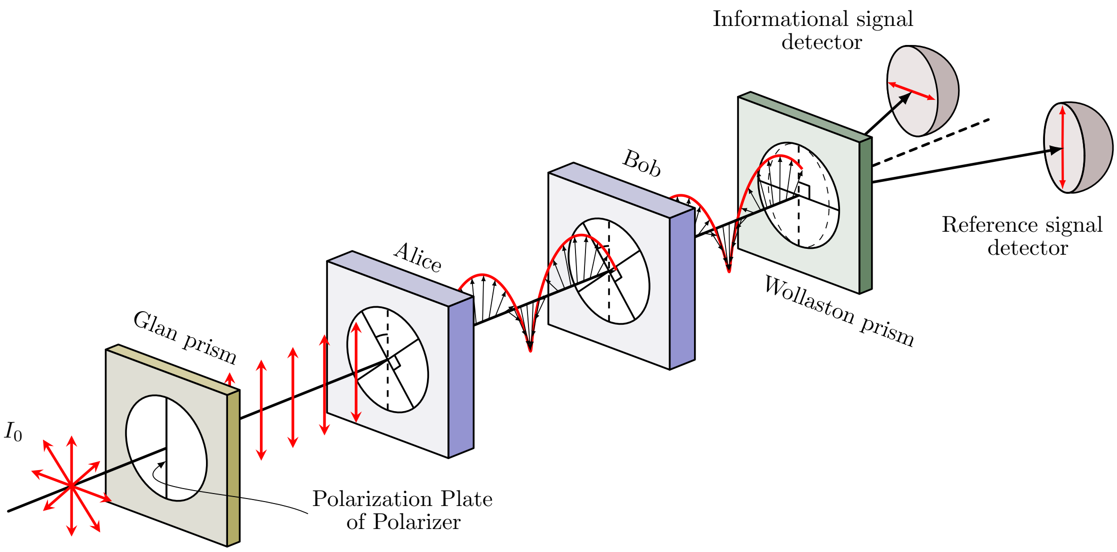


Figure 1: General scheme of the experiment. Light propagates through a Glan prism and becomes vertically polarized. After passing through the electro-optical crystals ("Alice" and "Bob" stations), polarization changes depending on the sign of the applied voltage. The Wollaston prism separates the signal into two orthogonal polarizations: the original vertical (reference signal) and horizontal (informational signal), and separates them spatially, sending them to the detectors.

## References

[1] *B. Huttner, N. Imoto, N. Gisin, and T. Mor*, Quantum cryptography with coherent states. Phys. Rev. A **51**, 1863 (1995)

[2] *Bennett, C. H., Brassard, G.*, Quantum cryptography: Public key distribution and coin tossing. Theoretical Computer Science **560**, 7–11. (2014).

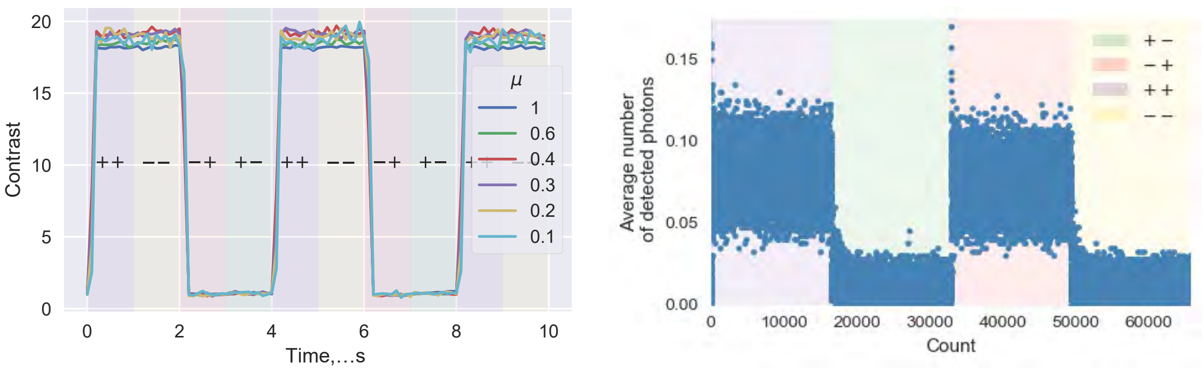


a) b)

Figure 2: Informational signal count statistics. a) Normalized signal, measured for different values of the average number of photons, displays the contrast of the scheme. Voltage switching frequency is 1 Hz, . b) Probability of detecting photons at a switching frequency of 2 MHz, obtained by averaging 400 experiments. The length of the voltage configuration block on the crystals is 16384 counts.

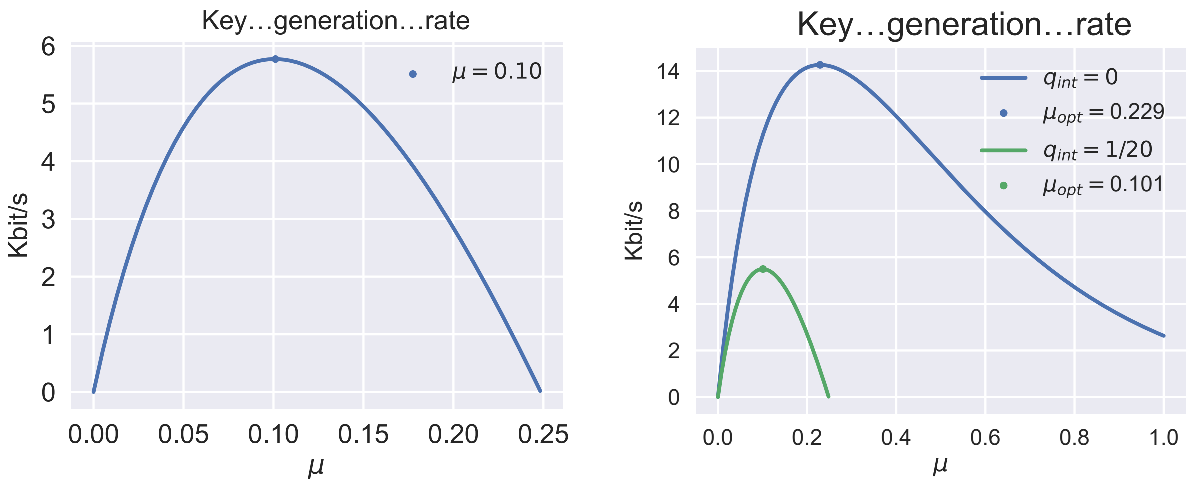


a) b)

Figure 3: a) Estimated key generation rate. Pulse repetition rate of 2 MHz b) Comparison of the key generation rate for ideal contrast and the measured experimental value of 1:20.

# Phase-encoded QKD over a multi-mode communication line

**Vladislav Tretiakov**[1*], **Konstantin Kravtsov**[1]

[1] *MSU Quantum Technology Centre, 119991 Moscow, Russia*
*E-mail: tretiakov.vv18@physics.msu.ru

**Abstract**

Quantum key distribution (QKD) is a quantum communication protocol based on principles of quantum mechanics, information carriers in which are quantum objects such as photons. Implementations of QKD utilizing fiber communication lines are widespread. The phase encoding is commonly used in such lines. Meanwhile, in free-space channels, polarization-encoded protocols are usually used due to their relative implementation simplicity. Also note the robustness of polarization in free-space propagation. It would seem to be impractical to use a phase encoding across free-space channels due to distortions of temporal and spatial modes of photons during propagation through an atmospheric turbulence. Here, we investigate free-space delay interferometer for quantum communications with a multimode signal. So far we have observed the visibility of 0.88, which allows us to believe that practical QKD implementation with this interferometer is possible.

## Introduction

Quantum key distribution (QKD) [1] is a method of sharing secret keys between two legitimate parties involved in the communication process. QKD over fiber communication channels has achieved great results and QKD experiments over 421 km fiber were demonstrated [2]. However, there is a fundamental limitation in increasing of communication distances over optical fibers. Free-space QKD experiments are usually based on polarization-states protocols, since they are simple to implement and the polarization is almost not affected by the atmospheric turbulence.

However, sometimes it's convenient to collect signal after the receiving telescope into optical fiber and transmit it to the place where it can be comfortably measured. Either single-mode or multi-mode optical fiber can be used for this purpose. In the first case, large losses occur when a signal enters a single-mode fiber so its usage become impractical. In the second case we need to refuse from polarization-states protocols because information about the polarization is lost when signal enters a multi-mode fiber. A convenient alternative to them is a phase encoding [4].

Here we investigate a free-space delay interferometer for analyzing phase-encoded photons. Such interferometer can be used in implementation of QKD protocols based on phase encoding. Experiments on visibility measurements with such an interferometer have been already conducted [3]. However, the delay value was only 2 ns, meanwhile we demonstrate free-space delay interferometer with the delay equal 5.7 ns. There are some limitations (lower bounds) on the delay time due to multi-mode dispersion, which leads to broadening of pulses propagating through the multi-mode fiber. So the phase encoding QKD implementations over installed multi-mode fiber communication lines is another purpose of this research.

## Phase encoding

Let us consider Fig.1 that shows a general setup for a phase encoding QKD experiment with an optic fiber. Alice and Bob both have delay interferometers with the same delay lengths. Laser source provides photons which pass Alice's interferometer, quantum channel and Bob's interferometer. The quantum state of such photons at the output of Bob's interferometer is given by

$$|\Psi\rangle = \frac{|SS\rangle\, e^{-i\Delta\phi_B} + |SL\rangle + |LS\rangle\, e^{i(\Delta\phi_A - \Delta\phi_B)} + |LL\rangle\, e^{i\Delta\phi_A}}{2}, \tag{1}$$

where $|SS\rangle$ corresponds to two passes through short arms, $|SL\rangle$ - one pass through a short arm and one through a long, etc. States $|SL\rangle$ and $|LS\rangle$ interfere with one another. The expression (1) shows that the result of this interference depends on the relation of phase shifts introduced by Alice and Bob. So QKD protocols such as BB84 can be implemented with phase encoding.

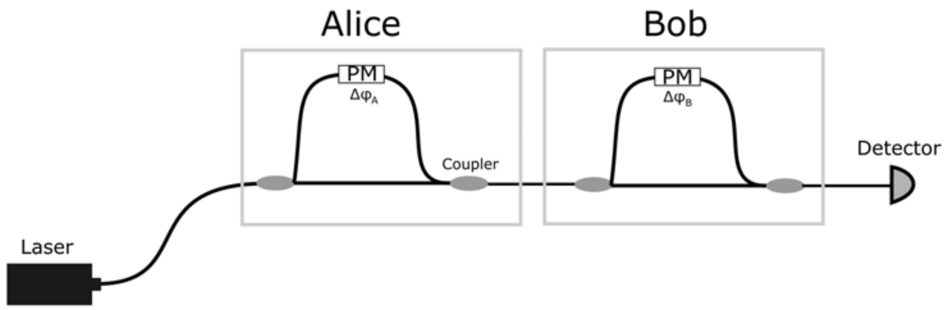


Figure 1: General scheme of phase-encoded QKD setup. A laser source produces faint pulses which split in both Alice's and Bob's interferometer. Alice and Bob are able to introduce phase shifts $\Delta\phi_A$ and $\Delta\phi_B$ respectively to pulses passing through long arms of their interferometers resulting to either constructive or destructive interference at the detector D.

## Visibility of interference at the output of interferometer

The setup for investigating a visibility of interference is shown in Fig.2. We used a 850 nm laser source of nanosecond pulses. These pulses pass through the attenuator and the fiber delay interferometer, split here in half, pass through the free-space Michelson delay interferometer, split again, and then finally reach the single photon detector $D$. The intensity of pulses at the input of Michelson interferometer is controlled by two fiber polarization controllers $PC_1$ and $PC_2$ and the polarizer $P$. It is necessary for tuning the interference visibility.

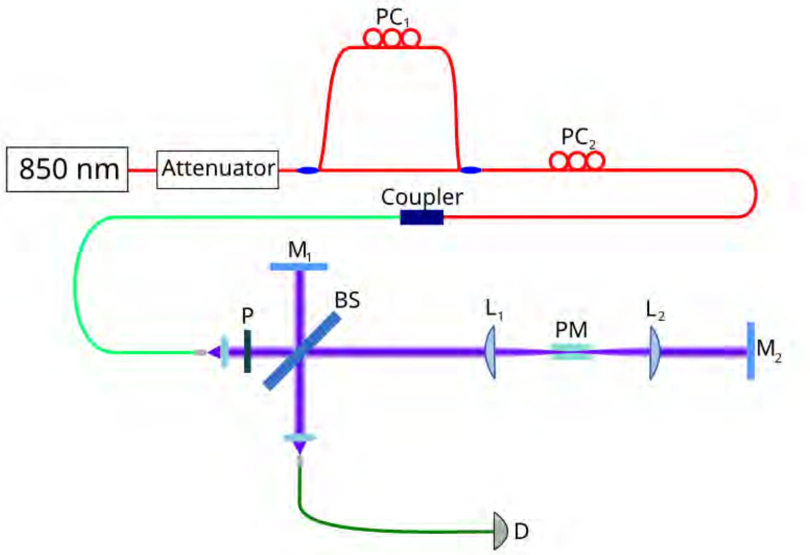


Figure 2: Experimental setup. $PC_1$, $PC_2$ - fiber polarization controllers, $P$ - polarizer, $M_1, M_2$ - flat mirrors, $L_1, L_2$ - thin lenses, $BS$ - 50/50 beam splitter, $PM$ - phase modulator, $D$ - single photon detector.

A pulse repetition rate was 2 MHz. Using the FPGA we measured the time between sending a pulse into the setup and detecting it at the output. Each time 32768 pulses had been sent we got an information about the amount of counts in each registration window, which size is 1.67 ns due to technical limitations. We measured histograms shown in Fig.3. We were able to observe changes of this histograms in real time, so we could adjust our experimental setup based on this information. Here, we investigated interference visibility using 5 different optic fibers at the input of the Michelson interferometer. Results of these experiments are presented in table1. Now our work is on the stage of implementing QKD protocol with the setup described above.

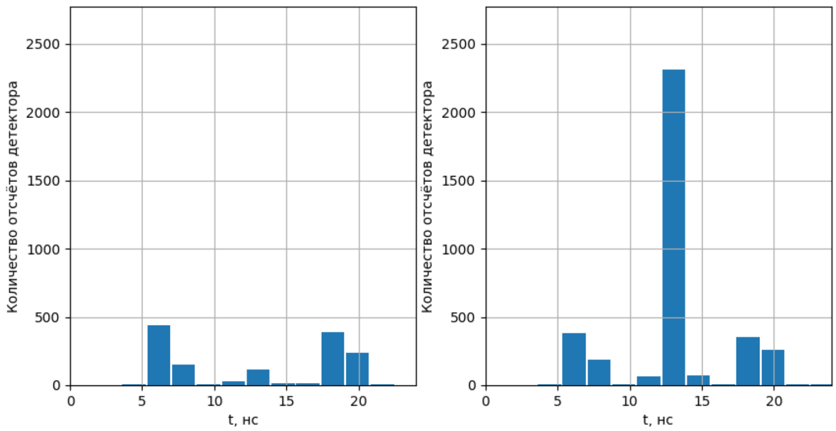


Figure 3: Amount of detector's counts in different registration gates.

Table 1: Values of interference contrast for different optic fibers at the input of free-space delay interferometer.

| Fiber type | Contrast |
|---|---|
| Single-mode 780-970 nm | 30.90 |
| Single-mode 1460-1620 nm | 20.12 |
| Multi-mode ø10 um, 0.10 NA | 20.65 |
| Multi-mode ø25 um, 0.10 NA | 15.05 |
| Multi-mode ø50 um | 15.56 |

# References

[1] C. H. Bennett and G. Brassard. Quantum cryptography: Public key distribution and coin tossing. In *Proceedings of IEEE International Conference on Computers, Systems, and Signal Processing*, page 175, India, 1984.

[2] Alberto Boaron, Gianluca Boso, Davide Rusca, Cédric Vulliez, Claire Autebert, Misael Caloz, Matthieu Perrenoud, Gaëtan Gras, Félix Bussières, Ming-Jun Li, Daniel Nolan, Anthony Martin, and Hugo Zbinden. Secure quantum key distribution over 421 km of optical fiber. *Phys. Rev. Lett.*, 121:190502, Nov 2018.

[3] Jeongwan Jin, Sascha Agne, Jean-Philippe Bourgoin, Yanbao Zhang, Norbert Lütkenhaus, and Thomas Jennewein. Demonstration of analyzers for multimode photonic time-bin qubits. *Phys. Rev. A*, 97:043847, Apr 2018.

[4] Xiao-Tian Song, Dong Wang, Xiao-Ming Lu, Da-Jun Huang, Di Jiang, Li-Xian Li, Xi Fang, Yi-Bo Zhao, and Liang-Jiang Zhou. Phase-coding quantum-key-distribution system based on sagnac–mach-zehnder interferometers. *Phys. Rev. A*, 101:032319, Mar 2020.

# Laser Damage Attack on a Simple Optical Attenuator Widely Used in Fiber-based QKD Systems

**Bugai K.E.**[1,3*], **Zyzykin A.P.**[1], **Bulavkin D.S.**[1,3], **Dvoretskiy D.A.**[1,3]

[1] *SFB Laboratory, Ltd, Moscow, 127273, Russia*
[2] *Bauman Moscow State Technical University, 2nd Baumanskaya str. 5-1, Moscow, Russia 107005*
*E-mail: kirillbugajjwork@yandex.ru

**Abstract**

We present the results of an experimental study of laser damage attack (LDA) from the CW laser power up to 5.5 W at a wavelength of 1561 at a simple type of commercially available attenuator widely used in telecommunications and fiber-based QKD systems.

## Introduction

Quantum key distribution (QKD) System provides a secure exchange of information between legitimate users, guaranteed by the laws of quantum mechanics. However, if the eavesdropper (Eve) changes the absorption of the fiber optic attenuator widely used for single-photon state preparation, then the safety of such a system will be at great risk [1]. In Alice, a fiber optical attenuator is usually the last component that interacts with laser radiation before passing through the quantum channel. However, for eavesdroppers, the attenuator is the first component, which can be attacked by high-power laser radiation.

## Experimental setup and results

The experimental setup for LDA is shown in Fig. 1. CW laser radiation with a high power up to 5.5 W at a wavelength of 1561 nm (1) is directed along with the fiber to the studied sample of the attenuator (DUT). As a result of DUT heating, the absorption of the attenuator may increase providing single-photon state corruption [1]. To monitor the change in the DUT absorption, another CW laser is installed in the experimental setup at a wavelength of 1547.315 nm (2). High power coupler of 90/10 was used both to control the 2 laser power (10%) and to transmit laser power to the DUT (90%). High power circulator was used on one hand to deliver the CW high-power radiation to the DUT and another hand to transmit 2 laser power to the detection system after the DUT. The spectral filter (set for the 2 wavelength) is installed in the detection setup to cut off the reflected radiation from the high-power CW laser. The attenuator in front of the SF was used to prevent laser damage from the reflected radiation of the high-power laser. High power optical isolator after LD2 was used to prevent laser seeding effect from high power laser [2]. The fiber fuse effect from high power radiation may occur in the DUT. A fiber spool with 100 m of SMF-28 fiber was added to the setup as protection for high-power laser.

We have studied the LDA effect on 5 same pieces of widely used commercially available attenuators with 20 dB absorption depicted in Fig. 2b. Experimental data on the attenuation deviation of DUT under high power CW radiation is shown in Fig. 2a. Obtained results show that attenuation deviation of DUT randomly changes under high power radiation and thus used 20-dB attenuators are not resistant to LDA.

As a defense against LDA, a new method based on the occurrence of fiber fuse effect in an optical fiber can be offered. Our experiments show that it is possible to protect the QKD system when high-power CW laser radiation riches only 200 mW of optical power.

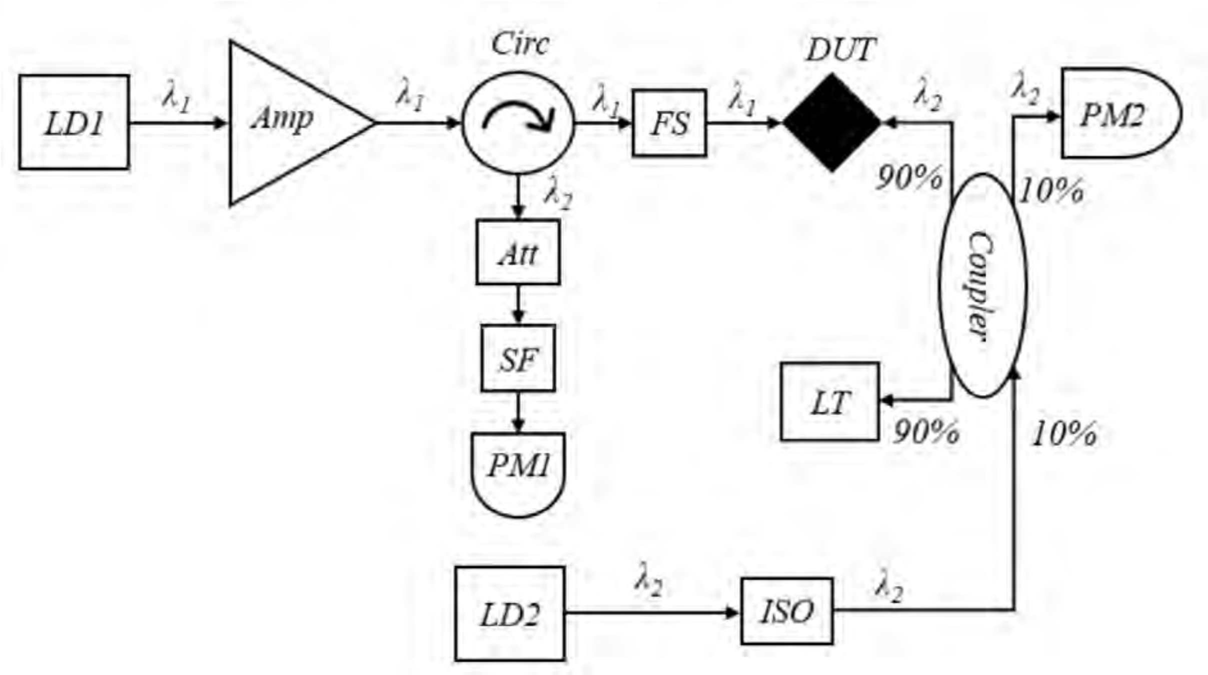


Figure 1: The experimental setup. LD1 — 1 laser diod ; Amp — er-doped fiber amplifier, Circ— fiber-optic circulator; FS — fiber spool; Coupler —90/10 fiber optical coupler; PM1, PM2 —power meters; SF — spectral filter, Att — attenuator; ISO —high-power fiber optical isolator; DUT— device under test, LD2 — 2 laser diode; LT - fiber optical light trap

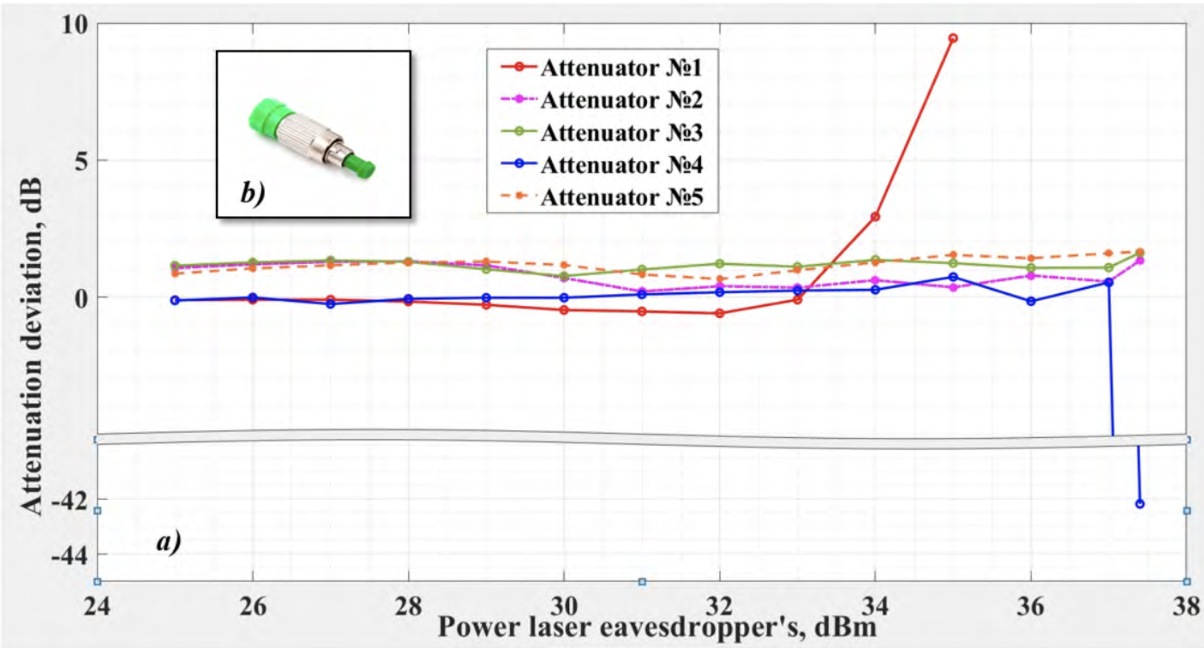


Figure 2: (a) Attenuation deviation of DUT under high-power CW radiation, (b) Image of used 20-dB attenuator

# References

[1] *Anqi Huang, Ruoping Li, et.al.,* Phys. Rev. Applied 13, 034017 (2020).

[2] *Anqi Huang, Alvaro Navarrete, et.al.,* Phys. Rev. Applied 12, 064043 (2019).

# Influence of QKD apparatus parameters on the “backflash” attack

**Sergey Bogdanov**[1,2*], **Ivan Sushchev**[1,3], **Andrey Klimov**[1]

[1] *Quantum Technology Centre of Moscow State University, Moscow, 119991, Russia*
[2] *National Research University Higher School of Economics, Moscow, 101000, Russia*
[3] *Faculty of Physics, Moscow State University, Moscow, 119991, Russia*
*E-mail: `king16061999@gmail.com`

**Abstract**

For examining QKD systems for sustainability to the “backflash” attack, it is necessary to measure the probability of photon re-emission and calculate the maximum possible information leakage. We present an experimental setup for the research of ”backflash” of a single-photon detector depending on parameters of QKD systems. The obtained experimental data demonstrate the variation of the backflash probability of the single-photon detector depending on the SPAD gate width and the mean photon number per pulse sent by Alice to Bob.

Quantum key distribution (QKD) systems provide a secure exchange of information between legitimate users, guaranteed by the laws of quantum mechanics [1]. Nevertheless, QKD systems may be vulnerable to optical attacks due to the imperfection of the equipment [2, 3]. One of the possible attacks on QKD systems using single-photon avalanche InGaAs detectors is a ”backflash attack” [4]. Since secondary photons are emitted back into the communication channel during events related to the counting of avalanche photodetectors (SPAD), Eve (the eavesdropper) can take advantage of this lack of SPAD to reveal the secret key by passively registering photons using a circulator between Alice and Bob’s communication channel, and thus obtain information about the encoded state of light.

However, in classical optical reflectometry [5], strobes are applied to the measuring detector at each probing laser pulse, which leads to significant noise during measurement. Indeed, with probing quasi-one-photon emission containing an average of 0.1 photons per pulse, the quantum efficiencies of the detectors are 10 % and the probability of re-emission is 1 %, the measuring SPAD will register 10 re-emitted photons per pulse, which is comparable to the SPAD’s dark noise.

To reduce errors associated with noise and other parasitic readings of the measuring SPAD, a time correlator must be introduced into the measurement scheme. In correlation measurements of the re-emission of a single-photon detector, the strobe is applied to the measuring SPAD only if the detector under test is triggered. This will increase the signal-to-noise ratio. The scheme of correlation measurements of the re-emission of a single-photon detector by optical reflectometry with a time correlator is shown in Figure 1.

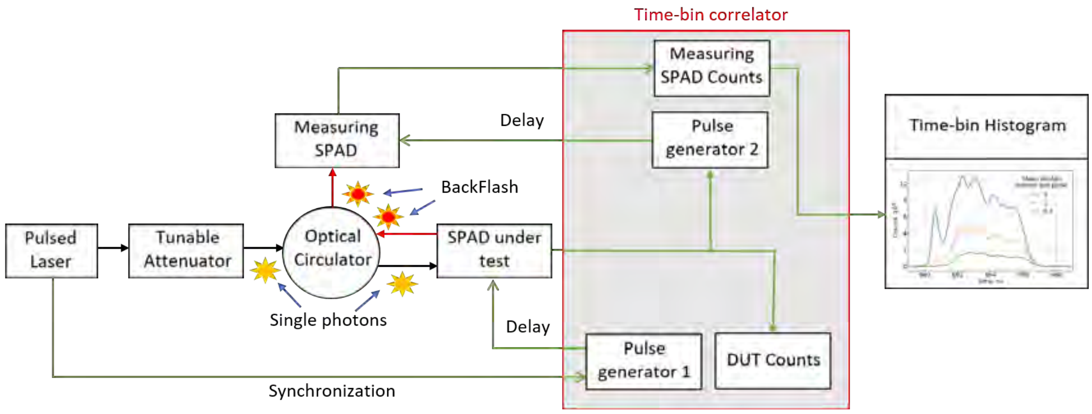


Figure 1: The scheme of correlation “backflash” measurements by optical reflectometry (Laser - pulsed laser, ATT - attenuator, Meas SPAD - measuring SPAD, DUT SPAD – SPAD under test, Time correlator for setting delays and synchronization settings)

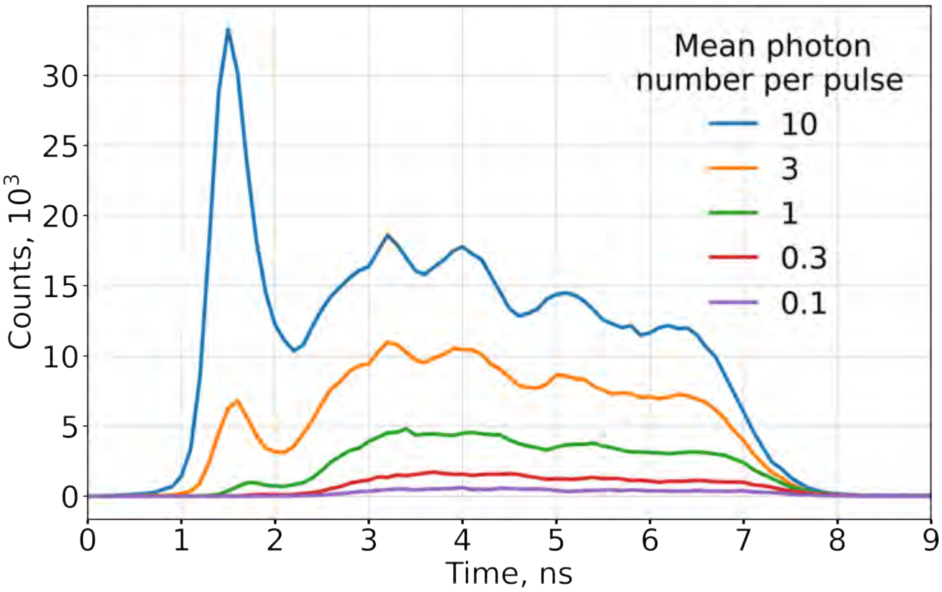


Figure 2: Histograms of “backflash” counts distribution for different mean photon number per pulse ($\mu$)

The width of the probing laser pulse was less than 150 ps. The laser pulse should be shorter than the effective strobe of the detector under test so that all emitted photons can be registered, and on the histogram, it is possible to separate the reflected photons from the re-emitted photons (”backflash”). Another advantage of the described correlation measurements is that the number of counts of the measuring detector at the peak of reflection will depend on the mean photon number per pulse (µ). With a sufficiently small µ, the contribution of reflected photons to the integral number of counts of the measuring detector can be made, however small, in the limit - zero at µ = 0, as when working only with dark counts of the test detector.

Therefore, the experimental setup makes it possible to obtain a ”backflash” picture for the detector under study demonstrated in Figure 2 with a higher signal-to-noise ratio than in the classical optical reflectometry scheme, and a couple of minutes is enough for a set of statistics. Moreover, by changing the parameters of the time delay, our experimental setup allows us to accurately investigate the dependence of the ”backflash” on the arrival of the probing pulse at the beginning, middle, or end of the SPAD gate with a step of 1 ns. Also, by changing the parameters of the SPAD, for example, the gate width of SPAD, it is possible to investigate the dependencies of the ”backflash” probabilities on the gate width of SPAD.

## References

[1] *S. N. Molotkov*, Journal of Experimental and Theoretical Physics, **114**, 168 (2014).

[2] *N. Jain, B. Stiller, I. Khan, D. Elser, C. Marquardt, G. Leuchs*, Contemporary Physics, **57(3)**, 366-387 (2016).

[3] *I. Sushchev*, Proceeding of SPIE, Emerging Imaging and Sensing Technologies for Security and Defence VI, **11868**, (2021).

[4] *C. Kurtsiefer*, Journal of Modern Optics **48(13)**, 2039-2047 (2001).

[5] *A. Meda*, Light: Science & Applications, **6**, (2017).

# Experimental security analysis of fiber-based QKD systems outside the telecom spectral region

**Ivan Sushchev**[1,2*], **Bogdanov S.A**[2,3], **Andrey Klimov**[2]

[1] *Faculty of Physics, Moscow State University, Moscow, 119991, Russia*
[2] *Quantum Technology Centre of Moscow State University, Moscow, 119991, Russia*
[3] *National Research University Higher School of Economics, Moscow, 101000, Russia*
*E-mail: `sushchev.is16@physics.msu.ru`

**Abstract**

We present an experimental setup for spectral transmission measurements of fiber-optical components in visible and near infrared spectral range. The dynamic range of measurements reaches 120 dB with the wavelength resolution down to 1 nm.

Modern commercial quantum key distribution (QKD) systems are usually equipped with a number of fiber-optical elements aimed to decrease the power of light propagating in one or two directions in various spectral ranges to prevent such well-known attacks as the Trojan-horse attack or the Backflash attack. Spectral transmission measurements of optical elements in telecom spectral range (1200 – 1700 nm) are available by means of conventional spectrometry setups [1, 2]. Previously, we have shown that full security analysis is only reachable using photon-counting method [3]. Here we demonstrate that photon-counting method is applicable outside the telecom spectral range.

The experimental setup for spectral transmission measurements is shown in Fig.1. The supercontinuum laser covering visible and infrared spectral region up to 2000 nm is used as the source of optical pulses. Tunable acousto-optics filter sets the wavelength selected on the connected computer. The filter contains a free-space-to-fiber coupler with the FC/APC output and the SMF-28 patch cords are used as the interlink between next elements. However, the single-mode regime is limited by the cutoff wavelength, which is equal to 1260 nm. It means that operating in visible region is accompained by additional losses on optical connections and bend instability, which dictates the strict requirements on the setup alignment and disturbence minimization.

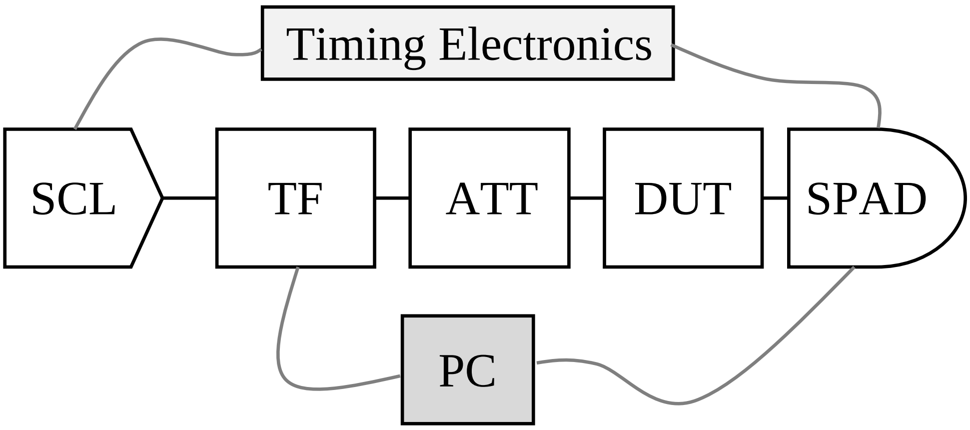


Figure 1: Measurement setup (SCL – supercontinuum laser, TF – tunable filter, ATT – variable attenuator, DUT – device under test, SPAD – single-photon avalanche diode, PC – personal computer)

The photon-counting mode is provided by the set of optical attenuators, which decrease the radiation power to less than single photon per pulse on the detection side. Variable attenuators are usually calibrated on paticular wavelengths and their attenuation outside the calibrated region is unpredictable. Considering this and that the overall setup transmittance is likely to drop significantly in visible region, it is convinient to exploit a set of low-loss constant attenuators with pre-measured on classical spectrum analyzer transmission spectra. The radiation passes through the device under test, which may be an fiber-optical isolator, circulator, attenuator, band-pass filter, wavelength-division multiplexer, etc. The detection is carried out by the single-photon avalanche diode (SPAD), running in Geiger mode, being syncronized with the laser by the timing electronics. Both Si an InGaAs SPADs are used depending on the spectral region of measurements (visible or infrared). Note that InGaAs diodes provide valid measurements even after 1800 nm, where their quantum effieciency drop significantly but remains non-zero, however, the dynamic range of measurements in this region decreases in severeal orders.

Thus, our setup allows to provide spectral transmission data outside the telecom spectral region and make it possible to carry out the security analysis of both red-shifted and blue-shifted Trojan-horse attack or Backflash attack on a fiber-based QKD system.

## References

[1] *N. Jain, B. Stiller, I. Khan, V. Makarov, C. Marquardt and G. Leuchs*, IEEE Journal of Selected Topics in Quantum Electronics, **21**, 168 (2014).

[2] *A. Borisova, B. Garmaev, I. Bobrov, S. Negodyaev and I. Sinil'shchikov*, Optics and Spectroscopy **128**, 1892 (2020).

[3] *I. Sushchev, et al*, Emerging Imaging and Sensing Technologies for Security and Defence VI **11868**, 57-63 (2021).

# Raman cooling in attenuators doped with optically active impurities

V.G. Krishtop[1,2*], V.G. Popov[1], K.E. Bugay[3], D.A. Dvoretskiy[3]

[1] *Centre of Perspective Development and Scientific Research, JSC Infotecs, Moscow, Russia.*
[2] *Instutute of Microelectronics Technology of RAS, Chernogolovka, Russia.*
[3] *JSC SFB Laboratory, Moscow, Russia*
*E-mail: `Vladimir.Krishtop@infotecs.ru`

**Abstract**

The report discusses the prospects of using phosphorus-doped optical fiber in devices such as optical radiation attenuators with a submicron gap. The propagation of light in such a fiber is characterized by strong Raman scattering by P-O molecular vibrations. These oscillations are weakly related to the surrounding $SiO_2$ matrix, which makes it possible to efficiently redirect optical power without absorption, accompanied by heating. This property allows you to create attenuators resistant to powerful optical radiation.

## Introduction

The development of integrated waveguide optics and its miniaturization set new challenges for physics, microelectronics, and materials science. Microelectronic technology implementation into optics systems leads to a size decrease of optical elements on a chip and an increase in the density of elements. The task is to increase the efficiency of heat distribution in optical chips, and this task is very urgent in integrated optics.

Heat dissipation problem is a critical in quantum key distribution (QKD) systems. Attenuators with a large attenuation of tens of decibels are used in QKD systems to provide a quasi-single-photon mode [1, 2]. The attenuators are strongly heated under the powerful laser radiation. Due to heating, the attenuation coefficient changes and leads to a violation of the single-photon regime.

It is shown in Ref. [3], using the example of spliced fiber attenuators, that external laser action can lead to a violation of the single-photon regime in QKD systems. The pulses become multiphoton, which makes the QKD protocol vulnerable to a photon splitting attack.

With the progress of optical systems on a chip, miniaturization of elements is accompanied by a heat dissipation deterioration and worsening heat problems. The classical thermal conductivity of materials becomes insufficient for effective heat dissipation. The challenge is to develop smart materials that can dissipate heat through more efficient physical processes.

## Discussion

Heating is caused by the dissipated optical power, which can transfer energy to vibrations of atoms, for example, through Raman scattering of light (RSL). There are optically active vibrations, for example, molecular vibrations of Si-O, which absorb the power of optical radiation and transfer it to acoustic phonons, with which they interact well. As a result, the RSL spectrum for such vibrations broadens.

A feature of phosphorus-doped $SiO_2$ is strong RSL. In the presence of phosphorus impurity in $SiO_2$, optically active P-O vibrations weakly interact with the $SiO_2$ lattice, which demonstrates a sharp peak in the RSL spectrum (see Fig. ). Optically active P-O vibrations can effectively redistribute energy in a material, reducing its conversion to heat. Although the intensity of spontaneous RSL is rather low, it should be taken into account that high intensity of optical radiation leads to stimulated scattering. The intensity of stimulated RSL increases by several orders of magnitude and can become comparable to the pump intensity.

Moreover, RSL can occur both in the Stokes regime and in the anti-Stokes one. Anti-Stokes RSL is associated with an increase in the photon energy due to the absorption of energy from the phonon subsystem. Anti-Stokes RSL can effectively cool the attenuator. Thus, scattering by dopants molecules can significantly change the energy redistribution in optical elements, ensure efficient energy transfer, and reduce local heating. For the case of planar waveguides made with an epitaxial crystal lattice,

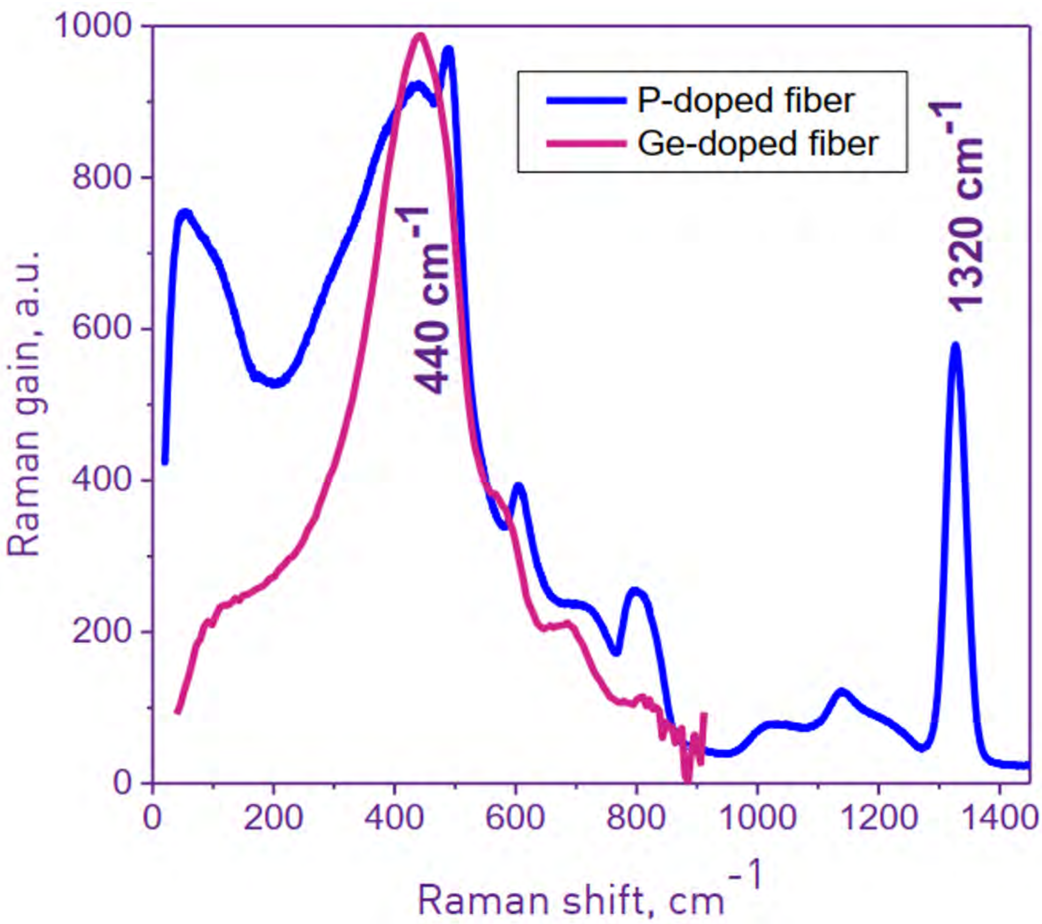


Figure 1: The RSL spectra in a doped fiber with phosphorus and germanium impurities. The maximum at 400 cm$^{-1}$ corresponds to scattering by Si-O vibrations. The maximum at 1320 cm$^{-1}$ corresponds to P-O vibrations.

this effect is described in terms of selective pumping of the optical phonon subsystem. The dissipated optical power causes local heating due to the energy transfer to acoustic phonons via interaction with LO-phonons appeared in RSL. Selective pumping of a phonon system by LO-phonons leads to efficient energy extraction from the region with a high optical density. We study attenuators based on phosphorus-doped $SiO_2$, in which the role of RSL by molecular P-O vibrations is essential. Preliminary measurements of spliced fiber attenuators demonstrated that attenuators with high attenuation based on standard fiber are susceptible to damage at a radiation power of 2.5 W. The attenuation coefficient is reduced by 20-25dB. This effect was confirmed in Ref. [3]. Next, we used a phosphorus-doped fiber, and the power threshold has increased to 3.6 W. This is evidence of efficient energy transfer by impurity vibrations.

## References

[1] *E. Diamanti, H.-K. Lo, B. Qi, and Z. Yuan*, "Practical challenges in quantum key distribution," npj Quantum Information, **2**, 1, (2016).

[2] *E. Diamanti and A. Leverrier*, "Distributing secret keys with quantum continuous variables: principle, security and implementations," Entropy, **17**, 6072, (2015).

[3] *A. Huang, R. Li, V. Egorov, S. Tchouragoulov, K. Kumar and V. Makarov*, "Laser-Damage Attack Against Optical Attenuators in Quantum Key Distribution" Phys. Rev. Appl., 034017, (2020).

# Study of the Vulnerability of Neutral Optical Filters Used in Quantum Key Distribution Systems against Laser Damage Attack

**Sergei Alferov**[1*], **Kirill Bugai**[2], **Ivan Pargachev**[1]

[1] *JSC "InfoTeCS",Moscow, Russia*
[2] *SFB Laboratory, Moscow, Russia*
*E-mail: `Sergey.Alferov@infotecs.ru`

**Abstract**

Quantum key distribution systems are accessible to an eavesdropper; i.e., the eavesdropper can attack not only quantum states but also the equipment. In the former case, vulnerabilities are removed by fundamental constraints (e.g., no-cloning theorem) or theoretical foundations for their removal exist. In the latter case, vulnerability is determined by the practical implementation of equipment. An attack with laser damage of optical components called laser damage attack can allow the eavesdropper to reduce the attenuation of optical elements and compromise distributed keys. In this work, a method based on neutral optical filters has been described for protection from laser damage attack against optical components. A scheme imitating actions of the eavesdropper in the process of laser damage attack has been presented. An approach has been proposed to calculate the parameters of optical elements after the attack. Processes occurring in samples exposed to intense laser radiation have been analyzed.

## Introduction

The security of quantum key distribution (QKD) is traditionally associated with fundamental laws of quantum mechanics. However, practical implementations usually have imperfections, resulting in vulnerability. Such vulnerabilities are described in a number of works [1, 2, 3]. Optical pulses attenuated to a quasi-single-photon level by an optical attenuator of various configurations are often used in quantum key distribution systems. In particular, as shown in [4] , some types of attenuators are invulnerable to laser damage attack (LDA) with limited duration and power of laser action.

In our previous work it has been shown [5] that a neutral optical filter with bilateral coating of metal-dielectric layers serving as an attenuator is vulnerable to LDA at a power above 34 dBm. Here we present a device based on bulk-colored neutral optical filters which have uniform absorption throughout the volume.

## Experimental setup and testing method

The optical attenuator (DUT) was tested through the scheme shown in Fig. 1.

**The main characteristics of the scheme**:

- Power of ALAS (1544 nm) 18 dBm;
- Power of ELAS (1561 nm) 25 $\div$ 37.4 dBm, 1 dB step;
- Coupler: 10 % - DET1, 90 % - DUT;
- Filter suppression of attack radiation $>$ 50 dB;
- Acquisition time / time step: 60 sec. / 10 ms

**The main characteristics of the DUT**:

- Type of glass: SZS-16 (analog is KG3 Schott);
- Optical density (OD): 2.0 (2 qty.) and 3.0 (1 qty.);
- Dimensions: 12 mm. diam., 1.25 (OD=2.0) and 2 mm. thickness;
- Holder: system of two collimating lenses with $NA = 0.13$

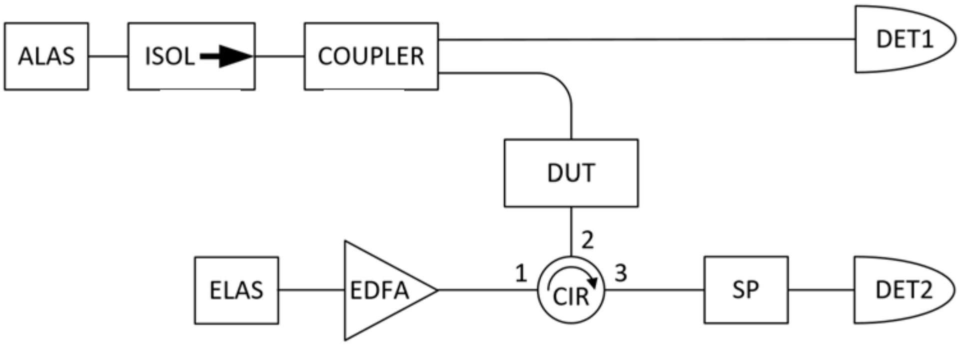


Figure 1: Layout of the measurement
(ALAS) control laser, (ISOL) high-power isolator, (COUPLER) 90/10 beam splitter, (DET1) power meter no. 1 for detection of control laser radiation, (DUT) device under test, (ELAS) attack laser, (EDFA) amplifier of laser radiation, (CIR) circulator with terminals marked by digits, (SP) optical filter, (DET2) power meter no. 2 for detection of control laser radiation passed through the DUT.

**Stages of measurement:**

- the measurement of the initial attenuation $A_0$ of light by the DUT before its exposure to intense radiation;
- the estimate of the noise component induced by the reflection and scattering of attack radiation;
- the calculation of change in the attenuation of light by the DUT exposed to intense radiation.

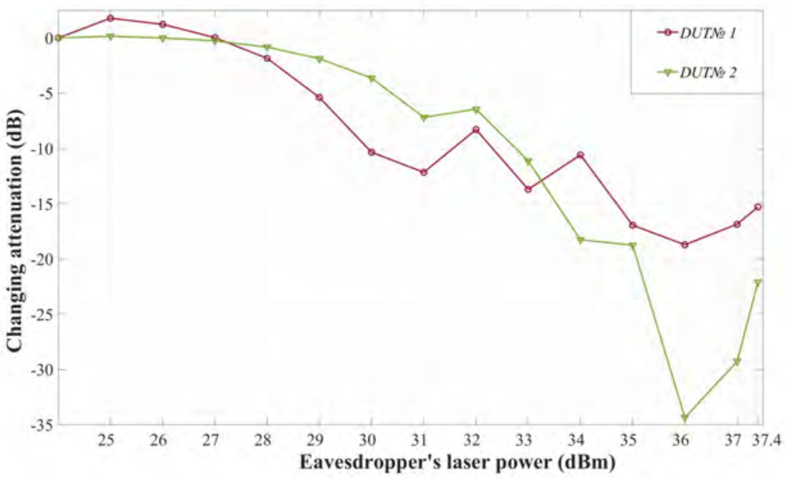


Figure 2: Change in the attenuation of optical filter nos. 1 and 2 with respect to the initial value

The attenuation was calculated by the formula (dB):

$$A = P_1 + K_c - P_2 - A_s \tag{1}$$

$K_c$ is the coupling ratio of the beam splitter (dB), $A_s$ is the losses in the path between the output of the beam splitter and DET2 in the absence of the sample (dB), $P_1$ - readout from DET1, $P_2$ - readout from DET2. Change in the attenuation for each sample was obtained as difference $A_0 - A$. Figure 2 shows a decrease in the attenuation (positive values) in the power range of $25 \div 27$ dBm of optical filter nos. 1 and 2 with respect to the initial value. Figure 3 doesn't reveal a decrease in the attenuation of optical filter no. 3 in the entire range of the power of attack radiation. Figure 4 shows a circular crater with a diameter of about 900 $\mu$m induced by LDA and the formed crack is observed in Fig.5.

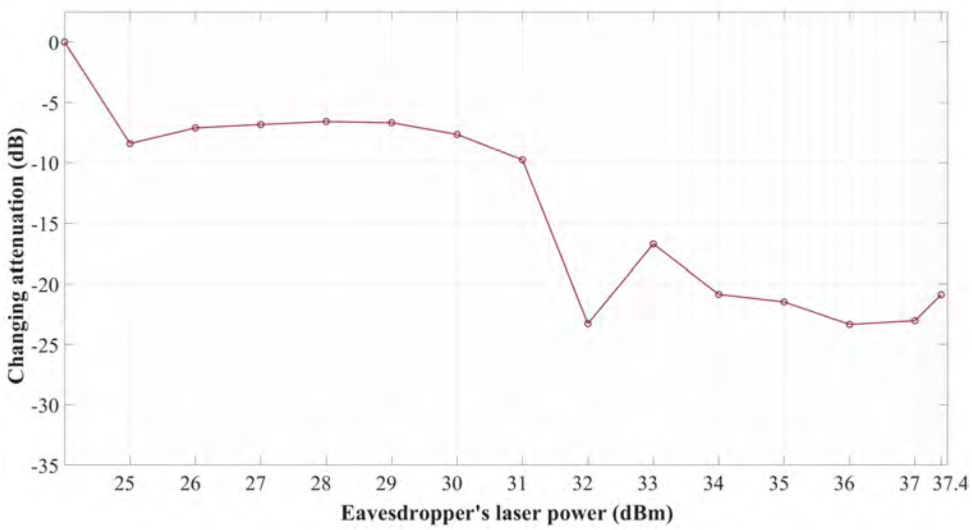


Figure 3: Change in the attenuation of optical filter no. 3 with respect to the initial value

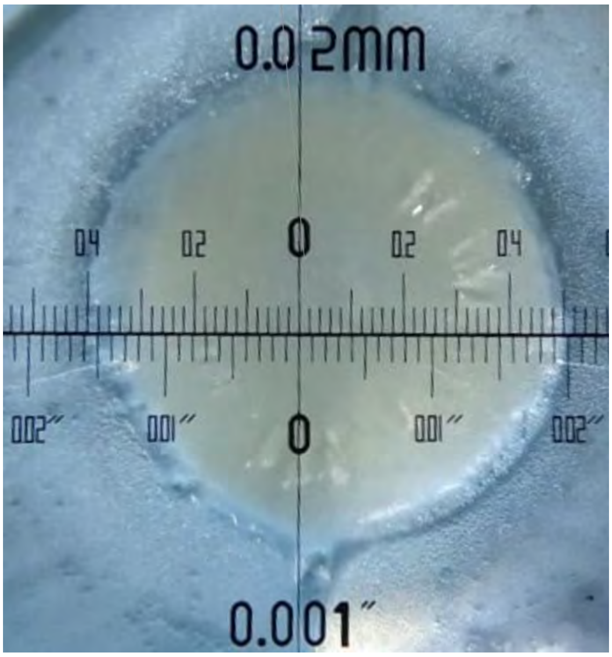


Figure 4: Magnified view of the crater

## Discussion

The decrease in attenuation of 1.25-mm-thick filters can be explained in the following way. Losses in the system of two collimating lenses without a filter are about 1.5 dB. At low powers of 25 ÷ 27 dBm, see Fig. 2, heating induces the thermo-optic effect leading to the formation of a thermal lens [6], which changes the trajectory of radiation inside the DUT. As a result, losses in the equipment decrease, which is interpreted as a decrease in the attenuation.The following measures can be used to increase resistance against LDA. First, heat removal from the surface of optical filters should be increased by means of active or passive cooling. The second measure is an increase in the area of action on the optical filter. This can be reached by increasing either the numerical aperture of collimators or the distance between the input collimator and optical filter. The third way is the choice of optical filters more resistant to laser irradiation. Fourth, devices with minimum losses should be used to reduce intrinsic losses of equipment.

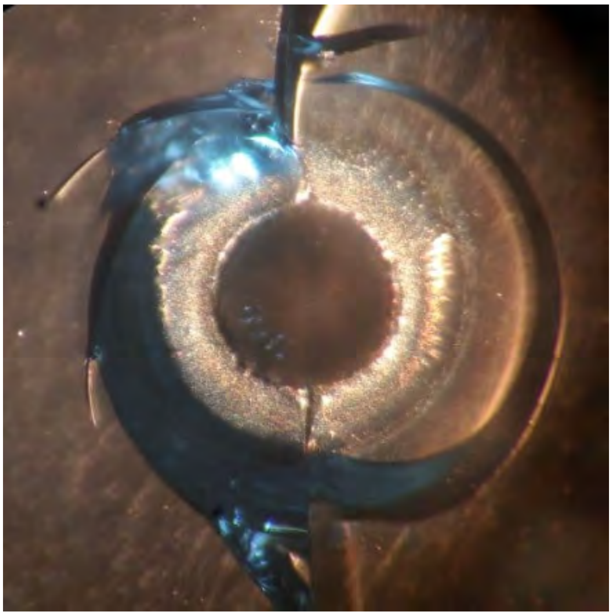

Figure 5: Crack around the crater

## Conclusion

The performed experiments have shown that bulk-colored neutral optical filters are vulnerable to laser damage attack against optical elements in the power range of $25 \div 27$ dBm because a decrease in attenuation is observed in this range. A further increase in the power of attack radiation leads to an increase in the attenuation of optical filters. It has been shown that intense laser radiation results in the irreversible degradation of an optical filter, which is, in our opinion, responsible for an increase in the attenuation of optical filters. It is noteworthy that the described attack is the simplest to implementation because there are much finer and nearly undetectable methods to irreversibly damage optical components of the apparatus part of quantum key distribution.

# References

[1] *A. Lamas-Linares and C. Kurtsiefer*, Breaking a quantum key distribution system through a timing side channel. Opt.Express **15**, 9388 (2007).

[2] *Shihan Sajeed, Igor Radchenko, Sarah Kaiser, Jean-Philippe Bourgoin, Anna Pappa, Laurent Monat, Matthieu Legré, and Vadim Makarov*, Attacks exploiting deviation of mean photon number in quantum key distribution and coin tossing. Phys. Rev. A. **91**, 032326 (2015).

[3] *F. Xu, B. Qi, and H.-K. Lo*, Experimental demonstration of phase-remapping attack in a practical quantum key distribution system. New J. Phys. **12**, 113026 (2010).

[4] *A. Huang, R. Li, V. Egorov, S. Tchouragoulov, K. Kumar and V. Makarov*, Laser-Damage Attack Against Optical Attenuators in Quantum Key Distribution. Phys. Rev. Appl. **13**, 034017 (2020).

[5] *S. Alferov, K. Bugai, I. Pargachev*, 4th International School on Quantum Technologies, Poster Session No. 16. http://qutes.org/wp-content/ uploads/2021/11/Poster_session.pdf. (2021).

[6] *Penano et al.*, Optical quality of high-power laser beams in lenses. J. Opt. Soc. Am. B. **26**, 3 (2009).

# Localization microscopy of single photon emitters in locally strained monolayer semiconductor

**Artem Abramov**[1*], **Igor Chestnov**[1],
**Ivan Iorsh**[1] , **Vasily Kravtsov**[1]

[1]*School of Physics and Engineering, ITMO University, Russia*
*E-mail: artem.abramov@metalab.ifmo.ru

**Abstract**

Integration of single photon emitters with nanophotonic structures on a chip is key for the development of future quantum optoelectronic devices. Here we study the formation of single photon emitters in a $WSe_2$ monolayer by local nanoindentation with an atomic force microscope probe. Using the bichromatic photoluminescence-imaging approach, we define the spatial locations of single photon emitters with deep sub-wavelength accuracy. From atomic force microscopy profiles, we calculate strain field maps in the nanoindented regions of the $WSe_2$ monolayer and extract local strain parameters at the experimentally determined emitter locations.

Single photon emitters (SPEs) are important elements for applications in quantum communication and computing devices [1]. One of the promising platforms for creating single photon emitters is provided by two-dimensional transition metal dichalcogenides (TMDs) [2]. Deformation of a two-dimensional material, for example, by the probe of an atomic force microscope (AFM), can lead to the formation of SPEs in TMD monolayers [3, 4]. The practical advantage of this approach is the possibility of forming arrays of emitters in specified locations on the chip due to the precise positioning of the AFM probe and the integration of emitters with nanophotonic structures on the chip. However, the integration accuracy is limited by the size of the nanoindent.

In this work, we investigate the formation process of SPEs in a $WSe_2$ monolayer by local deformation with an AFM probe. To this end, we detect photoluminescence (PL) signal and determine the position of each emitter within the nanoindented region on a deep sub-wavelength scale using the bichromatic photoluminescence-imaging (PL-imaging) approach [5, 6]. Our experimental sample is $SiO_2$(1 µm)/Si substrate with silver alignment marks on the surface, covered with a thin layer of PMMA polymer. $WSe_2$ monolayer is transferred to the polymer. The array of single photon emitters is fabricated in the $WSe_2$ monolayer by the method of local deformation by the AFM probe (Fig. 1a). SPEs with wavelength greater than 750 nm are selected spectrally and by polarization (Fig. 1b). We verify the single-photon character of the fabricated emitters via second order correlation function measurements, and we have the best achieved value $g^{(2)}(0) = 0.019 \pm 0.003$.

The bichromatic PL-imaging approach consists in simultaneous illumination of the sample with 632.8 nm HeNe laser to excite the photoluminescence of the SPE and with light with a longer wavelength to illuminate the alignment marks. Reflected light and PL of SPE are imaged on the CMOS camera (Fig. 1c). The alignment marks are also visible on the AFM map due to the swelling of the PMMA above them (Fig. 1d). The coordinates of the centers of the alignment marks and the emitters were obtained from orthogonal linear scans of the AFM map and the optical image using Gaussian function fitting (Fig. 1e). The exact position of the SPE is defined by converting the coordinates of the alignment marks and the SPE from the optical image to the AFM map of the structure. On average, the uncertainty of the SPE position obtained from a series of images was less than 60 nm. We then superimpose the SPE positions with the map of strain fields, which was calculated from the AFM profiles (Fig. 1f). The parameters of local deformation obtained via this procudure will help better understand the process of formation of single photon sources in a two-dimensional semiconductor at the microscopic level.

The results of our research work are important for the practical application of the local deformation method in the creation of single photon generators for quantum communication and computing devices.

This work was funded by the Russian Science Foundation under grants №21-72-10100.

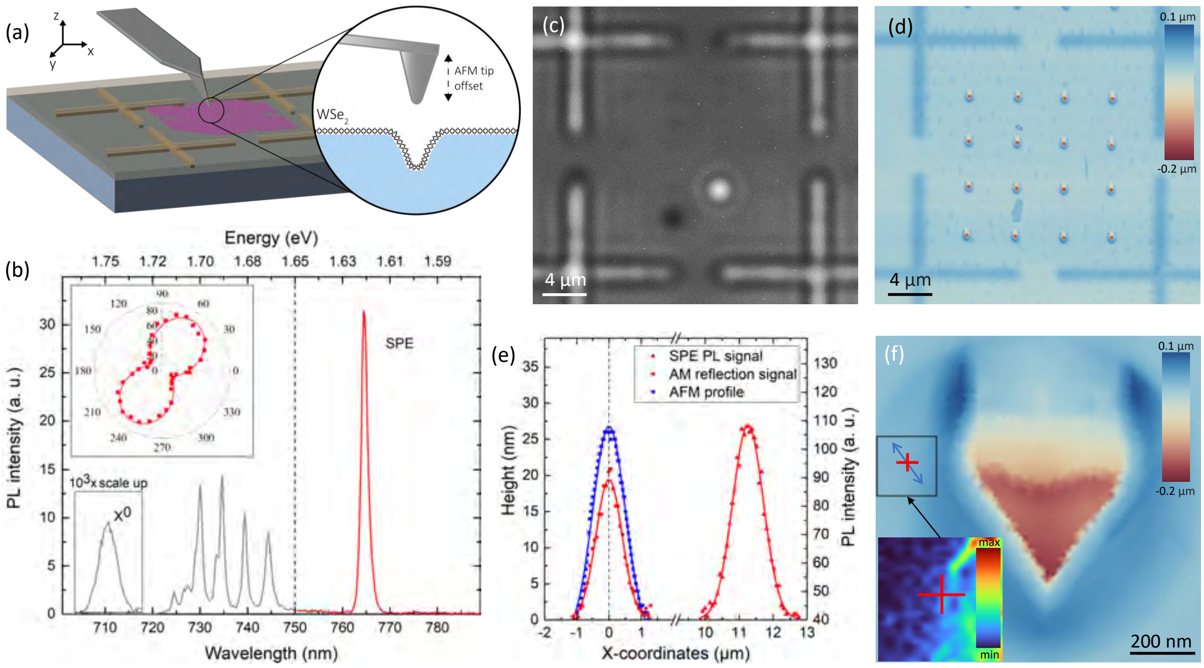


Figure 1: (a) Schematic of SPE fabrication process in $WSe_2$ monolayer by the AFM probe on the sample with alignment marks. (b) The photoluminescence spectrum one of the SPE in $WSe_2$ monolayer formed on a nanoindet (the wavelength of the emitter radiation is 764 nm). The filtration of 750 nm LPF is schematically shown. The spectrum of neutral exciton $X^0$ of $WSe_2$ monolayer is shown in the down inset. The polarization dependence is shown in the upper inset. (c) Optical image of the photoluminescence from a single SPE and reflected light by the alignment marks. (d) AFM scan of a sample with an array of nanoindents in a $WSe_2$ monolayer and alignment marks (coincides with Fig. 1c). (e) Orthogonal line cuts ($x$-axis) of the photoluminescence image, showing the profile of the SPE emission (red triangle symbols) and of the image of the alignment mark (red square symbols) and their Gaussian fits (red lines). Orthogonal line cut of the AFM scan, showing the profile of the alignment mark (blue square symbols) and its Gaussian fit (blue line). (f) The exact position of the SPE near the indent (the size of the cross shows uncertainty). The blue arrow shows the polarization of the SPE. The inset shows the position of the SPE on the strain map.

## References

[1] Aharonovich, I., Englund, D. & Toth, M. Solid-state single-photon emitters. *Nature Photonics* **10**, 631–641 (2016).

[2] Koperski, M. *et al.* Single photon emitters in exfoliated wse2 structures. *Nature nanotechnology* **10**, 503–506 (2015).

[3] Rosenberger, M. R. *et al.* Quantum calligraphy: writing single-photon emitters in a two-dimensional materials platform. *ACS nano* **13**, 904–912 (2019).

[4] Li, X. *et al.* Proximity induced chiral quantum light generation in strain-engineered wse2/nips3 heterostructures. *arXiv preprint arXiv:2203.00797* (2022).

[5] Thompson, R. E., Larson, D. R. & Webb, W. W. Precise nanometer localization analysis for individual fluorescent probes. *Biophysical journal* **82**, 2775–2783 (2002).

[6] Sapienza, L., Davanço, M., Badolato, A. & Srinivasan, K. Nanoscale optical positioning of single quantum dots for bright and pure single-photon emission. *Nature communications* **6**, 1–8 (2015).

# Radial Index Operator of Laguerre-Gaussian Modes and Zernike Modes

**D.D. Reshetnikov**[1*], **A.S. Losev**[1]

[1] *7/9 Universitetskaya nab., St. Petersburg, 199034 Russia*
*E-mail: d.d.reshetnikov@gmail.com

**Abstract**

We present an analysis of the operator of the radial index of Laguerre-Gaussian modes, show the relationship of the radial index with the total number of rotating quasiparticles. The connection of the probability density distribution in the transverse plane with the Zernike polynomials is also shown.

## Laguerre-Gaussian modes

Laguerre-Gaussian (LG) beam (1) is a solution of wave equation in paraxial approximation

$$LG_{p,l}(r_z,\varphi,z) = \frac{N_{p,l}}{w_z}\; r_z^{|l|}\; e^{(iz-1)r_z^2/2}\; L_p^{|l|}(r_z^2)\; e^{-i\varphi_{p,l}(z)}\; e^{il\varphi}, \tag{1}$$

where

$$N_{p,l} = \left(\frac{2p!}{\pi(p+|l|!)}\right)^{1/2} - \text{normalization constant}, \tag{2}$$

$$w_z^2 = 2(z^2+z_R^2)/(kz_R) - \text{beam width}, \tag{3}$$

$$z_R = \frac{1}{2}kw_0^2 - \text{Rayleigh length}, \tag{4}$$

$$\varphi_{p,l}(z) = (2p+|l|+1)\arctan z/z_R - \text{Gouy phase}, \tag{5}$$

$$k \equiv k_z \in \mathcal{R} - \text{wavenumber}, \tag{6}$$

and we made renaming and substitution:

$$z/z_R \to z, \tag{7}$$

$$r_z \equiv \sqrt{2}\,\rho/w_z \tag{8}$$

It is also important to mention two indexes: azimuthal index $l$ and radial $p$. The azimuthal index shows us the number of phase incursions with a rotation of $2\pi$ of the beam propagating along the $z$ axis. The radial index is responsible for the number of dark and light rings in the probability density distribution of the field in the transverse plane.

## Radial index operator

The azimuthal index $l$ is eigenvalue of orbital angular momentum operator $\hat{\ell}_z = -i\partial/\partial\varphi$ with LG modes as eigenfunctions:

$$\hat{\ell}_z LG_{p,l}(r_z,\varphi,z) = l\cdot LG_{p,l}(r_z,\varphi,z) \tag{9}$$

We can also write operator [1] with radial indexes $p$ as eigenvalues and LG modes as eigenfunctions:

$$\hat{\mathcal{P}}_z LG_{p,l}(r_z,\varphi,z) = p\cdot LG_{p,l}(r_z,\varphi,z), \tag{10}$$

where

$$2\,\hat{\mathcal{P}}_z = \hat{n} - |\hat{\ell}_z| + \frac{1}{2}z^2\,\hat{p}_\perp^2 - z\,\hat{p}_\rho \tag{11}$$

and $\hat{n}$ — quasiparticles number operator, $\hat{p}_\perp$ — orthogonal quadrature operator, $\hat{p}_\rho$ — radial quadrature operator. The last two terms are related to the diffraction broadening of the beam traveling along the z axis. Also, we can rewrite this equation and show, that the first two terms have a physical meaning of the number of rotating quasiparticles in the transverse plane of the beam.

Using two rotating bosonic operators [2]

$$\hat{a}_{\pm} = \frac{1}{\sqrt{2}}(\hat{a}_x \mp \hat{a}_y), \tag{12}$$

where

$$\hat{a}_{x,y} = \frac{1}{\sqrt{2}}\left(\hat{q}_{x,y} - i\,\hat{p}_{x,y}\right) \quad \text{– canonical field annihilation operator,} \tag{13}$$

with $\hat{q}_{x,y}$, $\hat{p}_{x,y}$ – corresponding quadrature operators, we can write such relations:

$$\hat{n} = \hat{n}_+ + \hat{n}_-, \tag{14}$$

$$\hat{\ell}_z = \hat{n}_+ - \hat{n}_-, \tag{15}$$

where

$$\hat{n}_{\pm} = \hat{a}^{\dagger}_{\pm}\,\hat{a}_{\pm} \quad \text{– rotating quasiparticles number operator.} \tag{16}$$

Finally, if we choose $z = 0$, we can write

$$\hat{\mathcal{P}}_{z=0} = \frac{1}{2}(\hat{n} - \hat{l}) = \begin{cases} \hat{n}_-, & l > 0 \\ \hat{n}_+, & l < 0 \\ \hat{n}_+ + \hat{n}_-, & l = 0 \end{cases} \tag{17}$$

## Zernike polynomials

Zernike polynomials can be expressed as

$$Z_n^l(r,\phi) = R_n^l(r)\cos(l\phi) \text{ for } l >= 0 \tag{18}$$

and

$$Z_n^{-l}(r,\phi) = R_n^l(r)\sin(l\phi) \text{ for } l < 0, \tag{19}$$

where $2p = n - l$, $p \in \mathbb{Z}$ and

$$R_n^l(r) = \sum_{k=0}^{p} \frac{(-1)^k (n-k)!}{k!(\frac{1}{2}(n+l)-k)!(\frac{1}{2}(n-l)-k)!} r^{n-2k}. \tag{20}$$

We show the relationship of Zernike polynomias parameters $p, n, l$ with eigenvalues of operators $\hat{\mathcal{P}}_z$, $\hat{n}$, $\hat{\ell}_z$.

# References

[1] *Plick W.N., Krenn M*, Physical meaning of the radial index of Laguerre-Gauss beams. Phys. Rev. A. **92**, 063841.

[2] *E. Karimi, R. W. Boyd, P. de la Hoz, H. de Guise, J. Řeháček, Z. Hradil, A. Aiello, G. Leuchs, and L. L. Sánchez-Soto*, Radial quantum number of Laguerre-Gauss modes. Phys. Rev. A **89**, 063813

# Impact of finite squeezing of non-Gaussian resource state on Schrödinger cat states prepared by a measurement-based logical gate and applicability of monotones

Baeva A.V.*, Sokolov I.V.

*St Petersburg State University, 7/9 Universitetskaya nab., 199034, St. Petersburg, 199034 Russia*
*E-mail: alexandrabaeva@mail.ru

**Abstract**

One of the possible resources for a logical gate based on quantum entanglement and projective measurement, which allows one to generate Schrödinger cat-like states as two "copies" of the target state on the phase plane [N.I. Masalaeva, I.V. Sokolov, Phys. Lett. A **424**, 127846 (2022)] is a cubic phase state. In our work, we present the exact solution for the logical gate output state obtained for a case of a finite squeezed resource state. We show how finite squeezing affects the probability of obtaining Schrödinger's cat states and their fidelity. Since the overall efficiency of the conditional scheme should consider the probability of success, we argue that measures of non-Gaussianity of the resource state, such as Wigner negativity and non-Gaussianity, may not be directly applicable to assess the efficiency of non-Gaussian gates, which are based on quantum entanglement and subsequent projective measurement.

The problem of generating Schrödinger cat-like states in quantum optics is a hot topic, since such states may potentially be applied to quantum computing. For instance, they can be used for implementation error-resistant transformations of quantum information [1]. Several schemes for generating cat-like states in the microwave region [2], using strong light fields [3] and with a photon-number states as a resource [4] have already been proposed. An important role here is played by the nonlinearity in the scheme.

In our work, we consider a logical gate based on quantum entanglement and projective homodyne measurement [5, 6], for which the simplest non-Gaussian resource can be a cubic phase state generated by cubic nonlinearity [7]. The key feature of such a gate is that the result of the ancillary oscillator measurement provides multivalued information about the canonical variables of the output state.

Up to now, we have considered an "ideal" non-Gaussian resource state, which in the semiclassical approximation we have interpreted as an infinitely thin parabola on the phase plane. Here, we extend this approach and take into consideration that the squeezing of the vacuum state used to prepare the auxiliary state is finite. On the phase plane, the resource state has a finite size, as shown in Fig. 1.

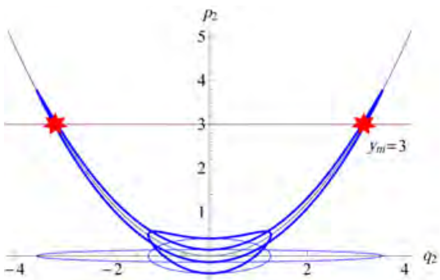


Figure 1: A visual representation of the ancillary oscillator support region on the phase plane before and after the cubic deformation with $\gamma = 0.1$ for the initial squeezing of 5 and 14 dB respectively.

We present the exact solution for the state at the output of the logical gate. We show how the squeezing parameter affects the probability of obtaining states Schrödinger's cat-like and their fidelity (Fig. 2). It is easy to see that an increase in squeezing will not lead to an increase in fidelity starting from some threshold. At the same time the squeezing significantly affects the probability of the expected measurement result (see Fig. 2a). With a small squeeze parameter, the quasicubic resource state has a low probability density close to $p_2 = y_m$. As the squeezing increases, the support region of the resource state stretches along the momentum axis, and the probability of the expected result first increases and then becomes smaller.

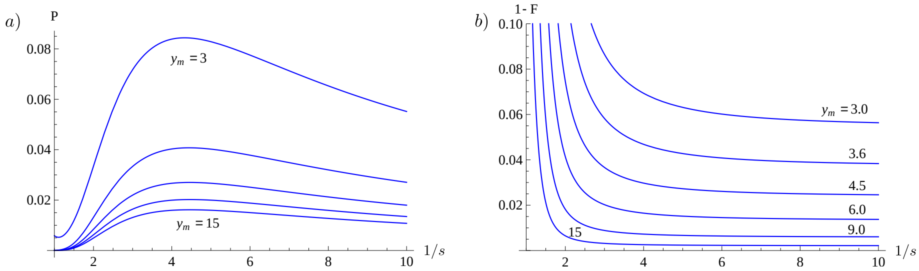


Figure 2: a) Probability density $P(y_m)$ of the measurement outcome depending on the initial squeeze of the ancillary state. b) The infidelity $1 - F_{cat}$ between the actual output state and the state of an ideal Schrödinger's cat. Here $1/s \geq 1$ is the stretching factor of the ancilla coordinate quadrature.

Recently, the problem of universal measures of non-Gaussianity of states, which can serve as a resource for universal quantum computing [8], has been widely discussed. One could expect that a non-Gaussian resource state for which a well-chosen measure is larger can more effectively derive the result of quantum evolution from the class of Gaussian schemes with optimal use. For the squeezed cubic phase state, such measures as the non-Gaussianity and Wigner negativity will be monotonic functions of the parameter $\gamma/s^3$ [9]. We show that with a sufficiently large cubic nonlinearity parameter, our logical gate can conditionally produce a state very close to the cat-like superposition of Glauber states almost regardless of the squeezing parameter (after some threshold value, see Fig. 2b). If the measured ancilla momentum $y_m$ falls within the range specified before measurement, the "amount of non-Gaussianity" in the output cat-like state becomes almost independent of the squeezing value with sufficiently large squeezing, regardless of which measure is used. However, it is necessary to take into account not only the fidelity of the prepared states, but also the probability of obtaining the necessary measurement result. In our scheme, the "amount of non-Gaussianity" in the output state, weighted by its probability shown in Fig. 2a, disappears in the limit of ideal squeezing. It means that using a cubic phase state with a large value of the $\gamma/s^3$ and, consequently, with large non-Gaussianity and Wigner negativity, can make the gate less efficient in the sense mentioned above. It is likely that non-Gaussian measures based on global properties of the resource state may be generally unsuitable for schemes based on entanglement and projective measurements. Physically speaking, the effectiveness of such schemes may depend more on the behavior of the resource state in the phase space region, where it overlaps with the state detected by the measuring device, than on its global properties.

# References

[1] *M. Mirrahimi, Z. Leghtas, V.V. Albert, S. Touzard, R. J. Schoelkopf, L. Jiang, and M.H. Devoret*, Dynamically protected cat-qubits: a new paradigm for universal quantum computation. New J. Phys. **16**, 045014 (2014).

[2] *Z. Bao, Z. Wang, Y. Wu, Y. Li, W. Cai, et al.*, Experimental preparation of generalized cat states for itinerant microwave photons. Phys. Rev. A, **105**, 063717 (2022).

[3] *J. Rivera-Dean, Th. Lamprou, E. Pisanty, P. Stammer, A. F. Ordóñez, A. S. Maxwell, M. F. Ciappina, M. Lewenstein, and P. Tzallas*, Strong laser fields and their power to generate controllable high-photon-number coherent-state superpositions. Phys. Rev. A **105**, 033714 (2022).

[4] *A. Ourjoumtsev, R. Tualle-Brouri, J. Laurat, and P. Grangier*, Generating optical Schrödinger kittens for quantum information processing. Science **312**, 83 (2006).

[5] *I. V. Sokolov*, Schrödinger cat states in continuous variable non-Gaussian networks. Phys. Lett. A **384**, 126762 (2020).

[6] *N. I. Masalaeva and I. V. Sokolov*, Quantum statistics of Schrodinger cat states prepared by logical gate with non-Gaussian resource state. Phys. Lett. A **424**, 127846 (2022).

[7] *D. Gottesman, A. Kitaev, and J. Preskill*, Encoding a qubit in an oscillator. Phys. Rev. A, **64**, 012310 (2001).

[8] *M. Walschaers*, Non-Gaussian quantum states and where to find them. PRX Quantum, **2**, 030204 (2021).

[9] *F. Albarelli, M.G.Genoni, M.G.A.Paris, and A.Ferraro*, Resource theory of quantum non-Gaussianity and Wigner negativity. Phys. Rev. A **98**, 052350 (2018).

# Improvement of Kerr QND Measurement Sensitivity via Squeezed Vacuum Input Field

Dariya Salykina[1,2*], Stepan Balybin[1,2]

[1] *Lomonosov Moscow State University, 119991 Moscow, Russia*
[2] *Russian Quantum Center, Skolkovo 143025, Russia*
*E-mail: koil257@mail.ru

**Abstract**

In Ref. [1], the scheme of quantum nondemolition measurement of optical quanta which uses a resonantly enhanced Kerr nonlinearity in whispering gallery mode (WGM) optical resonators was analyzed theoretically. Here we show, that by using a squeezed quantum state of the probe mode, it is possible to significantly increase the sensitivity of that scheme.

## Intorduction

One of the differences between quantum and classical physics lies in the fact that a precise measurement in the microscopic world is not possible without the introduction of a perturbation or 'back action' inherent to the very procedure of measurement. The idea of a quantum non-demolition (QND) measurement is to control this back action noise by redirecting it into the observable conjugated to the one being measured.

Schemes of quantum non-demolition measurement of number of photons are based on the coupling of two optical waves by means of the cross-phase modulation (XPM) effect resulting from the cubic (Kerr) nonlinearity of an optical material were proposed in [2, 3]. The goal is the indirect measurement of the number of photons in the signal beam by coupling it to another (probe) beam in a nonlinear medium, without absorption of the signal photons.

Recent advantages in fabrication of high-Q whispering gallery mode (WGM) microresonators [4] give hope to realization of such a measurement. The scheme of quantum nondemolition measurement of optical quanta which uses the resonantly enhanced Kerr nonlinearity in a WGM optical resonators was analyzed in detail in Ref. [1]. It was shown that the modern WGM resonators with the Q-factors excceding $10^9$ allow achieving the measurement imprecision several times better than the standard quantum limit.

## QND measuremnt using a squeezed state of light

The well known way to improve the sensitivity of optical measurement scheme is the use of squeezed states, as it was proposed in Ref. [5]. Nowadays squeezed states of light are widely used in gravitational wave detectors to achieve better phase sensitivity [6, 7].

Here we consider the configuration shown in Fig. 1(left). Squeezed light is fed into one of the input ports of Mach-Zehnder interferometer. On a beam splitter it is combined with the pump beam in the coherent state giving us a probe mode. The microresonator with $\chi^{(3)}$ nonlinearity couples probe mode and signal mode, which results in equation:

$$\phi_p = \Gamma_X \hat{n}_s, \tag{1}$$

where $\Gamma_X$ - nonlinearity factor, $\hat{n}_s$ is the number of photons in signal mode. Measurement of the phase shift in the probe mode allows to find the number of quanta in the signal mode, as shown in Fig. 1(right). Black circles show the case of coherent probe and red ellipses - the case of squeezed coherent probe mode. It is obvious that squeezing makes uncertainties of that value smaller by the factor of $e^{-r}$. Thus by using squeezed states of light and choosing the right homodyne angle we can get an improvement in sensitivity.

With account of the parasitic nonlinear self phase modulation (SPM) of the probe beam, the phase measerement error can be presented as follows:

$$(\Delta\phi_p)^2 = \frac{e^{2r}}{4\alpha^2}\Big(\cot\zeta + 2\alpha^2\Gamma_S\Big)^2 + \frac{e^{-2r}}{4\alpha^2}\,, \tag{2}$$

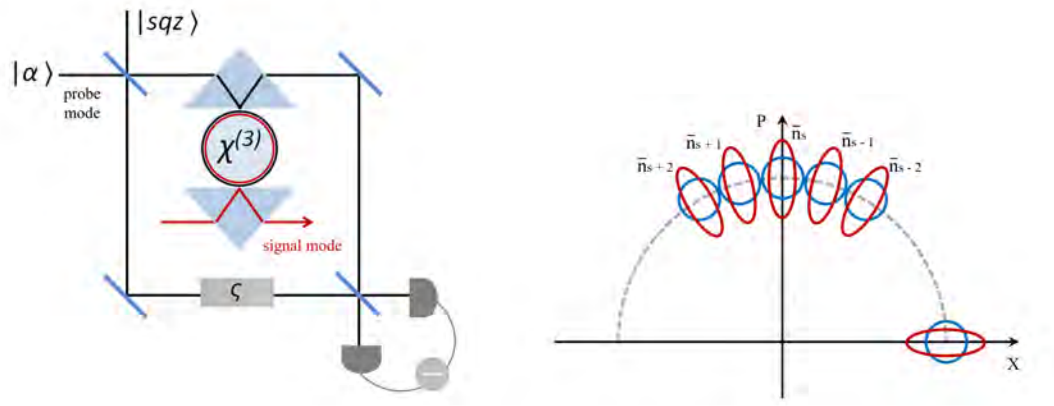


Figure 1: Left: Principal scheme of QND measurement of photon number in signal mode $S$ via XPM effect on probe squeezed coherent light in probe mode. Right: The evolution of probe field on the phase plate after cross phase interaction with signal field. The final phase of the probe depends on number of photons in the signal field.

where $\Gamma_S$ is the SPM factor. One can see that by choosing the value of homodyne angle so that $\cot\zeta = -2\alpha^2\Gamma_s$ the expression in brackets can be eliminated, giving the following simple formulae:

$$\Delta\phi_p = \frac{e^{-r}}{2\alpha} \tag{3}$$

It follows from Eqs. (1, 3), that the measurement error for the number of quanta in the signal is equal to

$$\Delta n_s = \frac{e^{-r}}{2\Gamma_X\alpha} \tag{4}$$

The squeezed states of light are strongly affected by optical losses. Let $\eta$ be an overall quantum efficiency of our scheme. In this case,

$$(\Delta n_s)^2_\eta = (\Delta n_s)^2 + \frac{1-\eta}{\eta}\frac{1}{2\alpha^2\Gamma_X^2\sin^2\zeta}, \tag{5}$$

## Conclusions

We showed that using the squeezed state of the probe, an improvement of sensitivity equal to the squeeze factor $e^{-r}$ can be obtained. The interfering effect of SPM was taking into account and it was shown that it can be compensated by using the right homodyne angle.

# References

[1] *S. N. Balybin, A. B. Matsko, F. Y. Khalili, D. V. Strekalov, V. S. Ilchenko, A. A. Savchenkov, N. M. Lebedev, and I. A. Bilenko*, Quantum nondemolition measurements of photon number in monolithic microcavities. Phys. Rev. A 106, 013720 (2022).

[2] *V. B. Braginsky and S.P. Vyatchanin*, Sov. Phys. Dokl. 26, 686 5 (1981).

[3] *G. J. Milburn and D. F. Walls*, Quantum nondemolition measurements via quadratic coupling. Phys. Rev. A **28**, 2065 (1983).

[4] *D. V. Strekalov, C. Marquardt, A. B. Matsko, H. G. L. Schwefel, and G. Leuchs*, Nonlinear and quantum optics with whispering gallery resonators. Journal of Optics 18, 123002 (2016).

[5] *C. M. Caves*, Quantum-mechanical noise in an interferometer. Phys. Rev. D 23, 1693 (1981).

[6] *M. Tse et al.*, Quantum-Enhanced Advanced LIGO Detectors in the Era of Gravitational-Wave Astronomy. Phys. Rev. Lett. **123**, 231107 (2019).

[7] *F. Acernese et al.*, Increasing the Astrophysical Reach of the Advanced Virgo Detector via the Application of Squeezed Vacuum States of Light. Phys. Rev. Lett. **123**, 231108 (2019).

# High fidelity quantum logic gate for OAM single qudits

Elizaveta Bashmakova*, Evgenii Vashukevich, Tatiana Golubeva, Yuri Golubev

*St. Petersburg State University, St. Petersburg, Russia*
*E-mail: bashmakova.elizaveta@mail.ru

**Abstract**

In this work, we propose a method for implementing multidimensional single-qudit gates for qudits based on light modes with orbital angular momentum (OAM) using the protocol for converting the OAM of light in the Raman quantum memory scheme. For different dimensions of qudits, we have shown that such transformations have an exceptionally high level of fidelity. We also compare quantum gates' properties of systems of different dimensions and find the optimal conditions for carrying out transformations in the protocol under consideration.

Today high-dimensional ($d-$dimensional) quantum systems (qudits) capture the attention of scientists. First of all, this is due to researchers are attracted by the possibility of increasing the information capacity of the channel – the amount of information that can be encoded in one physical carrier, that turns out to be very useful in the problems of quantum communication and quantum information processing [1]. Moreover, in quantum cryptographic protocols based on qudits, the security of the protocol appears to be higher, the larger the dimension of the system [2]. Nevertheless, there are still blind spots in the problem of efficient manipulation of multidimensional quantum states.

The orbital angular momentum (OAM) is one of the exciting resource for constructing a qudit since the OAM can take any integer values, which allows us to work in the Hilbert space of high dimension [3]. A significant factor is also that Laguerre– Gaussian modes with OAM show high stability and a relatively high decoherence time when propagating in a turbulent atmosphere [4].

To achieve the universality of quantum computation, it is necessary to be able to implement a universal set of quantum logic operations. Gates $\hat{X}_d^m$ and $\hat{Z}_d^m$ can be considered as single-qudit gates. The $\hat{X}_d^m$ gate performs modulo $d$ addition of the value of the qudit with $m$, and the $\hat{Z}_d^m$ gate adds a relative phase to the terms of the superposition. Since the gate $\hat{Z}_d^m$ and its powers can be quite easily obtained using the Dove prism [5], we focused on constructing the gate $\hat{X}_d^m$. In this work, based on the protocol for converting the OAM of light in the Raman quantum memory scheme [6], we propose a method for implementing quantum single-qudit gates for various dimensions of qudits encoded in OAM numbers.

We have shown that the success probability of the conversion by adding an OAM quanta for the qudit dimension $d = 3$ increases with the value of the OAM $l$ [7]. At the same time, in the case of subtracted OAM quanta ($m = -1, -2$), a higher probability can be achieved in the region of small values of $l$ (see Fig. 1). The resulting conversion asymmetry is caused by the asymmetry of the mode overlapping functions and can be considered as an advantage of the protocol, which makes it possible to control in a wide range of values of $l$. Moreover, all transformations provide an exceptionally high level of fidelity (up to $F \geq 97$). Furthermore, we select the control parameter $\lambda$, which is the normalized relative shift of the beam waists of the driving and quantum fields. In particular, for each transformation a specific value of the parameter $\lambda$, provides high probabilities over a wide range of $l$ values, could be calculated.

We have compared the characteristics of the $\hat{X}_d^m$ gates for different dimensions of qudits with the trivial case of a qubit. The values of probability and fidelity were taken into account, along with the potential gain from information capacity increased with the dimension of a qudit. We have evaluated the optimal qudit dimension for transformations. An estimation based on all these factors shows that working with qudits of dimensions $d = 3$ and $d = 4$ turns out to be preferable for performing quantum computations in the proposed protocol. Especially the drop in probability associated with an increase in the dimension of the system, is beaten by the high value of the information capacity of the channel.

This research was supported by Russian Science Foundation (project No. 22-22-00022) and Theoretical Physics and Mathematics Advancement Foundation "BASIS" (project No. 22-1-4-20-1).

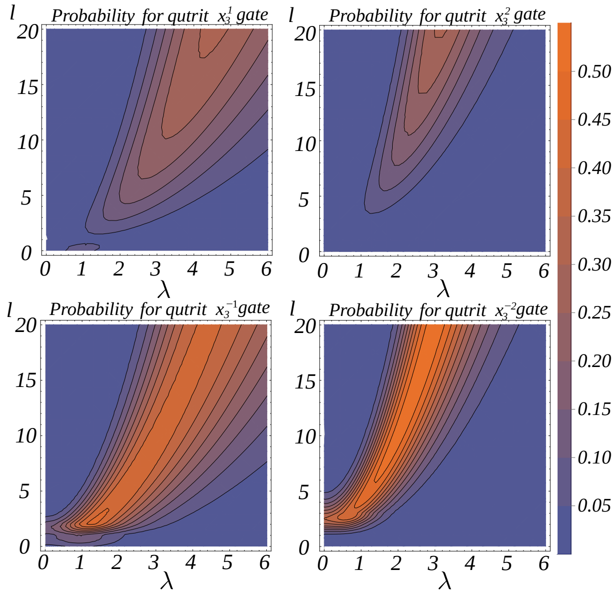


Figure 1: The probabilities of success of the qutrite gates $\hat{X}_3^1$, $\hat{X}_3^2$ (top), $\hat{X}_3^{-1}$, $\hat{X}_3^{-2}$ (bottom) depending on the values of $l$ and of the parameter $\lambda$ that controls the geometry of the modes.

## References

[1] *M. Erhard, R. Fickler, M. Krenn and A. Zeilinger*, Twisted photons: new quantum perspectives in high dimensions. Light Sci. Appl. **7**, 17111 (2018).

[2] *L. Sheridan, V. Scarani*, Security proof for quantum key distribution using qudit systems. Phys. Rev. A. **82**, 82 030301(R) (2010).

[3] *L. Allen, M. W. Beijersbergen, R. J. C. Spreeuw and J. P. Woerdman*, Orbital angular momentum of light and the transformation of Laguerre-Gaussian laser modes. Phys. Rev. A. **45**, 8185 (1992).

[4] *S. Li, S. Chen, C. Gao, A.E. Willner and J. Wang*, Atmospheric turbulence compensation in orbital angular momentum communications: Advances and perspectives Opt. Commun. **408**, 68 (2018).

[5] *Y. Zhang, F.S. Roux, T. Konrad, M. Agnew, J. Leach, and A. Forbes*, Engineering two-photon high- dimensional states through quantum interference. Science advances. **2**, e1501165 (2016).

[6] *E.A. Vashukevich, T.Y. Golubeva, and Y.M. Golubev*, Conversion and storage of modes with orbital angular momentum in a quantum memory scheme. Phys. Rev. A. **101**, 033830 (2020).

[7] *E.A. Vashukevich, T.Y. Golubeva, E.N. Bashmakova and Y.M. Golubev*, High-fidelity quantum gates for OAM qudits on quantum memory. Laser Phys. Lett. **19**, 025202 (2022).

Khosta, Sochi, Russia October 2–8, 2022
5th International School on Quantum Technologies

# Feedback Control Outside of the Controlled System

**Vladimir Tomilin**

[1] *Institute of Automation and Electrometry SB RAS*
*E-mail: 8342tomilin@mail.ru

**Abstract**

A novel scheme of measurement-based quantum feedback control is investigated. Instead of controlling the parameters of the system of interest, the feedback adjusts the measurement apparatus based on the history of measurement outcomes. As an illustration, the feedback control of two-mode atomic Bose-Einstein condensate is considered. One mode is probed by an external field in the dispersive regime, and the field is then detected at the output of Mach-Zehnder interferometer. The master equation for the BEC state is derived and its steady-state solution is analyzed by calculating Kullback-Leibler divergences from various reference distributions.

Quantum feedback control has several features that make it distinct from classical control theory. Unlike classical physics, the system-environment interaction channels for quantum systems can be effectively engineered and controlled. If all these channels are connected to the controller, it generates a series of registered events of various types (for example, detections of photons of a certain polarization). It is then possible to adjust the type of these events by reconfiguring the controller after each registration. In this way, the feedback loop is closed within the controller and does not contain the system itself. This principle has been previously investigated for continuously monitored solid-state system [1].

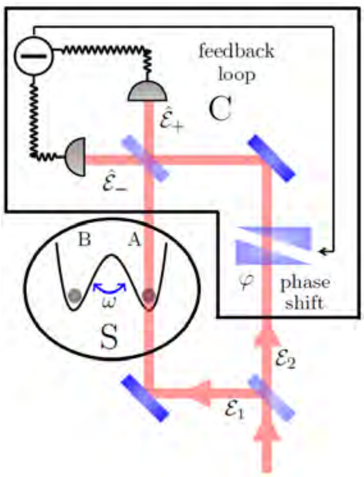


Figure 1: Double-well atomic BEC controlled by a feedback that modifies the phase shift $\varphi$. Labels S and C within black boxes indicate the "boundaries" of the system and the controller, respectively

The system state becomes a function of recorded history of events generated by controller. The scheme becomes most simple when there are only two types events possible (say, "+" and "-"), so that the conditioned density operators of the system are $\hat{\varrho}^{(\pm)}$. To illustrate it with a physical example, consider a model presented in Fig. 1 (a predecessor of this scheme previously appeared in [2]). Bose-Einstein condensate (BEC) of non-interacting atoms consists of two localized modes. One of the modes is probed by a an optical beam in one of the arms of Mach-Zender interferometer (MZI). The radiation propagating through MZI is then detected by two photodetectors operating in the photon counting regime. The two types of events are the detections in one or the other output channels.

The master equation governing the evolution of the BEC can be constructed on the basis of Lindblad equation. We consider the radiation interacting with the BEC in the dispersive regime (typical for the phase-contrast imaging technique). In this case the net effect of the interaction is a phase gain by the field, proportional to the number of atoms in the beam. Assume that this number is entire number of atoms in the mode. The Lindblad operators then are $\hat{\mathcal{E}}_{\pm}(\varphi) \doteq \left(e^{\imath\chi\hat{a}^{\dagger}\hat{a}} \pm e^{\imath\varphi}\right)/\sqrt{2}$, where $\varphi$ is the phase shift placed in the other arm of the MZI. It is this very parameter that is subject to feedback control. As there are two types of events, the most simple control scheme becomes the following: the phase shift $\varphi$ is switched into $\varphi_+$ position upon detecting the photon in the "+" channel, or into $\varphi_-$ position upon detecting the photon in the "-" channel. A single master equation then becomes a coupled system for conditioned density operators:

$$\begin{aligned} \frac{d}{dt}\hat{\varrho}^{(+)} + \imath[\hat{H}, \hat{\varrho}^{(+)}] &= \sum_{\sigma=\pm}\left(2\hat{\mathcal{E}}_{+}(\varphi_{\sigma})\hat{\varrho}^{(\sigma)}\hat{\mathcal{E}}_{+}^{\dagger}(\varphi_{\sigma}) - \{\hat{\mathcal{E}}_{\sigma}^{\dagger}(\varphi_{+})\hat{\mathcal{E}}_{\sigma}(\varphi_{+}), \hat{\varrho}^{(+)}\}\right), \\ \frac{d}{dt}\hat{\varrho}^{(-)} + \imath[\hat{H}, \hat{\varrho}^{(-)}] &= \sum_{\sigma=\pm}\left(2\hat{\mathcal{E}}_{-}(\varphi_{\sigma})\hat{\varrho}^{(\sigma)}\hat{\mathcal{E}}_{-}^{\dagger}(\varphi_{\sigma}) - \{\hat{\mathcal{E}}_{\sigma}^{\dagger}(\varphi_{-})\hat{\mathcal{E}}_{\sigma}(\varphi_{-}), \hat{\varrho}^{(-)}\}\right). \end{aligned} \tag{1}$$

For the eigendynamics of the system we take the simplest model of non-interacting identical modes: $\hat{H} = \omega\left(\hat{a}^{\dagger}\hat{b} + \hat{b}^{\dagger}\hat{a}\right)$. Eqs. (1) are then solved in the weak decoherence limit.

We are interested in the capability to control the steady-state atomic distributions in the modes, $p_n^{(\pm)} = \langle n|\hat{\varrho}^{(\pm)}|n\rangle$, $|n\rangle = |n\rangle_a \otimes |N-n\rangle_b$. To this end, we evaluate the Kullback-Leibler(KL) divergences [3] from the uniform distribution and the no-feedback distribution ($\varphi_+ = \varphi_-$) (Fig. 2).

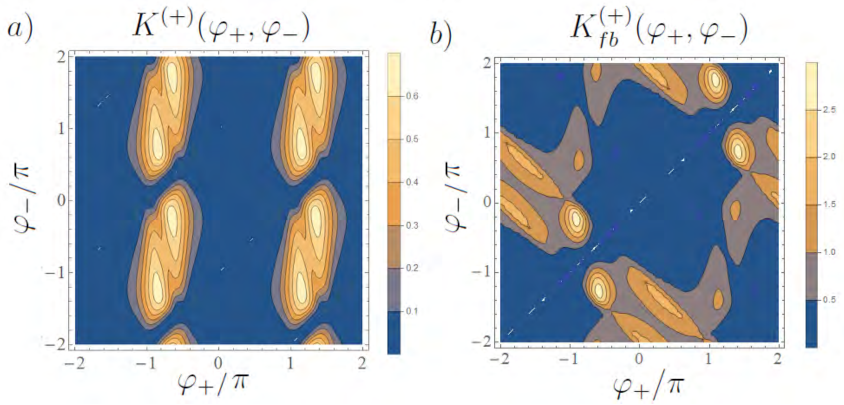


Figure 2: KL-divergences: a) between $P_n^{(+)}(\varphi_+, \varphi_-)$ and $p_n = \frac{1}{N+1}$; b) $P_n^{(+)}(\varphi_+, \varphi_-)$ and $P_n^{(\pm)}(\frac{\varphi_+ + \varphi_-}{2}, \frac{\varphi_+ + \varphi_-}{2})$. Capital letters stand for distributions normalized to 1

The maxima of the KL-divergence lie to the side of the plot diagonals (corresponding to no-feedback case). While this fact is peculiar by itself (meaning that manipulation with the radiation already scattered from the BEC still impacts the BEC state), it can also be utilised for preparing highly asymmetrical BEC states. The feedback is capable of enhancing the asymmetry between the atomic distribution in the modes, which follows from the higher values of maxima in Fig. 2b) compared to 2a).

This work was supported by the State Order (project AAAA-A21-121021800168-4) at the Institute of Automation and Electrometry SB RAS.

# References

[1] *L.S. Martin et al.*,, Implementation of a canonical phase measurement with quantum feedback. Nat. Phys. **16**, 1046-1049 (2020).

[2] *V.A. Tomilin, L.V. Il'ichov*, BEC Dynamics in a Double Well with Interferometric Feedback. Ann. Phys. (Berlin) **528**, 619-625 (2016).

[3] S. Kullback, L.A. Leibler, *Information and Statistics* (Wiley, 1959).

# Development of tomography methods for photon-number-resolving single-photon detectors, and their approbation on the simplest models

Semyon Zarutskiy[1,2*], Konstantin Katamadze[2,3], Grant Avosopiants[2,3], Boris Bantysh[2,3], Nadezhda Borshchevskaya[2,3]

[1] *Russian Quantum Center, Moscow, Russia*
[2] *Quantum Technology Centre, Faculty of Physics, Lomonosov Moscow State University, Moscow, Russia*
[3] *Institute of Physics and Technology, Russian Academy of Sciences, Moscow, Russia*
*E-mail: `zarutskiysy@gmail.com`

**Abstract**

Single-photon detectors, including those that resolve the photon number, play a key role in experimental research in the field of quantum optics and quantum computer science. However, such detectors have a number of disadvantages, and the choice of a detector is always a trade-off [1] between such characteristics as quantum efficiency, dead time, etc. In view of this, part of the information is lost and distorted during measurements, which negatively affects the experimental data obtained. The study suggests method for tomography of photon-number-resolving single-photon detectors. By means of the proposed method, the main characteristics of detectors and radiation sources are restored. The proposed method is tested on the simplest models.

The object of the study is an avalanche photodiode with a non-zero number of dark counts and a significant dead time, having the photon number resolve capability by means of time multiplexing. The considered mathematical model of the detector depends on the following parameters: $\eta$ – quantum efficiency, $t_{\mathrm{dead}}$ – dead time, $\mu_{\mathrm{n}}$ – average number of dark counts. The paper considers a model in which the quantum efficiency of an avalanche photodiode instantly turns to 0 when a photon is registered and is instantly restored after dead time passes. The noise is considered to be evenly distributed over the measurement interval. To conduct a numerical experiment, the transfer matrix of the detector is calculated. Its elements carry information about the probability of registering $k$ photocounts with $n$ photons at the input.

## Direct problem of the number of photocounts distribution

Using a transfer matrix, the dependence of the number of photocounts over the number of photons at the input is constructed, see Fig. 1.

The dependence of the average number of photocounts over the average number of photons at the input is approximated by the formula (1). The correction coefficient 0.95 was obtained empirically, and with the detector parameters used in the work, its value is close to constant.

$$f = \mu\eta\frac{1-0.95\gamma\mu}{1+0.95\gamma\mu\eta} + \mu_n, \tag{1}$$

The average relative error of the detector parameters recovery is given in the Table 1.

Table 1: Average relative error of the detector parameters recovery.

| | |
|---|---|
| $\gamma$ | 0.012 |
| $\eta$ | 0.020 |

## Inverse problem of the number of photocounts distribution

When solving the inverse problem of the number of photocounts distribution, we considered a thermal source described by a two-parameter Compound Poisson distribution [2]:

$$P_{\mathrm{CP}}(n|\mu,a) = \frac{(a)_n}{a^n}\frac{\mu^n}{n!}\frac{1}{(1+\mu/a)^{n+a}}, (a)_n = \frac{\Gamma(a+n)}{\Gamma(a)}, \tag{2}$$

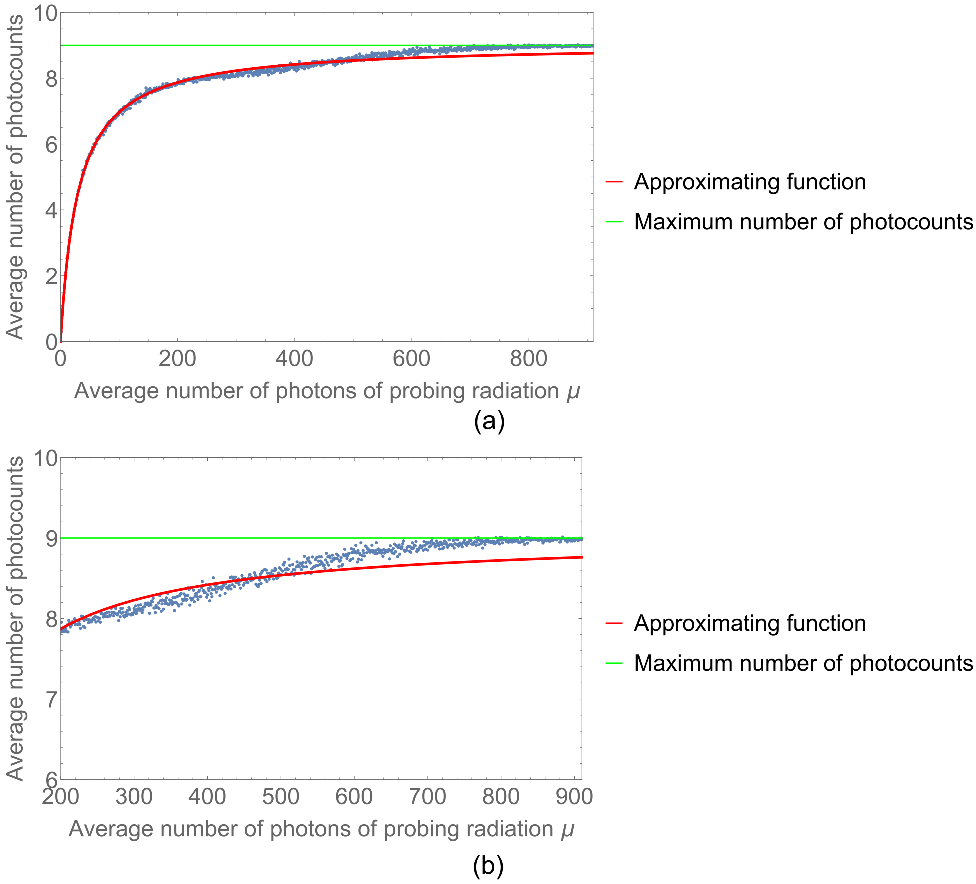


Figure 1: The dependence of the average number of photocounts over the average number of photons at the input. Its approximation by the approximation function: a – general sight; b – close-up. Detector Parameters: $\gamma = 0.117188$, $\eta = 0.3$, $\mu_n = 0.115 * 10^{-3}$

.

In the Equation (2) $\mu$ is the average number of photons of the source, $a$ is the coherence parameter.

The source parameters are restored by minimizing expressions that depend quadratically on the experimentally obtained values of the average number of photocounts and the average square of the number of photocounts. The average relative error of the detector parameters recovery is given in the Table 2.

Table 2: Average relative error of the source parameters recovery.

| | |
|---|---|
| $a$ | 0.03 |
| $\mu$ | 0.021 |

## References

[1] *Migdall A. et al.* Single-photon generation and detection: physics and applications. Academic Press (2013).

[2] *Yu. I. Bogdanov, N. A. Bogdanova, K.G. Katamadze, G.V. Avosopiants, V.F. Lukichev* Study on the photon statistics using Poisson's Compoung distribution and quadrature measurements. Optoelectronics, Instrumentation and Data Processing, **52** (2016).

# PCF Source of Visible-Telecom Photon Pairs

**Albert F. Khairullin**[1*], **Maxim A. Smirnov**[1], **Ilya V. Fedotov**[1,2], **Sergey A. Moiseev**[1], **Alexey M. Zheltikov**[1,2]

[1] *Kazan Quantum Center, Kazan National Research Technical University n.a. A.N. Tupolev-KAI, Kazan, Russia*
[2] *Physics Department, International Laser Center, M.V. Lomonosov Moscow State University, Moscow, Russia*
*E-mail: `albert.captaen@gmail.com`

**Abstract**

The source of entangled photon pairs is one of the basic elements of a quantum repeater[1]. When photon pairs propagate along fiber optic communication lines, an important role begins to be played by optical losses in the fiber, the minimum values for which are achieved in the range from 1530 to 1565 nm (standard transparency window), which imposes requirements on the spectral characteristics of the generated radiation[2]. Optical fibers themselves can act as such quantum sources, competing with nonlinear crystals due to their high radiation brightness and minimal losses when coupled to standard fiber optic systems[3]. In the course of the research, the possibilities of generating photon pairs near a standard transparency window based on a highly nonlinear photonic-crystal fiber (NL-PM-750) were studied. The generation of photon pairs with a generation rate of 5 MHz was experimentally obtained.

Photon pair sources are fundamental building blocks in the study of quantum entanglement and the creation of quantum communication systems. Currently, there are various methods for generating photon pairs,the most common are methods based on the use of photonic crystal fibers [4], nonlinear crystals [5], and generation in integrated structures is also of particular interest [6]. In this work, a photonic crystal fiber is used as a source, in which photon pairs are generated by the effect of spontaneous four-wave mixing. At the same time, methods for generating quantum light at a wavelength near 1550 nm, which is the standard for telecommunications, are of great interest. Four-wave mixing is a parametric process based on the third-order non-linearity $\chi^{(3)}$ of the fiber core, which converts two pump photons into two photons at different wavelengths. Usually, the received photons are called signal and idler. For the effect to occur, it is necessary to comply with the frequency and phase matching condition, which is written in the following form [7]:

$$k_i + k_s - 2k_p + 2\gamma P = 0, \tag{1}$$

$$\omega_i + \omega_s = 2\omega_p, \tag{2}$$

where $k_{i,s,p}$ - the wave vectors of the idler, signal, and exciting modes, $\omega_{i,s,p}$ - frequencies of idler signal pump wave $P$ - peak pump power, $\gamma$=$2\pi n_2/\lambda A_{eff}$ - coefficient of non-linearity of the fiber, where $n_2$ - non-linear refractive index, $A_{eff}$ - effective fiber mode area, $\lambda$ - pump wavelength.

The NL-PM 750 photonic crystal fiber with zero dispersion at a wavelength of 750 nm was studied as a source of photon pairs. A preliminary numerical analysis showed that states at a wavelength near 1530 nm can be realized in this PSF fiber. The FWM was excited using short pulses of a Ti:Sa laser with a wavelength near 780 nm. The frequency band of the pulses was additionally reduced in the duration adjustment block and amounted to 130 GHz. Idle lines with $\lambda_i$ near 1530 nm and signal lines with $\lambda_s$ near 520 nm generated as a result of a nonlinear process were cleaned from pump using filters and then sent to their own recording channel. Photons were recorded using the corresponding single-photon detectors: in the signal channel using a single photon detector in the visible range (SPDM Count NIR, Laser Components), in the idle channel using a single photon detector in the IR range (ID210, IDquantique). The count rates of the detectors and coincidences were recorded using a coincidence circuit, which received output electrical signals from the detectors. Fig. 1 shows the measurements of the statistical characteristics of the generated photon pairs in one of the scalar FWM regimes. At the pump power P= 2.2 mW, the measured second-order correlation is $g^2(0)$=10, the value of the pair generation rate obtained in the experiment (taking into account losses) is $r_0$=5 MHz. Note that the value $g^2(0) \geq$10

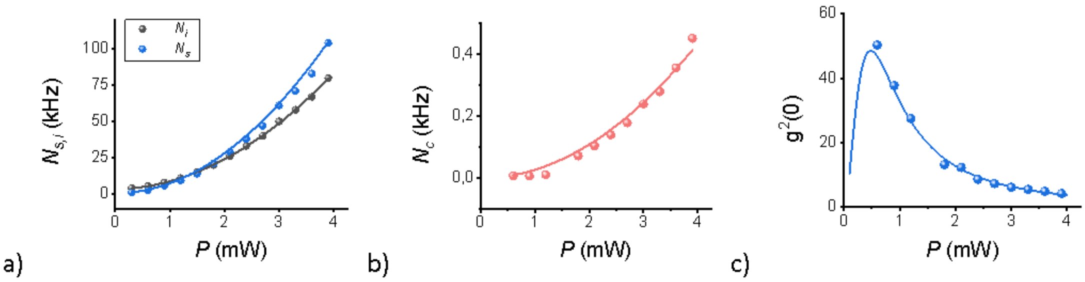

Figure 1: (a) Photon count rates in the signal channel $N_s$, idle channel $N_i$ as a function of the average pump power $P$: experiment (circles) and their approximations by quadratic functions (solid lines). (b) Coincidence count rates $N_c$ and second-order correlation function $g^2(0)$ as functions of power P (circles): experiment (circles) and their approximations by quadratic functions (solid lines). Experimental parameters: FWM scalar mode (ss-ss), $\lambda_p$=760 nm, $\lambda_s$=506 nm, $\lambda_i$=1526 nm.

is a criterion for the applicability of the source in quantum technologies. Thus, the value of $r_0$ can be considered optimal when using this source in quantum applications.

The key parameters of photon pairs with an idler photon wavelength near 1550 nm, generated by FWM in a PCF fiber, were experimentally studied. Generation of photon pairs was obtained at the output of an optical fiber with a generation rate of ≈5 MHz.

The study was carried out with the financial support of the Ministry of Education and Science of Russia Reg. number NIOKTR 121020400113-1.

# References

[1] *Yu, L., Natarajan, C.M., Horikiri, T., Langrock, C., Pelc, J.S., Tanner, M.G.,... Yamamoto, Y.*, Two-photon interference at telecom wavelengths for time-bin-encoded single photons from quantum-dot spin qubits. Nature Communications, 6, 2015.

[2] *Jones, C., Kim, D., Rakher, M.T., Kwiat, P.G., Ladd, T.D.*, Design and analysis of communication protocols for quantum repeater networks. New Journal of Physics, 18(8), 2016.

[3] *Söller, C., Brecht, B., Mosley, P.J., Zang, L.Y., Podlipensky, A., Joly,N. Y.,... Silberhorn, C.*, Bridging visible and telecom wavelengths with a single-mode broadband photon pair source. Physical Review A - Atomic, Molecular, and Optical Physics, 81(3), 2010.

[4] *Wang L.J., Hong C.K., Friberg S.R*, Generation of correlated photons via four-wave mixing in optical fibres. J. Opt. B Quantum Semiclassical Opt. 2001.V.3. №5.P.346.

[5] *Niizeki, K., Ikeda, K., Zheng, M., Xie, X., Okamura, K., Takei, N., ... Horikiri, T.*, Ultrabright narrow-band telecom two-photon source for long-distance quantum communication. Applied Physics Express, 11(4),2018.

[6] *O.A.Ermishev, M.A.Smirnov, A.F.Khairullin, N.M.Arslanov*, Optimization of parameters of a $LiNbO_3$ nanowaveguide with periodical polarization for the generation OF ultra-wideband biphotons in the near-IR range. Bulletin of the Russian Academy of Sciences: Physics.–2022.–V.86.–№.12.

[7] *Fulconis J. et al.* , High brightness single mode source of correlated photon pairs using a photonic crystal fiber. Optics Express.–2005.–V.13.–№.19.–P.7572-7582.

Khosta, Sochi, Russia October 2–8, 2022
5th International School on Quantum Technologies

# Multiqudit quantum hashing via orbital angular momentum of light

**Dmitriy Akat'ev**[1*], **Alexander Vasiliev**[2], **Nail Shafeev**[2]
**Farid Ablayev**[2], **Alexey Kalachev**[1,2]

[1]*Zavoisky Physical-Technical Institute, FRC Kazan Scientific Center, Russian Academy of Sciences, Kazan, Russia*
[2]*Institute of Computational Mathematics and Information Technologies, Kazan Federal University, Kazan, Russia*
*E-mail: `akatevdmitrijj@gmail.com`

**Abstract**

In this work we construct a quantum hash via a sequence of high dimensional single-photon states with orbital angular momentum and perform a proof-of-principle experiment. As a result, we experimentally verify the collision resistance of the quantum hash function depending on the number of qutrits in use.

## Inroduction

The hashing protocol is widely used in many branches of modern cryptography, such as verification of message integrity, digital signatures, fingerprinting, etc. [1], [2]. Hash function has several main properties. Firstly, it is a one-way function that is easy to compute on every input, but hard to invert given the image of a random input. Secondly, it has good collision resistance. The collision resistance property was the main object of our investigation. A promising generalization of the cryptographic hashing concept in the quantum domain has been suggested in [3]. The first realisation of a quantum hashing protocol was demonstrated on qubits with orbital angular momentum [4]. Now, we demonstrate the implementation of a multiqudit quantum hashing based on the high dimensional single photon states (qutrits) in the basis of Laguerre-Gaussian modes.

## High dimensional states

As an information carrier we used single photons with orbital angular momentum (M) under spontaneous parametric down-conversion conditionz. If pump radiation has OAM $l_p$, due to phase matching condition, generated biphoton pairs will also have OAM $l_p = l_s + l_i$. We created single qutrit states via fixing angular momentum of idler photon $l_i = 0$. In this case, information about the spatial structure of the signal photon reproduces that of the pump field $l_p = l_s$. In the present work, we realized this approach by preparing and measuring OAM carrying beams in the basis of Laguerre-Gaussian ($LG_p^l$) modes with $p = 0$. The single qutrit states were prepared in superposition of OAM modes $l = 2, 0, -2$.

$$|\psi_j(\phi_2, \phi_3)\rangle = \frac{1}{\sqrt{3}} \left(|2\rangle + e^{i\phi_2} |-2\rangle + e^{i\phi_3} |0\rangle\right) \tag{1}$$

To define states quality we take advantage of the quantum tomography approach developed in [5]. As an example, we carry out quantum tomographic measurements for a qutrit state $|\psi_j(0,0)\rangle$. The measured state fidelity is $F = 0.987 \pm 0.012$.

## Multiqudit quantum hash-function

When the information carriers are high dimensional states, quantum hash function can be constructed as follows.

$$|\Psi(x)\rangle = |\psi_1(x)\rangle \otimes \cdots \otimes |\psi_m(x)\rangle, \tag{2}$$

where

$$|\psi_j(x)\rangle = \frac{1}{\sqrt{d}} \left(|\ell_1\rangle + e^{i(2\pi s_{j,2}x/q)} |\ell_2\rangle + \ldots + e^{i(2\pi s_{j,d}x/q)} |\ell_d\rangle\right), \tag{3}$$

where $|\ell_j\rangle$ is a single-photon state corresponding to $\mathrm{LG}_0^{\ell_j}$ mode, $d$ is the dimension of its state space, $q$ is the size of the input space, $x \in \{0, 1, \ldots, q-1\}$ is a classical input that is encoded by the relative phase of $m$ qudit states, $s_{i,j}$ are numeric parameters of the quantum hash function that provide its collision resistance. The main idea of the collision resistance property is to provide minimum fidelity between different quantum hashes (quantum hash function images) with the minimal possible number of quantum information carriers. Furthermore, reaching reasonable balance between collision resistance property and one-way property for a quantum hash function is an important task.

The fidelity between two hash functions is described by the equation 4.

$$\left| \langle \Psi(x_1) | \Psi(x_2) \rangle \right|^2 = \frac{1}{d^{2m}} \prod_{j=1}^{m} \left| 1 + e^{i \frac{2\pi s_{j,2}(x_1 - x_2)}{q}} + \ldots + e^{i \frac{2\pi s_{j,d}(x_1 - x_2)}{q}} \right|^2 \tag{4}$$

The parameter set $\{s_{i,d}\}$ is chosen in such a way that the pairs of hashes $|\Psi(x_1)\rangle$ and $|\Psi(x_2)\rangle$ give the minimal fidelity for $x_1 \neq x_2$. In this work, we experimentally evaluate a collision probability for multiqudit quantum hash function for $q = 256, d = 3$ and different qutrit number in use $m = 1 \ldots 5$. To measure the collision probability we compare different quantum hashes in the worst-case scenario when hash codes formed from $x_1$ and $x_2$ have maximum fidelity for a given optimal (quasioptimal) set $\{s_{i,d}\}$. Table 1 demonstrates the result of collision probability evaluations. The experiential result demonstrates

Table 1: The collision probability for worst-case scenario.

| Qutrit number | Theory | Experiment |
|---|---|---|
| 1 | 0.9681 | $0.947 \pm 0.069$ |
| 2 | 0.5422 | $0.657 \pm 0.101$ |
| 3 | 0.1483 | $0.134 \pm 0.04$ |
| 4 | 0.0368 | $0.0072 \pm 0.008$ |
| 5 | 0.0063 | $0.0345 \pm 0.017$ |

that the collision probability decreases when the number of qutrits increases. However, it is necessary to find a balance between the one-way property and the collision resistance property because a larger number of qutrits also gives a higher inversion probability (i.e. low one-way resistance).

## Conclusion

In our work we have experimentally implemented multiqudit quantum hashing via separated qutrit states in orbital angular momentum basis. The experimental results suggest that the considered technique can be useful even for small sizes of input and output states. For instance, for m = 3 we “compress” the 8-bit input strings into 3-qutrit states, which provides some kind of a balance between inversion probability bounded by 27/256<0.11 and collision probability bounded by 0.15.

## Acknowledgements

The experimental part of the work was made within the government assignment for FRC Kazan Scientific Center of RAS.

# References

[1] *C. Paar and J. Pelzl*, Understanding cryptography: a textbook for students and practitioners. Springer Science & Business Media, New York (2009)

[2] *J. Katz and Y. Lindell,*, Introduction to Modern Cryptography, 2nd ed.. CRC press, Boca Raton (2014)

[3] *F. Ablayev and A. Vasiliev*, Cryptographic quantum hashing. Laser Phys. Lett. **11**, 05202 (2014).

[4] *D.A. Turaykhanov,D.O. Akat'ev,A.V. Vasiliev,F.M. Ablayev, A.A. Kalachev*, Quantum hashing via single-photon states with orbital angular momentum. Phys. Rev. A **104**(5), 052606 (2021).

[5] *M. Agnew, J. Leach, M. McLaren, F.S. Roux, R.W. Boyd* Tomography of the quantum state of photons entangled in high dimensions Phys. Rev. A **84**(6), 062101 (2011).

# Laser noises influence on Raman oscillations of rydberg atoms

**A.P.Gordeev***, **D.Schepanovich, I.B.Bobrov, S.S.Straupe**

*Quantum technology centre, Faculty of Physics M.V. Lomonosov Moscow State University, Moscow, Russia*
*E-mail: ar1emg0rdeev@gmail.com

**Abstract**

One of the factors restricting fidelity of quantum gates implementation in quantum computers based on cold atoms is laser technical noise. This work presents methods for measuring laser noises via signal from Pound–Drever–Hall system and heterodyne spectroscopy and provides a numerical model of rydberg atom excitation by solving Schrodinger equation using electric field noises recreated from experimental data in order to estimate quantum gate fidelity.

Rydberg atoms are promising platform for quantum simulation and computing as well as rydberg blockade is a practical way to entangle qubits by exciting high n states in two atoms simultaneously. Error sources for these systems are the following: finite lifetime of atomic states, Stark effect, thermal motion of atoms and noises in laser radiation. We provide description of experimental setup (detailed specification will be shown during presentation) for lasers' noise measurement and numerical simulation of Raman oscillations.

For practical purposes we used 2 lasers (red and blue) to excite rydberg states. Lasers' noise spectra were obtained via three methods: measurement of laser intensity with fast photodiode (so called intensity noise), heterodyne spectroscopy (lasers' spectra)[1] and signal from PDH-locking system (frequency noise spectra[2]).

For numerical simulation of the process there are two possible ways. First is to directly solve Schrodinger's equation for three level atom with following Hamiltonian

$$\widetilde{H} = UHU^\dagger + i\hbar\partial_t(U)U^\dagger = \begin{pmatrix} 0 & 0 & \sum\Omega_{1,i}e^{-i\Delta_{1,i}t+\phi_{1,i}} \\ 0 & 0 & \sum\Omega_{2,i}e^{-i\Delta_{2,i}t+\phi_{2,i}} \\ \sum\Omega_{1,i}e^{i\Delta_{1,i}t-\phi_{1,i}} & \sum\Omega_{2,i}e^{i\Delta_{2,i}t-\phi_{2,i}} & 0 \end{pmatrix}, \qquad (1)$$

where $\Delta_{1(2),i}$ is detuning of i-th spectral component from atomic resonance, $\Omega_{1(2),i}$ - Rabi frequency produced by i-th component, $\phi_i$ - random phases and indices 1 and 2 correspond to red and blue lasers.

Second way is to use adiabatic approximation[3] reducing three level system to two levels and solve Schrodinger's equation Hamiltonian:

$$\hat{H} = \hat{H}_0 + \hat{H}_1 = \frac{\hbar\Delta}{2}\sigma_z + \frac{\hbar\Omega}{2}\sigma_x + \frac{\hbar\nu(t)}{2}\sigma_z + \frac{\hbar\Omega\varepsilon(t)}{2}\sigma_x,$$

where $\nu(t)$, $\varepsilon(t)$ - functions proportional to oscillation of frequency and amplitude of lasers with mean values equal to 0. This method allows to compare modeling result with perturbation theory results[4] applied to two level system.

Using numerical simulation we demonstrated insignificant influence of low-frequency (intensity) noise and high-frequency ($> 10$ MHz) noise in our experimental setup, whereas mid-frequency noises have considerable impact which can be reduced from 0.2% to 0.1% infidelity for red laser and from 0.5% to 0.3% by adding Fabri-Perot resonator to the model.

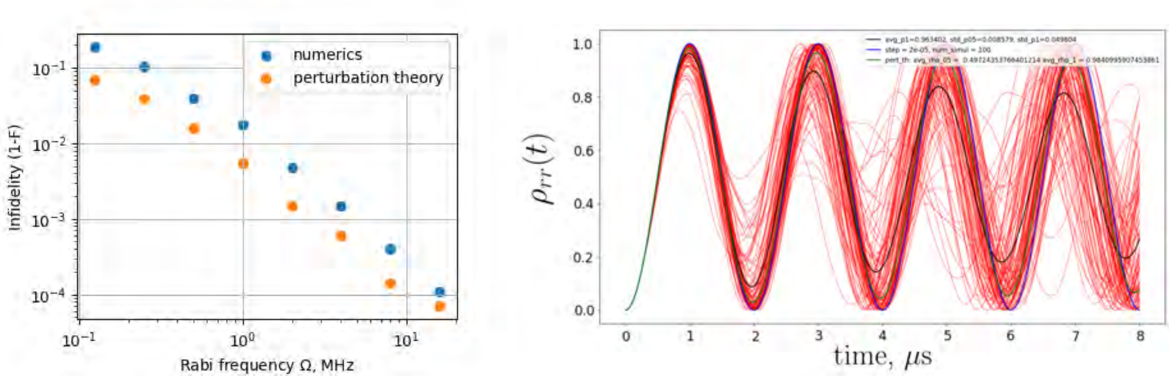


Figure 1: (a) - Infidelity of $\pi$-impulse at different Rabi frequencies in comparison with perturbation theory, (b) - Evolution of rydberg state obtained by numerics (Rabi freuency $\Omega = 0.5$ MHz). Red lines corresponds solutions with different sets of random phases $\phi_i$, black line is their average, blue line shows evolution without noise and green line represents perturbation theory for red laser spectra measured from PDH-locking signal.

## References

[1] *Hanne Ludvigsen and Mikael Tossavainen and Matti Kaivola*, Laser linewidth measurements using self-homodyne detection with short delay. **180-186**, 155 (1998)

[2] *E. Black*, An introduction to Pound-Drever-Hall laser frequency stabilization. American Journal of Physics **79-87**, 69 (2001).

[3] *D.A. Steck*, Quantum and Atom Optics, **269** (2007).

[4] *A. Kale*, Towards High Fidelity Quantum Computation and Simulation with Rydberg Atoms. Defended 5 June 2020.

# Graphene coated nickel tips for STM lithography with atomic precision

**Ekaterina Mirgazizova**[1,2*], **Tatyana Pavlova**[1], **Konstantin Eltsov**[1]

[1] *Prokhorov General Physics Institute Russian Academy of Sciences, Moskow, Russia*
[2] *National Research University Higher School of Economics, Moskow, Russia*
*E-mail: `emirgazizova@nsc.gpi.ru`

**Abstract**

STM lithography requires sufficiently robust conductive and inert probes. It is proposed to use graphene-coated nickel tips. A complete technological cycle has been developed for the creation of an atomically sharp carbon-coated Ni tip, including electrochemical etching of a nickel wire, ultrahigh-vacuum preparation, and synthesis of a tip coating by chemical epitaxy. Auger electron spectroscopy and STS methods were used to test the presence of a carbon layer on the surface of a nickel needle, including the tip. A high degree of matching of the electron density near the Fermi energy for the carbon coating on the tip of the Ni-needle and the graphene monolayer on the Ni(111) surface is shown.

At present, nanoelectronics based on single-atom impurity atoms in a silicon matrix (single-atom nanoelectronics) [1], which use both individually embedded atoms as quantum dots and two-dimensional arrays with a concentration enabling dielectric-metal transition to control quantum transport, are being actively developed. All process operations (in the standard planar technology approach) are carried out under controlled ultrahigh vacuum conditions. Monoatomic adsorbate layers (hydrogen [2], halogens [3]) are used as resist. Atomically-sharp-edged windows in the resist (mask) are formed using a scanning tunnelling microscope (STM) probe (tip). Adsorption of relevant molecules is used for doping and functionalisation. Low-temperature homoepitaxy is used to seal the circuit. A facet 100 is used as a substrate.

A sufficiently inert and robust surface of the probe apex is necessary for reproducible technological treatment of a solid surface with an STM probe. Experience shows that W- or Pt/Ro-tips, usually used in STM, in tunnel contact mode can change its state when pulse voltage is applied, which leads to poorly reproducible STM lithography results on silicon surface [4, 5]. This paper presents methods for creating and controlling STM tips coated with a monolayer of carbon. We use needles made of pure (99.98 %) nickel wire with a thermally programmed graphene growth on their surface [6]. The criterion for the presence of graphene on the Ni-needle tip is a specific density of electron states, which appears in the differential conductivity spectra $dI_t/dU_t$ during tunneling. Taking into account that $dI_t/dU_t$ is determined by the density of electronic states of both contacts, the Cu(100) facet with constant density of states near the Fermi energy, 1 eV, is chosen as the second contact [7]. Graphene synthesis conditions: propylene dose 500-1000 Langmuir at room temperature followed by annealing at 500 °C for 3-4 hours. Measurements and process procedures were performed in the same ultra-high vacuum chamber equipped with an electron Auger spectrometer, slow electron diffractometer and GPI-300 STM [8], at a residual gas pressure of less than $6\text{-}10^{-11}$ torr.

Fig. 1 shows the differential conductivity curve taken with a carbon-coated tip on Cu(100) surface. The shape of the curve agrees with the data of the ARPES experiment for the Ni(111) surface coated with a graphene monolayer (1x1) [8]. The ability of the tip to obtain atomic resolution on the metal surface is confirmed by the example of Cu(100) (inset on fig. 1).

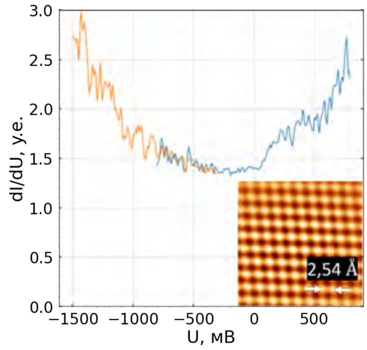


Figure 1: STS spectrum of Cu(100) surface taken with a carbon-coated needle ; inset: STM image (25x25 Å, I = 0.8 nA, U = -6.64 mV) of Cu(100) surface

This work was supported by the Russian Science Foundation (grant no. 21-12-00299).

## References

[1] *E. Prati, T. Shinada (Eds.)*, Single-atom nanoelectronics. Pan Stanford Publishing Pte Ltd. **1** (2000).

[2] *M.Y. Simmons, F.J. Ruess, K.E.J. Goh, W. Pok, T. Hallam, M.J. Butcher, T.C.G. Reusch, G. Scappucci, A.R. Hamilton, L. Oberbeck*, Atomic-scale silicon device fabrication. Int. J. Nanotechnol. **5**, 352-369 (2008).

[3] *T.V. Pavlova, V.M. Shevlyuga, B.V. Andryushechkin, G.M. Zhidomirov, K.N. Eltsov*, Local removal of silicon layers on Si(100)-21 with chlorine-resist STM lithography. Appl. Surf. Sci. **509**, 145235 (2020).

[4] *M. Rashidi, R. A. Wolkov*, Autonomous Scanning Probe Microscopy in Situ Tip Conditioning through Machine Learning. ACS Nano. **12**, 5185-5189 (2018).

[5] *T.V. Pavlova, V.M. Shevlyuga, B.V. Andryushechkin, K.N. Eltsov*, Dangling bonds on the Cl- and Br-terminated Si(100) surfaces. Appl. Surf. Sci. **591**, 153080 (2022).

[6] *S.L. Kovalenko, T.V. Pavlova, B.V. Andryushechkin, O.I. Kanishcheva, K.N. Eltsov*, Epitaxial growth of a graphene single crystal on the Ni(111) surface. JETP Letters. **105**, 185-188 (2017).

[7] *C. Baldacchini, L. Chiodo, F. Allegretti, C. Mariani, M. G. Betti, P. Monachesi, R. Del Sole*, Cu(100) surface: High-resolution experimental and theoretical band mapping. Phys. Rev. B. **68**, 195109 (2003).

[8] http://sigmascan.ru/index.php/ru/menu-uhvstm

Khosta, Sochi, Russia October 2–8, 2022
5th International School on Quantum Technologies

# Disorder-Induced Dynamical Quantum Phase Transitions in Transverse Field Ising Model

**Oleg Kulyashov**[1,2*], **Anton Markov**[2] **and Alexey Rubtsov**[2,3]

[1] *Moscow Institute of Physics and Technology (State University), Institutskii per. 9, 141700 Dolgoprudnyi, Moscow Region, Russia*
[2] *Russian Quantum Center, Bolshoy Boulevard 30, bld. 1, Skolkovo, Moscow 121205, Russia*
[3] *Department of Physics, Lomonosov Moscow State University, Leninskie Gory 1, 119991 Moscow, Russia*
*E-mail: `kulyashov.on@phystech.edu`

**Abstract**

Ground state of a many-body system may drastically change as its parameters are varied. These, intrinsically quantum, phase transitions have a counterpart out of equilibrium. Short-time dynamics of many-body systems may exhibit non-analytical behavior of the systems' properties at particular times, thus dubbed dynamical quantum phase transition. Simulations showed that in the presence of disorder new critical times appear in the quench evolution of the Ising model. We study the physics behind these new critical times. We discuss the spectral features of the Ising model responsible for the disorder-induced phase transitions. We found the critical value of the disorder sufficient to induce the dynamical phase transition as a function of number of spins.

*Introduction* Out of equilibrium collective phenomena are far worse understood than the equilibrium ones. Even what is a 'phase' and a 'phase transition' is not quite clear yet. Dynamical Quantum Phase Transitions (DQPT) [1], that is the points in time when the system's parameters evolve non-analytically in time is one of the more established concepts.

The theory of DQPT is built in close formal analogy to the theory of equilibrium quantum phase transitions. The key observation is that the Loschmidt Echo (LE) can be interpreted as a partition function of an equilibrium system at imaginary temperatures:

$$\mathcal{L}(t) = \langle\psi|e^{-it\mathcal{H}}|\psi\rangle \longleftrightarrow \mathcal{Z}(\beta) = e^{-\beta\mathcal{H}} = \sum_i \langle\psi_i|e^{-\beta\mathcal{H}}|\psi_i\rangle \tag{1}$$

Correspondingly, rate function $\lambda$ is analogous to free-energy density, but with complex time in place of inverse temperature:

$$\lambda(z) = -N^{-1}\log\mathcal{L}(z) \longleftrightarrow f(\beta) = -N^{-1}\log\mathcal{Z} \tag{2}$$

($N$ - number of degrees of freedom). And as points of non-analyticity of free-energy density are called phase transitions, so are points of non-analyticity of the rate function, which coincide with zeros of the LE. In general, zeros of the LE (also called Fisher zeros) may be complex, but only purely imaginary zeros correspond to real times. Such special zeros indicate times of DQPTs.

*Model and Results* We study the dynamics of the transverse field Ising model after a quench from ferromagnetic to paramagnetic phase with an additional disorder in the final field:

$$\mathcal{H}_0 = -\sum_{i=1}^{N}\sigma_x^i\sigma_x^{i+1} \longrightarrow \mathcal{H}_1 = -\sum_{i=1}^{N}\sigma_x^i\sigma_x^{i+1} + h_i\sigma_z^i\ ,\ h_i \in U[h-\Delta, h+\Delta], \tag{3}$$

here $\sigma$ are Pauli matrices, $h$ - are on-site magnetic fields drown from the the uniform random distribution $U[h-\Delta, h+\Delta]$. Varying the disorder amplitude $\Delta$ we see that without any disorder, the system features DQPTs with a period $T_1$ and logarithms of spin-spin correlators feature non-analyticities with the same period. In the weak disorder limit ($0 \neq \Delta \ll h$), LE acquires an additional series of DQPT with a different period $T_2$ as was first observed numerically in Ref. [2]. We derive analytically this new period $T_2$.

In general, it is not trivial to identify any kind of order parameter for DQPT [3]. As we can see, spin-spin correlators become non-analytic with the old period $T_1$ and do not "feel" the new period $T_2$. To explain this analytically we went through the following steps:

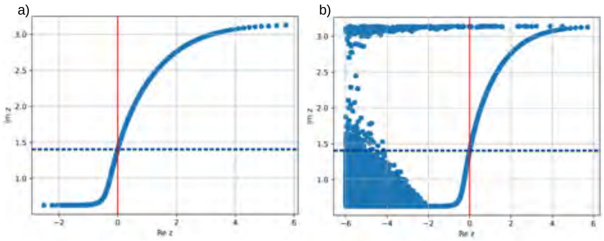


Figu $\neq 0$

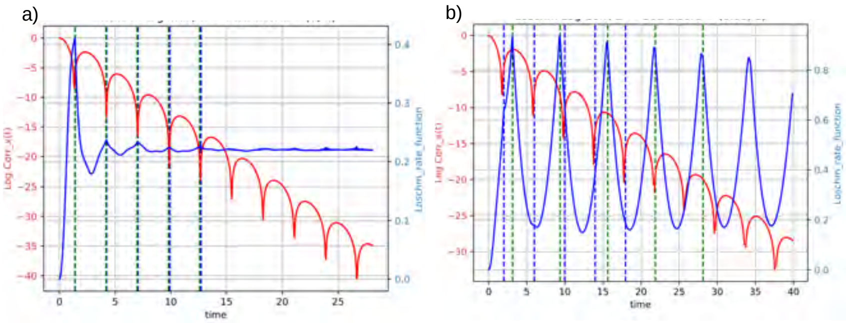


Figure 2: Loschmidt rate function (blue) and logarithm of spin-spin correlators (red); a) without disorder, $\Delta = 0$, b) with small disorder, $\Delta \neq 0$

1. In the limit of weak disorder we derived a formula for the change of Fisher zeros under disorder $\Delta = 0 \to \Delta \neq 0$ - see Fig. 1

2. As a corollary we obtained a lower bound on $\Delta$, such that disorder still induces a new series of DQPTs:
$$\Delta_{min} \geq \frac{3(2\pi)^3}{8}\left(\frac{h}{h-1}\right)^2 \frac{1}{N^3} \tag{4}$$
Importantly, this bound vanishes in the thermodynamic limit ($N^{-3} \to 0$ when $N \to \infty$)

3. Using the bound from the Eq. 4 we showed that for a sufficiently large system, the disorder may have an arbitrarily small effect on spin-spin correlators and still cause an additional series of DQPTs - see Fig. 2.

To sum up, we analytically demonstrated that at any disorder strength, in the thermodynamical limit the Ising model develops a new series of DQPT and derived the bound for the critical value for finite systems. We demonstrated that the ferromagnetic order is intact at the new critical times. Our results may be directly observed in experiments in modern quantum simulator platforms [4].

# References

[1] *M. Heyl, A. Polkovnikov, and S. Kehrein*, Dynamical Quantum Phase Transitions in the Transverse-Field Ising Model. Phys. Rev. Lett. **110**, 135704 (2013).

[2] *Kaiyuan Cao, Wenwen Li, Ming Zhong, and Peiqing Tong*, Influence of weak disorder on the dynamical quantum phase transitions in the anisotropic XY chain. Phys. Rev. B **102**, 014207 (2020).

[3] *Markus Heyl*, Dynamical quantum phase transitions: a review. Rep. Prog. Phys. **81**, 054001 (2018).

[4] *P. Jurcevic, H. Shen, P. Hauke, C. Maier, T. Brydges, C. Hempel, B.P. Lanyon, M. Heyl, R. Blatt, and C.F. Roos*, Direct Observation of Dynamical Quantum Phase Transitions in an Interacting Many-Body System. Phys. Rev. Lett. **119**, 080501 (2017).

# Breakdown of the topological charge pumping

**Ivan Dudinets**[1,2,3*]

[1] *Russian Quantum Center, Skolkovo, Moscow 143025, Russia*
[2] *Moscow Institute of Physics and Technology, Dolgoprudny, Moscow Region 141700, Russia*
[3] *Steklov Mathematical Institute of Russian Academy of Sciences, Moscow 119991, Russia*
*E-mail: `dudinets@phystech.edu`

**Abstract**

We study the topological quantum pumping (Thouless pumping) in the framework of the Rice-Mele model (RM) for the case of non-adiabatic driving and existence of interactions. We examine the charge transported in a single period in the non-adiabatic regime. We also consider how a finite initial temperature affects the charge pumping. Furthermore, we investigate the charge pumped after many cycles. Our analytical results for the quadratic RM model are supplemented by numerical results for an interacting version of the RM model. These results are relevant for future experimental realizations of Thouless pumps.

The dynamics of a system of noninteracting electrons governed by a time periodic Hamiltonian exhibits an interesting property discovered by Thouless: If the parameters of the Hamiltonian vary adiabatically and periodically in time, then the charge transported per cycle is determined by the Chern number and, consequently, is strictly quantized [1]. The interest to this phenomenon (called topological pumping or Thouless pumping) was renewed by its experimental realization in systems of ultracold atoms in optical lattices [2, 3]. Perfect quantization of the pumped charge is guaranteed only in the limit of infinite system size (thermodynamic limit) and infinite cycle duration (adiabatic limit). Establishing quantitative conditions for quantization away from these limits can be a subtle issue [4]. In particular, one should distinguish between two modes of operation of the Thouless pump, a transient mode (first few cycles) and a continuous mode (established after many cycles) [4]. Though finite-size corrections in the adiabatic limit are well understood [5], the investigation of the phenomenon out of the adiabatic limit as well as the interacting case is still lacking. Several studies addressed this issue from various perspectives [6, 7, 8].

We focus on the Rice-Mele model (RM), an archetypal model of the Thouless pump, a one-dimensional bipartite tight-binding lattice, described by the Hamiltonian

$$H_0(t) = -J_1(t)\sum_{j=1}^{N} c^\dagger_{jA}c_{jB} - J_2(t)\sum_{j=1}^{N} c^\dagger_{jB}c_{j+1A} + h.c. + \Delta(t)\sum_{j=1}^{N} c^\dagger_{jA}c_{jA} - c^\dagger_{jB}c_{jB}, \qquad (1)$$

where an operator $c^\dagger_{jA(B)}$ ($c_{jA(B)}$) creates (annihilates) an electron at $j$th site in $A(B)$ sublattice. A hoping amplitude $J_{1(2)}(t)$ and on-site potentials $\Delta(t)$ and $-\Delta(t)$ are periodic with the period $T$.

The charge transported over $m$th period is given by

$$Q_m = \int_{mT}^{(m+1)T} dt\, \langle\Psi(t)|\hat{J}|\Psi(t)\rangle, \quad \hat{J} = \frac{J_2(t)}{N}\sum_i \left(ic^\dagger_{jB}c_{j+1A} + h.c.\right) \qquad (2)$$

where $\Psi(t)$ is the many-body state of the electrons.

## Transient mode

The topological nature of the Thouless pumping is supported by the fact that the transported charge does not depend on the choice of the protocol provided the evolution of the system is adiabatic. To illustrate this we present the exact charge transferred after the first cycle in the RM model for three different paths in the parameter space of the system's Hamitonian (1) (see Fig. 1a). We observe that for the adiabatic evolution ($\omega = 2\pi/T \to 0$) the charge is strictly quantized regardless of the path chosen. The adiabatic condition is crucial since the charge deviates from the quantized value for increasing the frequency $\omega$.

We also regard the effect of a finite initial temperature on the Thouless pumping and obtain explicit expression for the transported charge.

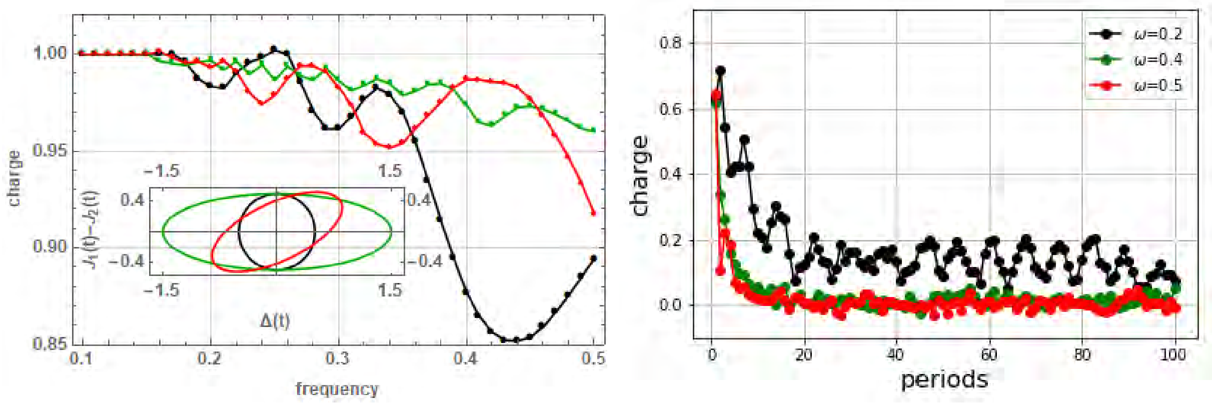


(a) (b)

Figure 1: (a) The charge transported over the first period, $Q_0$, versus the driving frequency $\omega$ for $N = 100$ particles. In the inset, three driving protocols of the Thouless pumping in the parameter space of the model. The quantized transport takes place when a closed path encircles the point $(\Delta, J_1 - J_2) = 0$. (b) The charge $Q_m$ (2) versus the number of periods $m$ for different values of the driving frequency $\omega$. The plot is obtained by the exact diagonalization of the Hamiltonian (3) with $N = 8$ particles.

## Continuous mode

Most of the studies devoted to the issue of the deviations from the perfect quantization are dedicated to integrable systems like the RM model (see, for example, [6]). Such systems have integral of motions which prevent the system from heating [9, 10]. We consider the long-time behaviour of the RM model with the time-independent interaction term $H_{int}$

$$H(t) = H_0(t) + H_{int}, \quad H_{int} = U \sum n_{jA} n_{jB} + n_{jB} n_{j+1A}, \tag{3}$$

where $n_{jA(B)} = c^{\dagger}_{jA(B)} c_{jA(B)}$ the number operator. The transported charge established after many cycles is depicted in Fig. 1b. We can observe the breakdown of the quantization for the system with interactions in the case of the steady operational regime of the Thouless pump. The breakdown is related to the heating of the system.

# References

[1] *D. J. Thouless*, Quantization of particle transport. Phys. Rev. B **27**, 6083 (1983).

[2] *S. Nakajima, T. Tomita, S. Taie, T. Ichinose, H. Ozawa, L.Wang, M. Troyer, and Y. Takahashi*, Topological Thouless pumping of ultracold fermions. Nature **12**, 296 (2016).

[3] *M. Lohse, C. Schweizer, O. Zilberberg, M. Aidelsburger, and I.Bloch*, A Thouless quantum pump with ultracold bosonic atoms in an optical superlattice. Nature **12**, 350 (2016).

[4] *O. Lychkovskiy, O. Gamayun, and V. Cheianov*, Time scale for adiabaticity breakdown in driven many-body systems and orthogonality catastrophe. Phys. Rev. Lett. **119**, 200401 (2017).

[5] *R. Li and M. Fleischhauer*, Finite-size corrections to quantized particle transport in topological charge pumps. Phys. Rev. B **96**, 085444 (2017).

[6] *L. Privitera, A. Russomanno, R. Citro, and G. E. Santoro*, Nonadiabatic breaking of topological pumping. Phys. Rev. Lett. **120**, 106601 (2018).

[7] *H. Wang, L. Zhou, and J. B. Gong*, Interband coherence induced correction to adiabatic pumping in periodically driven systems. Phys. Rev. B **91**, 085420 (2015).

[8] *S. Malikis, V. Cheianov*, An ideal rapid-cycle Thouless pump. SciPost **12**, 203 (2022).

[9] *A. Lazarides, A. Das, R. Moessner*, Periodic thermodynamics of isolated quantum systems, Periodic thermodynamics of isolated quantum systems. Phys. Rev. B, **112**, 150401 (2014).

[10] *N. H. Lindner, E. Berg, M. S. Rudner*, Universal chiral quasisteady states in periodically driven many-body systems, Phys. Rev. B, **7**, 011018 (2017).

# Quantum dissipative dynamics of a superconducting neuron

**Pavel Pikunov**[1], **Dmitriy Pashin**[1], **Marina Bastrakova**[1,2*]

[1] *Lobachevsky State University of Nizhni Novgorod, Nizhny Novgorod, Russia.*
[2] *Russian Quantum Center, Moscow, Russia*
*E-mail: `bastrakova@phys.unn.ru`

**Abstract**

The process of dynamic state switching in a modified scheme of a superconducting quantum parametron in a heat reservoir is studied numerically. In the Born-Markov approximation, the system evolution is reduced to an adiabatic generalized master equation for the density matrix in the instantaneous basis. The numerical solution of the equation is discussed Redfield and the possibility of using secular approximation and random phase approximation (Pauli equation).

## Introduction

One of promising applications of superconducting circuits in electronics and computing is the creation of elements of artificial quantum neural networks (QNN). These systems combine the ideas of quantum and neural network computing by using the possibilities of macroscopic quantum effects in superconductors [1].

In this paper, we consider a physical model of a superconducting neural cell that can function in both classical [2, 3] and quantum [4] modes. In our recent paper [4], we found conditions that provide the required sigmoidal activation function (conversion of the input magnetic flux into the average output current) for the operation of this cell in QNN as a perceptron [5]. However, an important unexplained issue in [4] remains the influence of dissipation on the dynamics of a neural cell.

## Phisical model

The basic element of a neural network, functioning in classical [3] and quantum [4] modes of operation, can be implemented on the basis of superconducting elements in the scheme of a parametric quantron with a SQUID instead of a Josephson junction (perceptron [2]).

The Hamiltonian of the quantum neural cell was derived in [4], and has the form

$$H(t) = \frac{p^2}{2M} + E_J \left\{ \frac{(b\varphi_{in}(t) - a\varphi)^2}{2a} + (1 - \cos\varphi) \right\}. \tag{1}$$

The system under consideration is similar to a moving particle with mass $M = \frac{\hbar^2}{2E_c}$ and momentum $p = -i\hbar\frac{\partial}{\partial\varphi}$ (where $E_C$ charge and $E_J$ Josephson energies) and the phase, $\varphi$, of the Josephson junction is the effective coordinate of the particle. The coefficients $a, b$ are parameters determined experimentally. Dynamic control of the system states is carried out by a changing external magnetic flux:

$$\varphi_{in}(t) = A\left[\left(1 + e^{-2D(t-\tau_1)}\right)^{-1} + \left(1 + e^{2D(t-\tau_2)}\right)^{-1}\right] - A. \tag{2}$$

The external flux is characterized by amplitude $A$, rise and fall times $\tau_1$ and $\tau_2 = 3\tau_1$, steepness parameter $D$.

As the simplest dissipation model, we consider the superconducting neuron to be coupled to a thermal reservoir, which is modeled as a collection of harmonic oscillators. The linear interaction between the quantum system and the reservoir can be written as

$$H_{int} = k\varphi \sum_i \left(b_i^\dagger + b_i\right), \tag{3}$$

where $b_i^\dagger$ and $b_i$ are creation and annihilation operators of the reservoir harmonic oscillators, and $k$ is the coupling constant.

## Results

In this paper the dissipative dynamics was calculated in the Born-Markov approximation, which is described by the generalized adiabatic master equation [6].The density matrix in terms of the instantaneous basis obeys the Redfield equation. Since the energy relaxation rate of the system is much smaller than the frequency of transitions between levels, we can calculate the evolution within the within the framework of the secular approximation. Moreover, if the system satisfies the additional condition that the phase relaxation rate is much larger than the energy relaxation rate, we can average over the phase (random phase approximation). In this case, keeping only the diagonal terms of the density matrix, we can obtain the basic Pauli equation.

The typical dependence activation functions are shown in Fig. 1 for various approximations. Note that the activation function is marked with different colors in the rise time ($\varphi_{in} = 0 \to A$) and the fall time ($\varphi_{in} = A \to 0$).

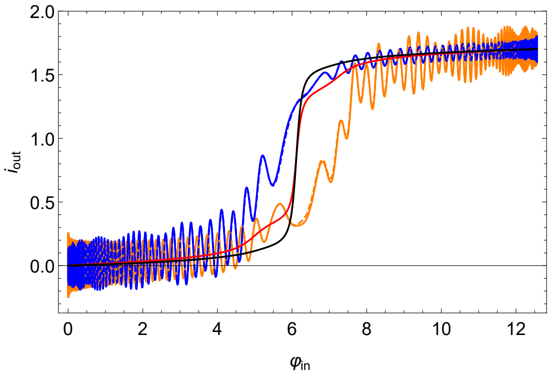


Figure 1: The activation function was calculated in three different ways, the black-red corresponds the Pauli master equation, the solid orange-blue corresponds to the Redfield equation, dashed orange-blue corresponds to the Redfield equation with secular approximation. Numerical calculations are made for $A = 2\pi$, $\tau_1 = 500$, $D = 0.008$, $a = 0.385$, $b = 0.198$, $E_J/E_C = 1$.

To summarize, we can conclude that the Pauli equation is completely unsuitable for describing dissipative dynamics. In turn, the Redfield equations and the equation in the secular approximation give practically the same results. We also found a range of parameters in which the activation function of the quantum neuron is close to the sigmoidal.

The work is supported by the Russian Science Foundation Grant (RSF) No. 22-72-10075.

## References

[1] *Schneider, M. L., Donnelly, C. A., Haygood, I. W., Wynn, A., Russek, S. E., Castellanos-Beltran, M., Dresselhaus, P. D., Hopkins, P. F., Pufall, M. R., Rippard, W. H.*, Synaptic weighting in single flux quantum neuromorphic computing. Scientific Reports **10**(1), 1–7 (2020).

[2] *Schegolev, A.E., Klenov, N.V., Soloviev, I.I., Tereshonok, M.V.,* Adiabatic superconducting cells for ultra-low-power artificial neural networks. Beilstein J. Nanotechnol. **7**, 1397-–1403 (2016).

[3] *Bastrakova, M., Gorchavkina, A., Schegolev, A., Klenov, N., Soloviev, I., Satanin, A., Tereshonok, M.*, Dynamic Processes in a Superconducting Adiabatic Neuron with Non-Shunted Josephson Contacts. Symmetry **13**(9), 1735 (2021).

[4] *Bastrakova, M., Pashin, D., Rybin, D., Schegolev, A., Klenov, N., Soloviev, I., Gorchavkina, A., Satanin A.*, A superconducting adiabatic neuron in a quantum regime. Beilstein J. Nanotechnol. **13**, 653—665 (2022).

[5] *da Silva, A. J., Ludermir, T. B., de Oliveira, W. R.*, Quantum perceptron over a field and neural network architecture selection in a quantum computer. Neural Networks **76**, 55-–64 (2016).

[6] *Albash, T., Boixo, S., Lidar, D. A., Zanardi, P.*, Quantum adiabatic Markovian master equations. New Journal of Physics **14**(12), 123016 (2012).

# Bifurcation oscillator as an advanced sensor for quantum state control

**Dmitrii Pashin**[1*], **Marina Bastrakova**[1,2], **Arkady Satanin**[3], **Nikolay Klenov**[1,2,4],

[1] *Lobachevsky State University of Nizhni Novgorod, Nizhny Novgorod, Russia*
[2] *Russian Quantum Center, Moscow, Russia*
[3] *Higher School of Economics, Russia National Research University, Moscow, Russia*
[4] *Skobeltsyn Institute of Nuclear Physics, Lomonosov Moscow State University, Moscow, Russia*
*E-mail: pashindmi@gmail.com

**Abstract**

We consider bifurcation behavior of a high-Q Josephson oscillator coupled to a superconducting qubit. A new measurement method for superpositions of qubit states based on the sensitivity of the probability of capture into either metastable equilibrium states of the driving nonlinear oscillator is proposed. The influence of the measuring oscillator on the process of qubit initialization by Rabi pulses is studied.

Scalable quantum computing and quantum error correction require high-precision projective measurements of qubit states at scales shorter than coherence time. In superconducting systems, measurements are usually based on qubit-microwave resonator coupling (dispersive readout) [1]. The qubit state can be measured due to its effect on the probability of signal transmission and reflection. Subsequently, high fidelity single-shot readout of transmon qubits states has been reached by using a Josephson bifurcation amplifiers (JBA) [2]. In this case, the probability of switching the oscillator between dynamic equilibrium states is sensitive to the qubit state.

Here, we propose a new measurement method for superpositions of qubit states using the discriminating property of a JBA. It's based on the sensitivity of the probability of capture into either metastable equilibrium states of the driving nonlinear oscillator. In the classical approximation, metastable equilibrium states are realized dynamically under the action of the drive force $f\cos(\omega t)$ (as in the case of the Duffing oscillator) and separated in phase space by a separatrix.

The prototype of the measured qubit is the "quantronium" system [3]. In the rotating wave approximation, the Hamiltonian can be written in terms of creation and annihilation operators as

$$H = H_q + \hbar(\omega_0(1+\frac{\lambda}{2}\sigma_z) - \omega)a^\dagger a - \beta(1+\frac{\lambda}{4}\sigma_z)aa^\dagger a^\dagger a - \frac{f}{\sqrt{2}}(a^\dagger + a), \tag{1}$$

where $\omega_0$ and $\beta$ are the natural frequency and non-linearity parameter of JBA, $\lambda$ is the coupling coefficient. The qubit Hamiltonian $H_q$ consists of two terms: $-\frac{1}{2}\hbar\Omega\sigma_z$ defines the qubit frequency, and the term with the control field $-\frac{1}{2}\epsilon(t)\sigma_x$.

The case $\lambda = 0$ was investigated in [4], where dissipation was taken into account and it was shown that for a quantum system with two attractors (which can be considered as an analogue of potential wells) the probability of capture into either depends on only the transition rates of levels near the separatrix energy. Because these transition rates are sensitive to the polarization of the qubit, it is possible to determine the qubit state by measuring the capture probability into one of the metastable equilibrium states. In our recent paper [5], we described in detail the mechanism for measuring the qubit state in this way.

At the initial moment we believe that the system of "qubit + JBA" is initialized near their ground states and their state is factorized. Then the process of preparation (recording) is carried out qubit states using the control field $\epsilon(t)$ and the system is described by the density matrix $\rho$.

Since the qubit continuously interacts with the measuring oscillator, it is necessary to analyze the influence of this interaction on the qubit (back action effect). To do this, we define the fidelity, $F$, of preparing qubit states by the Rabi pulse:

$$F = \frac{1}{6}\sum_{\alpha} \mathrm{Tr}\left(\rho_\alpha \cdot \rho^0_\alpha\right), \tag{2}$$

where $\rho_\alpha \equiv \mathrm{Tr}_{ocs}(\rho)$ is the reduced density operator for the qubit subsystem at the end of the Rabi pulse at the initial state of the qubit $|\alpha\rangle$, and $\rho_\alpha^0$ is the density matrix of the qubit after the pulse, but without taking into account the connection with the oscillator ($\lambda = 0$). The summation in (2) occurs over the six initial states of the qubit $|q\rangle = |\alpha\rangle$: $|\downarrow\rangle$, $|\uparrow\rangle$, $\frac{|\downarrow\rangle \pm |\uparrow\rangle}{\sqrt{2}}$ and $\frac{|\downarrow\rangle \pm i|\uparrow\rangle}{\sqrt{2}}$. It is obvious that the fidelity, $F$, depends not only on the parameters of the qubit control field, but also on the initial state of the measuring oscillator due to the connection of subsystems, which inevitably gives rise to entanglement of their states. The von Neumann entropy (an entanglement measure of subsystems) was calculated:

$$S = -\eta_+ \ln \eta_+ - \eta_- \ln \eta_-, \tag{3}$$

where $\eta_\pm = \frac{1}{2}(1 \pm |\mathbf{s}|)$. Note that the entanglement of the system is determined only by the length of the Bloch vector $\mathbf{s} = \mathrm{Tr}(\vec{\sigma}\rho_\alpha)$.

Figure 1 shows the results of the numerical calculation of the infidelity $1 - F$ and the von Neumann entropy $S$ for different the $2\pi$-pulse amplitude and initial states of the measuring oscillator averaged over the Pauli eigenstates. It can be seen from the analysis of this figure that the infidelity, $1 - F$, decreases with increasing $2\pi$-pulse amplitude $\epsilon_0$. This can be explained by the fact that the duration of the $2\pi$-pulse decreases with increasing amplitude $\tau_R \sim 1/\epsilon_0$, and, consequently, the interaction time of the qubit with the measuring oscillator also decreases. Note also that in Figure 1 a there is a clear local minimum near the value $\epsilon_0 = 2\hbar\omega$, at this pulse amplitude the Rabi frequency is equal to the JBA natural frequency.

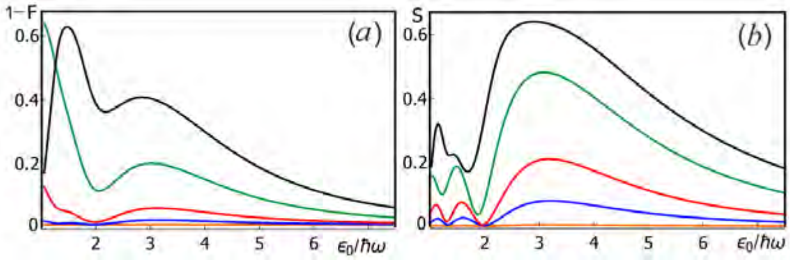


Figure 1: The infidelity **(a)** and the von Neumann entropy **(b)** of the system at the end of the Rabi pulse as a function of the amplitude of the qubit control field $\epsilon_0$ for various occupation numbers of the measuring oscillator initial state $n$: 0 (orange), 5 (blue), 10 (red), 20 (green), and 30 (black).

Another important result is that $1 - F$ and $S$ grow with an increase in the occupation number of the initial state of the measuring oscillator, see series of curves in Figure 1. Therefore that effective control (with minimal back action effect) of the qubit by pulses is possible only when the measuring oscillator is in a superposition of states with a small value of the occupation number $n$.

The development of the main idea of measuring is performed under support from Grant of the President of the Russian Federation No. MK-2740.2021.1.2. The numerical simulations were supported by the Russian Science Foundation No. 22-72-10075.

## References

[1] *A. Blais, R.-S. Huang,A. Wallraff, S.M. Girvin, R.J. Schoelkopf,* Cavity quantum electrodynamics for superconducting electrical circuits: An architecture for quantum computation. Phys. Rev. A , **69**, 062320 (2004).

[2] *F. Mallet, F.R. Ong, A. Palacios-Laloy, F. Nguyen, P. Bertet, D. Vion, D. Esteve,* Single-shot qubit readout in circuit quantum electrodynamics. Nature Physics, **5**, 791–795 (2009).

[3] *I. Siddiqi, R. Vijay, M. Metcalfe, E. Boaknin, L. Frunzio, R.J. Schoelkopf, M.H. Devoret,* Dispersive measurements of superconducting qubit coherence with a fast latching readout. Phys. Rev. B, **73**, 054510 (2006).

[4] *D. Pashin, A.M. Satanin, C.S. Kim,* Classical and quantum dissipative dynamics in Josephson junctions: An Arnold problem, bifurcation, and capture into resonance. Phys. Rev. E, **99**, 062223 (2019).

[5] *D.S. Pashin, M.V. Bastrakova, A.M. Satanin, N.V. Klenov,* Bifurcation Oscillator as an Advanced Sensor for Quantum State Control. Sensors , **22**, 6580 (2022).

# Generalized Toffoli Gate Decomposition with Qutrits

**A.S. Nikolaeva**[1,2*], **E.O. Kiktenko**[1], **A.K. Fedorov**[1,3]

[1] *Russian Quantum Center, Skolkovo, Moscow 143025, Russia*
[2] *Moscow Institute of Physics and Technology, Dolgoprudny, Moscow Region 141700, Russia*
[3] *National University of Science and Technology "MISIS", Moscow 119049, Russia*
*E-mail: anastasiya.nikolayeva@phystech.edu

**Abstract**

In this work, we propose a decomposition scheme for a generalized $N$-qubit Toffoli gate with the use of $2N-3$ two-qutrit gates. We show how to decompose $N$-qubit Toffoli gate on qutrits within arbitrary coupling map. We provide a blueprint of the realization of the proposed scheme for the Aspen-9 superconducting processor supporting quantum operations with qutrits.

One of the major challenges in the development of quantum computers is the significant error rate that occurs during the computational process. These errors are mostly caused by the imperfection of two-particle operations, a large number of which usually appear in multi-qubit gates decompositions into one-qubit and two-qubit operations. A promising way to reduce the number of two-qubit operations in the generalized Toffoli gate decomposition is to use the upper levels of multi-level quantum systems – qudits [1, 2]. From an experimental point of view, the most accessible dimension is that corresponds to the so-called qutrit ($d = 3$). Qutrits have been demonstrated experimentally not only in superconducting systems [3], but also in systems based on ultra-cold ions caught in traps [4]. We describe how the generalized Toffoli gate, which is used in many algorithms, can be efficiently implemented as a sequence of two-qutrit gates that can be implemented on superconducting processors [1].

The implementation of the $N$-qubit Toffoli gate $C^{N-1}X$, which inverts the state of the target qubit if and only if all $N-1$ control qubits are in the state $|1\rangle$, can be reduced to surrounding the generalized $N$-qubit controlled-phase gate $C^{N-1}Z$ by two single-qubit gates on the target qubit. For this reason, we further consider decomposition of $C^{N-1}Z$ gate. We also introduce $U_{i\to j}$ gate acting on $i$th and $j$th qutrit that leaves $i$th qutrit in state $|1\rangle_i$ only if both qutrits $i$ and $j$ are in the state $|1\rangle$. Otherwise, the state of $i$th qutrit becomes $|0\rangle_i$. The action of $U_{i\to j}$ on qubit levels of input qutrits is as follows:

$$\begin{aligned} U_{i\to j}\,|00\rangle_{ij} &= |01\rangle_{ij}\,, \\ U_{i\to j}\,|01\rangle_{ij} &= |00\rangle_{ij}\,, \\ U_{i\to j}\,|10\rangle_{ij} &= -\imath\,|02\rangle_{ij}\,, \\ U_{i\to j}\,|11\rangle_{ij} &= |10\rangle_{ij}\,. \end{aligned} \tag{1}$$

We note that the core operation in $U_{i\to j}$ is native for superconducting processors $iSWAP^{02}(0)$ gate (see Fig. 1).

To decompose $C^{N-1}Z$ gate, we consider the coupling map involved in decomposition qutrits as a tree, because superconducting processors typically have a restricted coupling map, which means that two-particle operation can be implemented on not any pair of qudits in the processor. By applying operation $U_{i\to j}$ to $N-2$ pairs of qutrits in accordance with their coupling map, we leave the last pair of qutrits in the states $|1\rangle$ if all other qutrits, which have a path to these two qutrits, are also in the state $|1\rangle$. After the sequence of $U_{i\to j}$, in order to apply phase factor -1 to the whole system, we implement $C^{N-1}Z$ gate on the last pair of qutrits. Then, as the third levels of qutrits were affected, we perform an uncomputation process, i.e., we apply Hermitian conjugate sequence of $U_{i\to j}$ gates in the reverse order. Thus, to implement the $C^{N-1}Z$gate, we employ $2N-3$ two-qutrit gates. We demonstrate the application of our approach to the existing superconducting quantum processor architecture on the Aspen-9 architecture, which supports quantum operations with qutrits [3].

The proposed method for decomposing the generalized Toffoli gate using the qutrit's upper level allows one to implement $C^{N-1}X$ with only $2N-3$ two-qutrit gates on any qutrit's connection topology, whereas its qubit-based realization requires $O(N^2)$ two-qutrit gates. We can improve the total fidelity of algorithm realizations on qutrit-based processors by reducing the complexity of generalized Toffoli gate

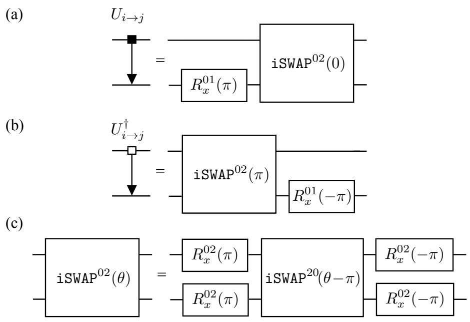


Figure 1: Decomposition of two-qutrit gate $U_{i\to j}$ (a) and its inverse $U^\dagger_{i\to j}$ (b) using $iSWAP^{02}$ gate, which is native for superconducting qutrit-based platforms, is shown. In (c) the transformation of $iSWAP^{02}$ into $iSWAP^{20}$ using local operations is depicted.

implementation. Therefore, this result is of importance for the realization of quantum algorithms with a considerable number of multi-qubit gates.

The research is supported by RSF grant No. 19-71-10091 and LRC program on Quantum Computing (Agreement No. 014/20).

## References

[1] *A.S. Nikolaeva, E.O. Kiktenko, and A.K. Fedorov*, Decomposing the generalized Toffoli gate with qutrits. Physical Review A **105**, 032621 (2022).

[2] *E.O. Kiktenko, A.S. Nikolaeva, P. Xu, G.V. Shlyapnikov, and A.K. Fedorov*, Scalable quantum computing with qudits on a graph. Physical Review A **101**, 022304 (2020).

[3] *A.D. Hill, M.J. Hodson, N. Didier, and M.J. Reagor*, Realization of arbitrary doubly-controlled quantum phase gates. arXiv preprint arXiv:2108.01652 (2021).

[4] *M. Ringbauer, M. Meth, L. Postler, et al.*, A universal qudit quantum processor with trapped ions. Nat. Phys. **18**, 1053–1057 (2022).

# Design and application of a broadband Josephson parametric amplifier for dispersive qubit readout

**A.E. Dorogov**[1,3*], **G.P. Fedorov**[1,2,3], **D.A. Kalacheva**[4,1,2], **A.Yu. Dmitriev**[1], **A.N. Bolgar**[1,4], **N.N. Abramov**[2], **O.V. Astafiev**[4,1]

[1] *Moscow Institute of Physics and Technology, 141701 Dolgoprudny, Russia*
[2] *National University of Science and Technology MISIS, 119049 Moscow, Russia*
[3] *Russian Quantum Center, 143025 Skolkovo, Moscow, Russia*
[4] *Skolkovo Institute of Science and Technology, 121205 Moscow, Russia*
*E-mail: Dorogov.AE@phystech.edu

**Abstract**

We examine the performance of a Josephson Parametric Amplifier (JPA) which uses an array of SNAILs (Superconducting Nonlinear Asymmetric Inductive eLements) as the source of nonlinearity and leverages the technique of impedance engineering (introducing a positive linear slope in the imaginary part of the input impedance seen by the SNAILs) to overcome a traditional gain-bandwidth product and increase the 1-dB compression point. We experimentally demonstrate an 18 dB gain over a 586 MHz band, along with a 1-dB compression point -101.9 dBm. All these characteristics are of great importance for the quantum devices measurements and in particular for the single-shot readout of a multi-qubit system. The signal-to-noise ratio after the application of the JPA was increased by 3 times. That led to the improvement of separation fidelity of single-shot dispersive measurements of a transmon qubit from 30.6% to 97.2%.

As the field of quantum computing is rapidly evolving, quantum devices incorporate more and more qubits, inevitably forming a demand for broadband parametric amplifiers which can be used for multiplexed qubit readout. Commercially available HEMT amplifiers are not sufficient because of high added noise, $T_{HEMT} = 3 \div 5$ K. Josephson Parametric Amplifiers (JPAs) are capable of reaching the minimum added noise imposed by quantum mechanics, $T_q \sim 0.3$ K, and consequently can increase the signal-to-noise ratio (SNR) several-fold. Enhancement of SNR is a vital task for qubit measurements because it allows to speed up readout and improve the fidelity.

Moreover, JPAs have to provide a decent gain $G_{JPA}$ to overcome the noise from the subsequent HEMT amplifiers, as follows from the expression for the chain noise:

$$T_{chain} = T_{JPA} + \frac{T_{HEMT}}{G_{JPA}}. \tag{1}$$

Thus, the crucial requirements which define the performance of the JPA are low added noise, high gain (15-20 dB), large bandwidth and dynamic range, as well as ease of operation.

## Design

Seeking the way to satisfy all of these, we study a JPA which uses an array of SNAILs (Superconducting Nonlinear Asymmetric eLements) as a nonlinear element [1]. This architecture offers great flexibility at the stage of device design.

The device under study leverages another technique to go beyond the gain-bandwidth product – impedance engineering [2]. The design uses a combination of a $\frac{\lambda}{4}$ and a $\frac{\lambda}{2}$ impedance transformers to introduce the frequency dependence of the environmental impedance:

$$Z_{in}[\omega] = R + \imath\xi\omega. \tag{2}$$

## Fabrication

The fabrication of the device starts with the aluminum evaporation on a silicon substrate followed by etching of a patterned optical resist mask in $Cl_2$ plasma. To minimize the amount of native oxide on silicon substrate, piranha solution and buffered HF treatment were implemented [3]. The Josephson junctions for the device were fabricated using electron lithography and the aluminum was evaporated using Dolan bridge technique [4].

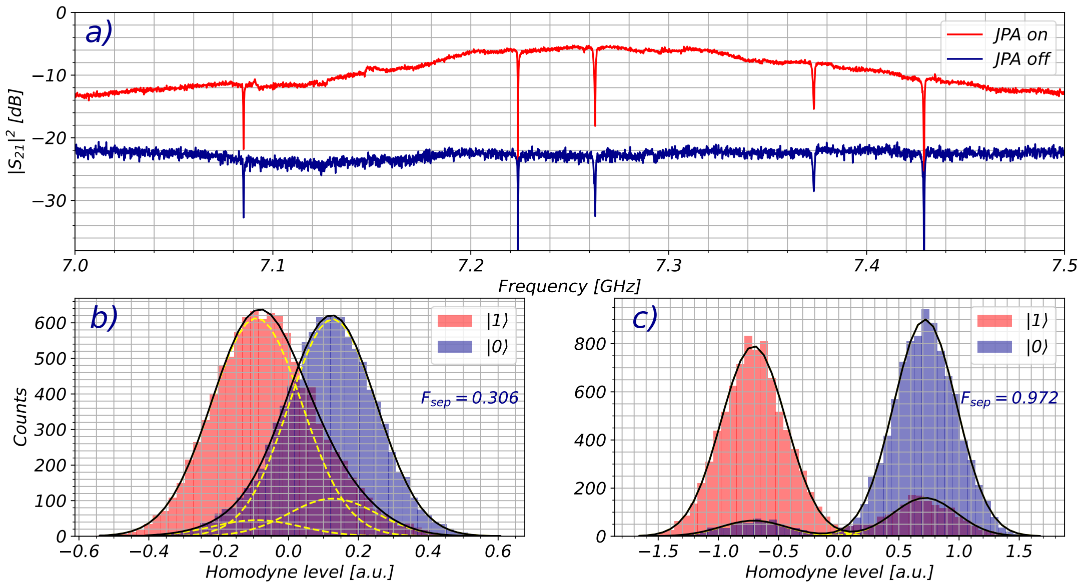


Figure 1: Application of the amplifier. **a)** Comparison between the transmission profiles through the readout line of the 5-qubit sample with active JPA (red, pump signal on) and inactive (blue, pump signal off). In 'off'-state, the JPA has almost no effect on transmission. The SNR at resonator frequencies (sharp dips in transmission) in 'on'-state is increased by approximately 3 times. **b), c)** Applying the device for single-shot qubit measurements (resonator II at 7.232 GHz). The $|0\rangle$ and $|1\rangle$ states are nearly indistinguishable after $I$-pulse (blue) and $\pi$-pulse (red) without JPA **b)**, providing poor separation fidelity of 30.6%. After turning on the JPA **c)**, the state histograms become well-separated with decent fidelity of 97.2%.

## Application and Results

For the ease of application of the amplifier for any quantum device, an optimization algorithm was developed. It receives the needed gain and bandwidth and seeks for the parameters (bias magnetic flux, pump frequency and power) which provide the best performance. Using it, a suitable working regime for a 5-qubit device was found. The improvement of the SNR is shown in Fig. 1 *a)*. Due to improved SNR, the fidelity of single-shot IQ-clouds measurement [5] was also enhanced (Fig. 1 *b)*, *c)*).

## Acknowledgements

The work was done in the frame of the Roadmap for the development in the Russian Federation the high-tech field of "Quantum Computation" for the period up to 2024. All samples were fabricated at the cleanroom facility of MIPT.

# References

[1] *N.E. Frattini, V.V. Sivak, A. Lingenfelter, et al.*, Optimizing the nonlinearity and dissipation of a snail parametric amplifier for dynamic range. Physical Review Applied **10**, 054020 (2018).

[2] *T. Roy, S. Kundu, M. Chand, et al.*, Broadband parametric amplification with impedance engineering: Beyond the gain-bandwidth product. Applied Physics Letters **107**, 262601 (2015).

[3] *D. Kalacheva, G. Fedorov, A. Kulakova, et al.*, Improving the quality factor of superconducting resonators by post-process surface treatment. AIP Conference Proceedings **2241**, AIP Publishing LLC (2020).

[4] *G. J. Dolan*, Offset masks for lift-off photoprocessing. Applied Physics Letters **31**, 337-339 (1977).

[5] *T. Walter, P. Kurpiers, S. Gasparinetti, et al.*, Rapid high-fidelity single-shot dispersive readout of superconducting qubits. Physical Review Applied **7**, 054020 (2017).

# Towards deep quantum learning in superconducting qubits

**Alexey Tolstobrov**[1*], **Gleb Fedorov**[1,2,3], **Darya Kalacheva**[3,1,2], **Viktor Lubsanov**[1], **Aleksey Bolgar**[1], **Shamil Kadyrmetov**[1] **and Oleg V. Astafiev**[3,1]

[1] *Moscow Institute of Physics and Technology*
[2] *National University of Scienece and Technology MISIS*
[3] *Skolkovo Institute of Science and Technology*
*E-mail: `tolstobrov.ae@phystech.edu`

**Abstract**

Single-qubit and two-qubit gates are components of algorithms for deep quantum machine learning in qubits. During this work, the control parameters and waveform shapes of single-qubit rotations were being optimized in the experiment. Two-qubit gates also were studied. The numerical model was developed to simulate the dynamics of multi-qubit systems. Predictions of this model were compared with experimental data.

## Introduction

Superconducting qubits remain one of the most rapid-growing and promising platforms for quantum computation. It is also possible to use them for quantum machine learning [1]. For the realization of quantum machine learning algorithms, single-qubit gates and two-qubit gates with high fidelity are necessary. In this work these operations were implemented in a 5-qubit quantum processor; different impulse correction techniques were applied.

## Experimental setup

The investigated sample was fabricated as 5-transmon[2] chain. Each transmon had its own measurement resonator, and 2 control lines - to control the flux through the SQUID of transmon and to excite it with microwave radiation. A photo of the processor in an optical microscope is shown in Fig. 1.

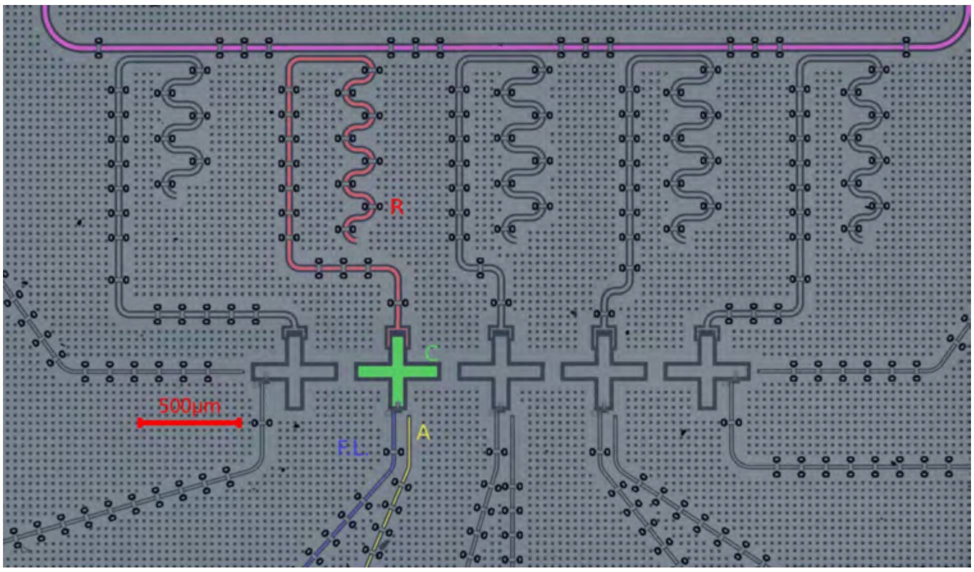


Figure 1: Micrograph of the 5-qubit quantum processor. Purple- Transmission line, yellow - microwave antenna(for excitation of the qubit), blue - flux line, green - shunted capacity of the qubit, red - measuring resonator

## Single-qubit operations

A common technique for single qubit operations is to infer $\pi$-pulse duration from Rabi-oscillations experiment and then use pulses of other durations or other amplitudes for other angles. This technique does not allow to reach high precision operations with transmons due to their low anharmonicity. We use HDRAG-correction technique to compensate leakage to higher states, manifesting itself as phase errors in computational subspace of two lowest levels [3]. We measure dependence of phase error of $\frac{\pi}{2}$-pulse from the number of pseudo-identity operators Fig. 2, Fig. 3. Without the correction, the phase error linearly increases with the number of pseudo-identity operators, which tells us about phase error approximately $-2°$ per pulse. For the pulse with correction, phase error practically does not depend on number of $\frac{\pi}{2}$-pulses, which leads to a notably higher fidelity of operations.

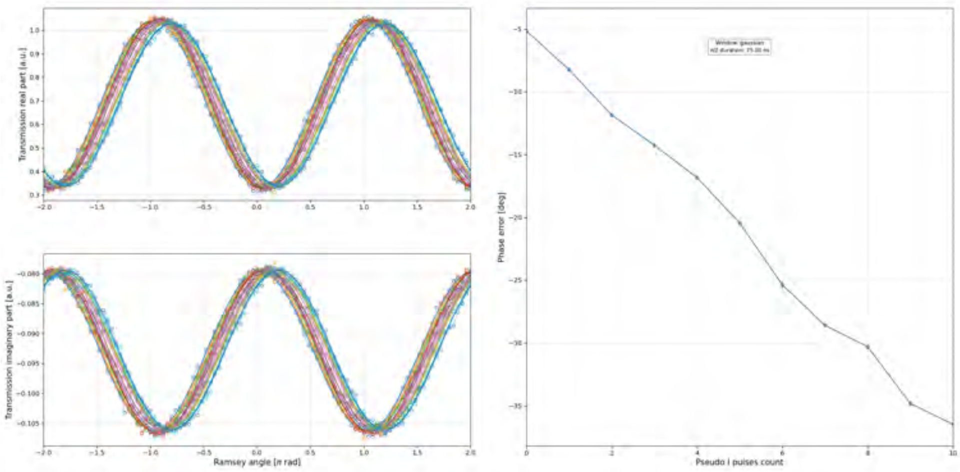


Figure 2: Phase error without any correction

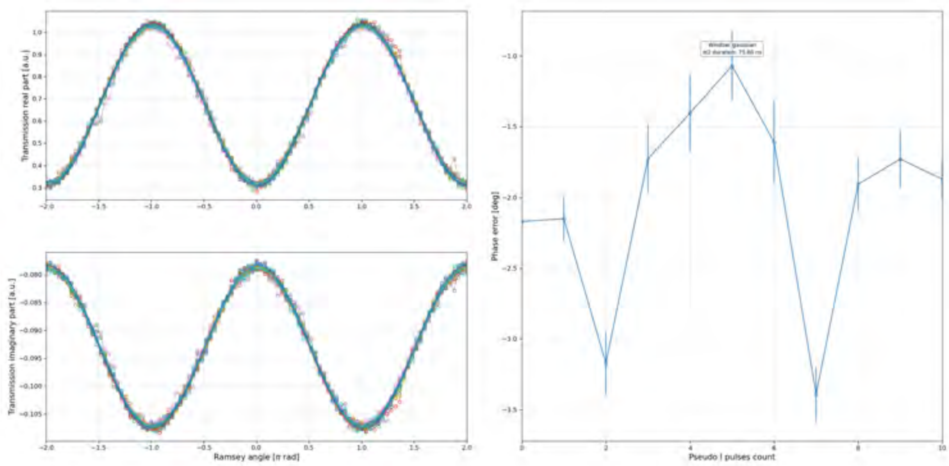


Figure 3: Phase error with HDRAG correction

## Two-qubit operations

Hamiltonian of two-qubit system has the following structure Eq. 1:

$$H = g(\hat{\sigma}^- \otimes \hat{\sigma}^+ e^{i\Delta t} + \hat{\sigma}^+ \otimes \hat{\sigma}^- e^{-i\Delta t}), \tag{1}$$

Where $\Delta = \omega_{q_2} - \omega_{q_1}$ For realizing two-qubit operations (i-Swap) the qubits were brought into resonance by changing the magnetic flux through one of them, in such a way that the exchange of energy turned out to be maximal. For calibration of this operations the experiment in observing two-qubit oscillations was realized. The scheme of this experiment is shown below, Fig. 4.

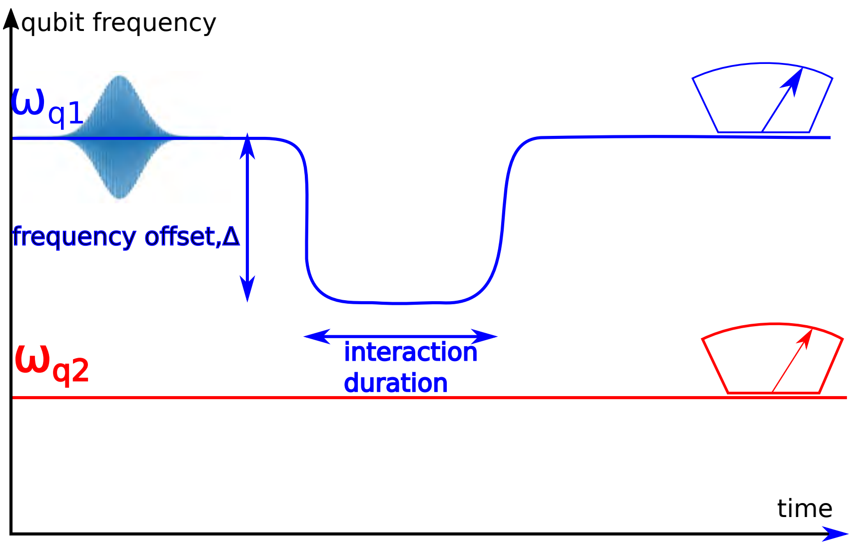


Figure 4: Scheme of two-qubit oscillations experiment

This experiment also was simulated numerically, comparison the result of simulations with experimental data is shown on Fig. 5. There is clearly visible asymmetry in the chevrons, which is associated with the distortion of the flux pulse [4]. Implementation of the flux-pulse correction technique is a subject of future research.

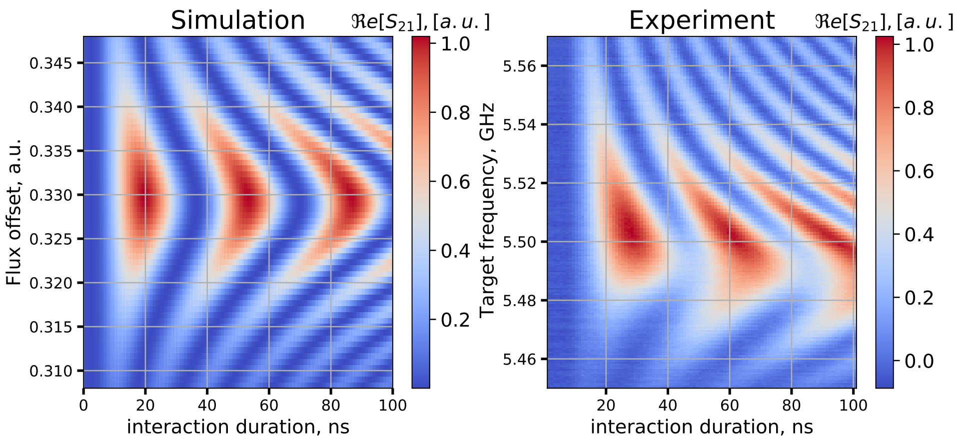


Figure 5: Two-qubit oscillations

## Conclusion

Single-gubit and two-qubit operations for 5-transmon quantum processor were demonstrated. Numerical model of the device was implemented and used for comparison with the experimental results.

### Acknowledgements

The work was done in the frame of the Roadmap for the development in the Russian Federation the high-tech field of “Quantum Computation” for the period up to 2024. All samples were fabricated at the cleanroom facility of MIPT.

## References

[1] Wenhui Ren, Weikang Li, Shibo Xu, Ke Wang, Wenjie Jiang, Feitong Jin, Xuhao Zhu, Jiachen Chen, Zixuan Song, Pengfei Zhang, Hang Dong, Xu Zhang, Jinfeng Deng, Yu Gao, Chuanyu Zhang, Yaozu Wu, Bing Zhang, Qiujiang Guo, Hekang Li, Zhen Wang, Jacob Biamonte, Chao Song, Dong-Ling Deng, and H. Wang. Experimental quantum adversarial learning with programmable superconducting qubits, 2022.

[2] Jens Koch, Terri M. Yu, Jay Gambetta, A. A. Houck, D. I. Schuster, J. Majer, Alexandre Blais, M. H. Devoret, S. M. Girvin, and R. J. Schoelkopf. Charge-insensitive qubit design derived from the cooper pair box. *Phys. Rev. A*, 76:042319, Oct 2007.

[3] Erik Lucero, Julian Kelly, Radoslaw C. Bialczak, Mike Lenander, Matteo Mariantoni, Matthew Neeley, A. D. O’Connell, Daniel Sank, H. Wang, Martin Weides, James Wenner, Tsuyoshi Yamamoto, A. N. Cleland, and John M. Martinis. Reduced phase error through optimized control of a superconducting qubit. *Phys. Rev. A*, 82:042339, Oct 2010.

[4] M. A. Rol, L. Ciorciaro, F. K. Malinowski, B. M. Tarasinski, R. E. Sagastizabal, C. C. Bultink, Y. Salathe, N. Haandbaek, J. Sedivy, and L. DiCarlo. Time-domain characterization and correction of on-chip distortion of control pulses in a quantum processor. *Applied Physics Letters*, 116(5):054001, 2020.

# Switching of superconducting logic element due to single flux quantum pulses

**Dmitriy A. Rybin**[1*], **Dmitrii S. Pashin**[1], **Marina V. Bastrakova**[1,2], **Andrey E. Schegolev**[3], **Nikolay V. Klenov**[1−3], **Igor I. Soloviev**[1−3]

[1] *Lobachevsky State University of Nizhni Novgorod, Nizhny Novgorod, Russia*
[2] *Russian Quantum Center, Moscow, Russia*
[3] *Skobeltsyn Institute of Nuclear Physics, Lomonosov Moscow State University, Moscow, Russia*
*E-mail: `rybin@asgap.ru`

**Abstract**

The article proposes the scheme of a modified rf-SQUID with rapid single flux quantum (RSFQ) control and finds the parameters of the system functioning in the logic element mode and neuron mode. The modification of the input SFQ pulse to suppress parasitic oscillations on the output function of the dynamic switching is found. Optimization of the scheme parameters with dissipation taken into account has been carried out.

Quantum and superconductor technologies are already demonstrating the potential of their application in the creation of quantum artificial neural networks and elements of digital electronics [1, 2]. The main advantage of superconductor technology compared to CMOS is its low power consumption and high speed performance.

The current work considers the possibility of implementing digital logic on superconductor elements. Such elements can be useful in the design of nodes where it is necessary to have the ability to represent information in digital form, as well as to combine quantum and silicon technologies in one device, which will take advantage of both technologies.

We study a parametric quantron scheme with a SQUID instead of a Josephson contact (parametron) without a resistive shunt, which has previously successfully proven itself as a basic element of a perceptron-type neural network [2, 3]. Within the framework of the resistive model for the scheme shown in Fig. 1(a), we can write down the equation defining the phase dynamics $\phi$ on the Josephson contact:

$$\frac{\beta}{\omega_c^2}\ddot{\phi} + \frac{1}{\omega_c}\dot{\phi} + \sin\phi = \frac{\phi_{in}\cdot(l_a + 2l_{out}) - 2\phi\cdot(l_a + l_{out})}{2(l\cdot l_a + l_{out}\cdot(l + l_a))}, \quad (1)$$

where the values $\beta = \frac{2\pi R^2 I_c C}{\Phi_0}$ – the McCumber parameter, $\omega_c = \frac{2eRI_c}{\hbar}$ – characteristic Josephson transition frequency, $\phi_{in} = \frac{2\pi\Phi_{in}}{\Phi_0}$ – external magnetic flux normalized per quantum of magnetic flux, $l$, $l_{out}$, $l_a$ – the corresponding inductances, defined in Fig. 1(a).

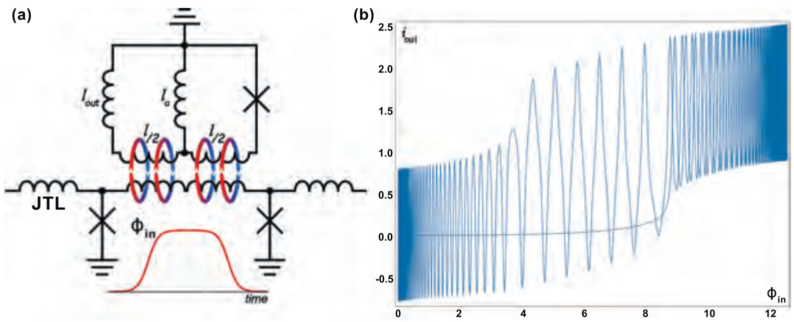


Figure 1: (a) Scheme of the modified rf-SQUID and a typical view of the SFQ control pulse. (b) Output current-flux characteristic .

The states are controlled within the concept of energy-efficient adiabatic superconductor logic due to $\phi_{in}(t)$ – single flux quantum (SFQ) pulse propagating along Josephson transmission lines. The typical view of the SFQ pulse shown in Fig. 1(a) can be represented as

$$\phi_{in}(t, t_1, t_2, D) = A_{in}\left((1 + \exp(-2D(t - t_1)))^{-1} + (1 + \exp(2D(t - t_2))^{-1}) - 1\right), \quad (2)$$

Where the pulse amplitude is defined as $A_{in}$, and the steepness of the front, at rise/fall times $t_1/t_2$ is defined by the parameter $D$. It was noticed in the work [2] that the single SFQ pulse (2) is not suitable for the circuit as a digital logic element $l > \sqrt{l_{out}^2 + 1} - l_{out}$ because it causes strong oscillations on the output characteristic $i_{out}(\phi_{in})$, see the characteristic example shown in Fig.1(b). In this connection, we proposed a method to modify the supply of the controlling external magnetic field, which consists of a superposition of three SFQ pulses, shown in Fig. 2(a), coming to the controlling logic cell. A typical view of such an effect can be represented as:

$$\widetilde{\phi}_{in}(t, t_1, t_2) = \phi_{in}(t, t_1, t_2, D) + \phi_{in}(t, t_3, t_4, 2D) - \frac{\delta}{10}\phi_{in}(t, t_5, t_6, 2D), \tag{3}$$

where $\phi_{in}(t, t_1, t_2, D)$ is the input flux by the equation (2). The asymmetry of the right branch is controlled by the parameter $\delta$. The view of the input flux at different parameters of $\delta$ is shown in Fig.2(a).

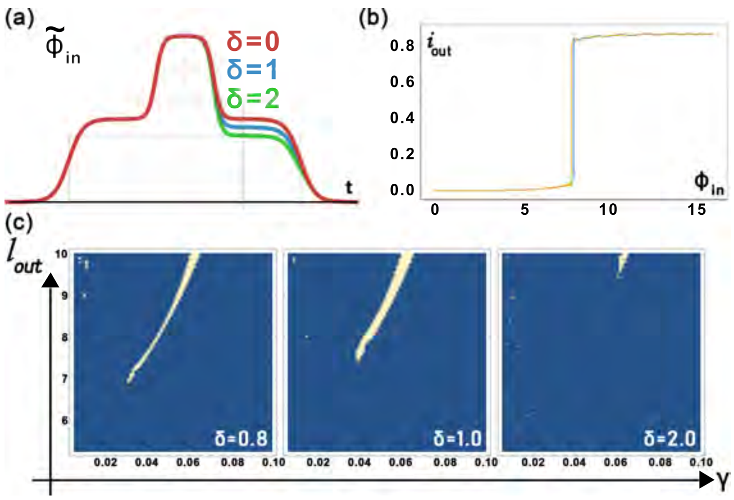


Figure 2: (a) Modified external flux $\widetilde{\phi}_{in}$ with $t_3 = 2.5t_1$, $t_4 = 0.7t_2$, $t_5 = 3.5t_1$, $t_6 = t_2$. (b) Output characteristic of a digital logic element. (c) Parameter plane $l_{out}(\gamma)$ at different values of flux asymmetry $\delta$.

Figure 2(b) shows the output characteristic of the system $i_{out}(\phi_{in})$, which is a stepped Heaviside function implementing digital logic. We have plotted the parameter planes $l_{out}$ and $\gamma = \omega_p\omega_c^{-1}$ (dissipation parameter) as a function of the asymmetry parameter $\delta$ of the external flux. The yellow dots in Fig.2(c) indicate areas where minimal oscillations in the output characteristic are observed, and where there is no hysteresis character of the curves.

Therefore, numerical analysis has shown that by controlling the external flux it is possible to switch between different modes of operation of the circuit to obtain the required output characteristic (sigmoid – for neuron or Heaviside – for digital logic).

The work is supported by the Russian Science Foundation Grant (RSF) No. 22-72-10075.

## References

[1] *M. Schneider, E. Toomey, G. Rowlands, J. Shainline, P. Tschirhart, and K. Segall*, SuperMind: a survey of the potential of superconducting electronics for neuromorphic computing. Supercond. Sci. Technol. **35**, 053001 (2022).

[2] *M.V. Bastrakova, A.A. Gorchavkina, A.E. Schegolev, N.V. Klenov, I.I. Soloviev, A.M. Satanin, and M.V. Tereshonok*, Dynamic Processes in a Superconducting Adiabatic Neuron with Non-Shunted Josephson Contacts. Symmetry **13(9)**, 1735 (2021).

[3] *M.V. Bastrakova, D.S. Pashin, D.A. Rybin, A.E. Schegolev, N.V. Klenov, I.I. Soloviev, A.A. Gorchavkina, and A.M. Satanin*, A superconducting adiabatic neuron in a quantum regime. Beilstein J. Nanotechnol. **13**, 653 (2022).

# Using ab initio methods for quantum technologies

Maria Kaplun, Valery Beskachko

*South Ural State University, Chelyabinsk, Russia*
*E-mail: kaplunmv@susu.ru

**Abstract**

We have explored the possibility of using ab initio numerical experiments for quantum technologies. This method makes it possible to study materials with the necessary characteristics and configuration for further implementation of experiments with their use for quantum applications.

With the development of quantum technologies, more and more stringent conditions are needed for the creation of certain experimental works. The development of such areas as photonics, spintronics, twistronics, quantum informatics speaks of the need to study a variety of materials. For example, for the further development of quantum information technologies, high requirements are placed on single-photon detectors, which leads to the search for new materials and architecture to improve the characteristics of the former: high detection efficiency, fast response, and photon-number-resolving ability, etc [1]. The initial theoretical study of materials and topology makes it possible to select materials with the required characteristics without significant costs for the experiment. Such a study is possible using first-principles methods (ab initio), based on the direct solution of the equations of quantum mechanics using various approximations and simplifications. One such method is density functional theory (DFT)[2]. DFT - replacement of many-electron wave function by electron density. This method is implemented in such software packages as SIESTA and VASP, while the approaches of these packages are different and, accordingly, using two such numerical packages, more accurate results can be achieved [3, 4].

A feature of numerical experiments is the ability to create almost any architecture of materials necessary for further experimental work, for example, we can explore 0D (quantum dots), 1D (nanotubes), 2D (small-layer materials) and 3D materials and their combinations (Fig. 1).

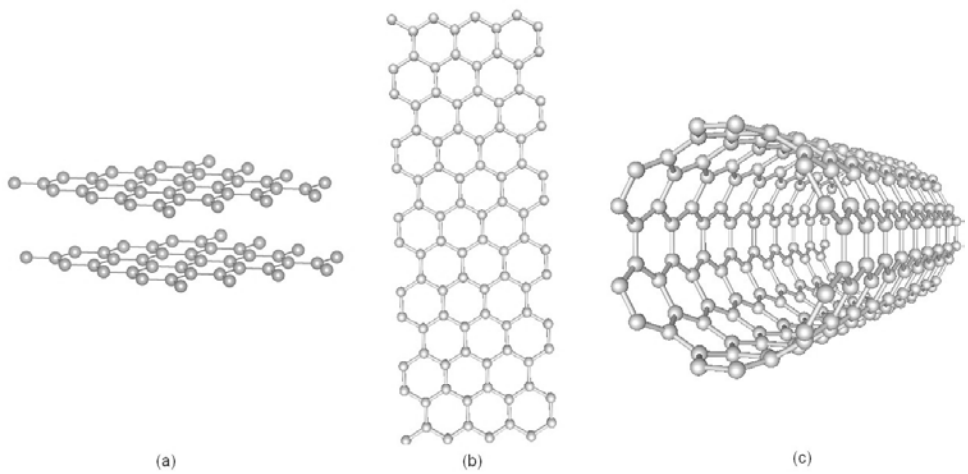


Figure 1: Examples of simulated structures. (a) two-layer graphene; (b) graphene nanoribbon; (c) graphene nanotubes.

Numerical experiments using ab initio methods make it possible to study the binding energy of the system and the energetically favorable configuration of materials, the electron density of states, electronic band structures, spin polarization, and other things that are relevant for quantum applications.

The work was supported as part of the implementation of the project under Decree 220 of the Government of the Russian Federation.

## References

[1] *H. Wang, J. Guo, J. Miao, W. Luo, Y. Gu, R. Xie, F. Wang, L. Zhang, P. Wang and W. Hu*, Emerging Single-Photon Detectors Based on Low-Dimensional Materials. Small **18**, 2103963 (2022).

[2] *R.O. Jones*, functional theory: Its origins, rise to prominence, and future. Rev. of Mod. Phys. **87**, 3 (2015).

[3] *J.M. Soler, E. Artacho, J.D. Gale, A. García, J. Junquera, P. Ordejón and D. Sánchez-Portal*, The SIESTA method for ab initio order-N materials simulation. Journal of Physics: Condensed Matter **14**, 11 (2002).

[4] *G. Kresse and J. Furthmüller*, $\lambda/4$ Efficient iterative schemes for ab initio total-energy calculations using a plane-wave basis set. Phys. Rev. B **54**, 16 (1996).

# GROUND STATE COOLING OF 171Yb ION VIA QUADRUPOLE TRANSITION

Vasilii Smirnov[1,2*], Ilia Semerikov[1,3], Ilia Zalivako[1], Alexander Borisenko[1], Mikhail Aksenov[1], Pavel Sidorov[1], Nikita Semenin[1], Igor Zhuravlev[1,2], Ksenia Khabarova[1], Nikolai Kolachevskiy[1,3]

[1] *P. N. Lebedev Physics Institute of the RAS, Moscow, Russia*
[2] *Moscow Institute of Physics and Technology (National Research University), Dolgoprudny, Russia*
[3] *Russian Quantum Centre, Skolkovo, Russia*
*E-mail: smirnov.vasilii@phystech.edu

**Abstract**

We numerically simulate ground state cooling of 171-Yb ion with usage of a quadrupole transition on the wavelength of 435 nm. Parasitic heating due to repumping process after each cooling pulse is also investigated. The optimal sequence of cooling pulses is found for the scheme with the excitation of the first and second red motional sidebands. For a time of about 5 ms and 240 cooling pulses, we theoretically achieve mean motional number $\bar{n} = 0.219$ and 81.4% population of the ground state.

## Equations

$$P_n = \frac{\bar{n}^n}{(\bar{n}+1)^{n+1}}, \tag{1}$$

where $\bar{n}$ is mean motional number. Equation (1) is the population of thermally distributed motional states.

$$\Omega_{n,\Delta n} = \Omega_0 e^{-\eta^2/2} \eta^{|\Delta n|} \sqrt{\frac{n!}{(n+\Delta n)!}} L_n^{|\Delta n|}(\eta^2), \tag{2}$$

where $\eta$ is the Lamb-Dicke parameter, $\Omega_0$ is the Rabi frequency not taking into account motional levels,$L_n^\alpha$ is generalized Laguerre polynomial, $n$ and $\Delta n$ are number of motional level and distinction of motional levels in transition [1]. Equation (2) is Rabi frequency for transitions between motional levels.

$$L_n^\alpha(X) = \sum_{m=0}^{n} (-1)^m \binom{n+\alpha}{n-m} \frac{X^m}{m!}. \tag{3}$$

Equation (3) is generalized Laguerre polynominal .

$$P_n \to P_n - P_n P_{n\to n-1} + P_{n+1} P_{n+1\to n}, \tag{4}$$

where $P_n P_{n\to n-1}$ is transition probability. Equation (4) is population change after applying cooling pulse [2].

$$P_{n\to n-1} = \sin^2\left(\frac{\Omega_{n,n-1} t}{2}\right). \tag{5}$$

Equation (5) is transition probability when applying $\pi$-pulse.

$$\Delta\bar{n} = P_n \cdot n + P_{n-1} \cdot (n-1) + P_{n+1} \cdot (n+1) - n = (P_{n+1} - P_{n-1}) \cdot 1. \tag{6}$$

Equation (6) is average heating of level $n$ in repumping process.

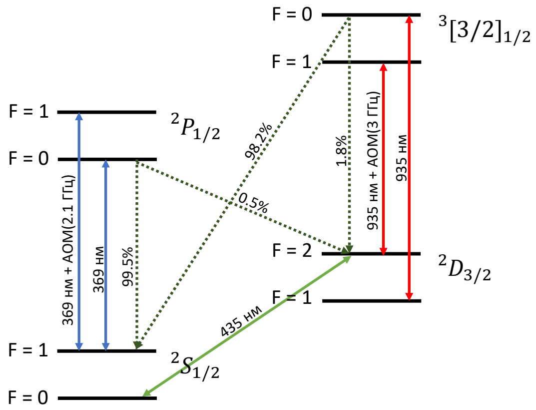


Figure 1: Relevant level scheme of $^{171}$Yb$^+$

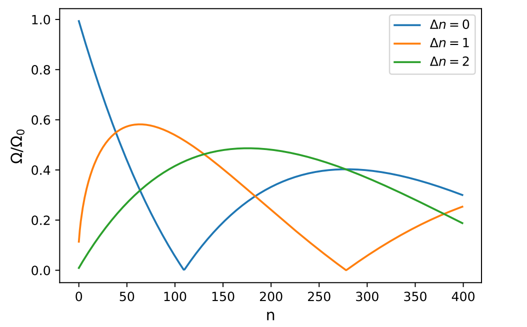


Figure 2: Rabi frequences depending on $n$ for carrier, 1-st and 2-nd red sidebands

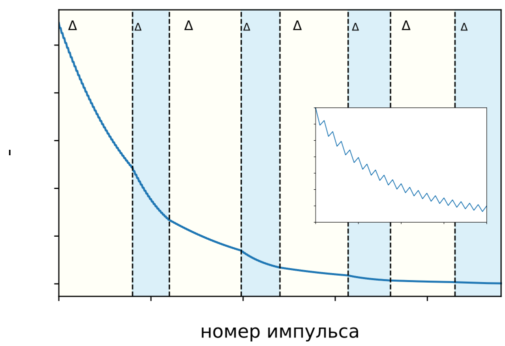


Figure 3: Mean motional number depending on pulse number during sideband cooli~~

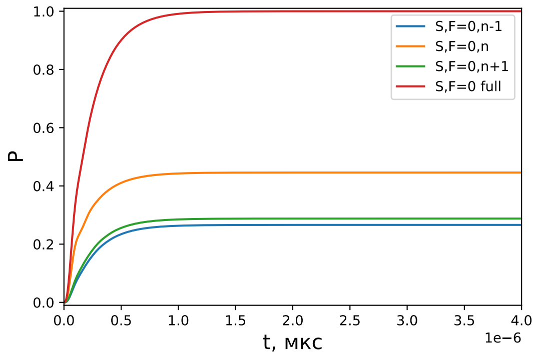


Figure 4: Population of initial state $^2S_{1/2}(F =$

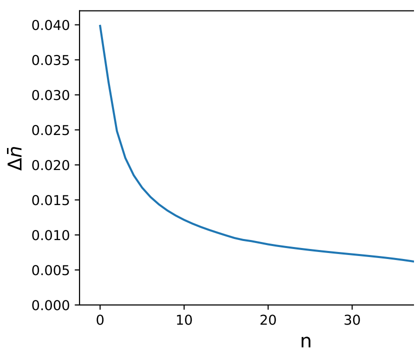


Figure 5: Average heating of eac| level in repumping process

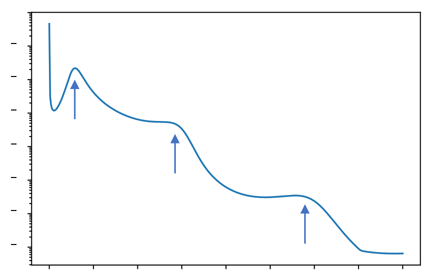

Figure 6: Population distribution of motional levels after applying 50 1-st sideband pulses

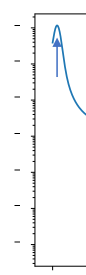

# References

[1] *Leibfried D., Blatt R., Monroe C., Wineland D.*, Quantum dynamics of single trapped ions. Reviews of Modern Physics, 2003.

[2] *H. Che, K. Deng, Z. T. Xu, W. H. Yuan, J. Zhang, and Z. H. Lu*, Efficient raman sideband cooling of trapped ions to their motional ground state. Phys. Rev. A, 96:013417, Jul 2017.

# Efficient Ultracold Atoms Source for Quantum Sensing

**A.E. Afanasiev[1,2], A.S. Kalmykov[1,2], R.V. Kirtaev[3], P.I. Skakunenko[1,3,4*], D.V. Bykova[1,2], A.A. Kortel[1,2], D.V. Negrov[3], V.I. Balykin[1,2]**

[1] *Institute of Spectroscopy Russian Academy of Sciences, Moscow, Troitsk, Russia*
[2] *National Research University Higher School of Economics, Moscow, Russia*
[3] *Moscow Institute of Physics and Technology, Dolgoprudny, Moscow Region, Russia*
[4] *Skolkovo Institute of Science and Technology, Moscow, Russia*
*E-mail: `skakunenko.pi@phystech.edu`

**Abstract**

We propose a new efficient source of ultracold atoms for quantum sensing based on the atom chip technology. It consists of a single-layer atom chip loaded by low-velocity intense beam (LVIS). We consider focusing of a low-velocity atomic beam into the atom chip's trapping region using 2D-MOT in overdamped regime. According to the calculations it would increase the loading rate by a factor of 160 compared to an unfocused atomic beam. We also developed a new wide-wire intermediate MOT on a chip which would increase the number of trapped atoms by a factor of 1.7 compared to the traditional MOT on a chip.

## Introduction

Localized atoms are used in many precise atomic interferometry experiments. The development of this trend has already resulted in the creation of a new generation of quantum sensors based on the measurement of the effect of physical fields on quantum degrees of freedom of atoms. Quantum sensors provide an accuracy higher than that of existing classical sensors. Sensors based on atomic interferometry for measuring inertial forces [1, 2], including gravimeters [2, 3], gradiometers [4, 5], and gyroscopes [6] belong to the most developed quantum sensors. The accuracy of modern atom gravimeters and gradiometers already exceeds the accuracy of many classical analogs [7], and their application demonstrates a high reliability [8,9].

## Atom chip technology

One of the main approaches in the implementation of atomic interferometry is currently the approach using the atom chip technology [10-12]. The use of atom chips for atomic interferometry is based on laser cooling of atoms and their subsequent localization near the surface of a solid-state chip. The design of the chip allows you to control the internal and external degrees of freedom of localized atoms by controlling the electric currents flowing through the microwires located on its surface. This approach makes it possible to integrate elements of cooling, localization, manipulation, and measurement of atomic ensembles in single device.

## Atomic beam focusing

One of the most important parameters of quantum sensors affecting their accuracy is the number of cooled atoms, because it determines signal-to-noise ratio. The maximum number of atoms that can be localized is given by the expression [11]:

$$N = R\tau, \tag{1}$$

where N is the number of atoms in the magneto-optical trap, R is the loading rate of atoms and $\tau$ is the lifetime of atoms in the MOT. We propose focusing of the atomic beam by 2D MOT into the trapping region of the atom chip (Fig. 1) to increase R and, consequently, N. In overdamped regime (when intensity of laser beams of 2D MOT is 10 times larger than saturation intensity) the focal length of such focusing element is given by:

$$f = \frac{kv_z}{\alpha g}, \tag{2}$$

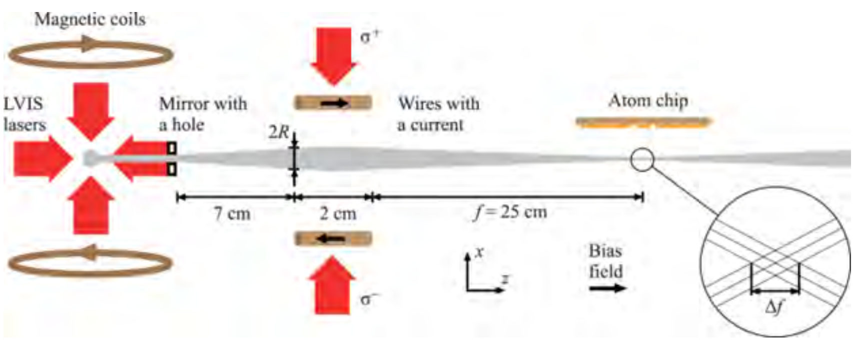


Figure 1: Scheme of loading an atom chip with focused low-velocity atomic beam [13]

where $\alpha = 2\pi \times 1.4MHz/G$ is the Zeeman shift of the resonance absorption line in the magnetic field $B = gx$, $k$ – laser field wavevector, $v_z$ – longitudinal velocity of the atom. We demonstrated [13] that, in spite of dependance of the focal length $f$ on the velocity of the atom $v_z$, low-velocity atomic beam can be focused into a spot 250 $\mu m$ in diameter. This would increase the loading rate by a factor of 160.

## Wide-wire U-trap

Additional method to increase R is to improve MOT on a chip. Usually, MOT on a chip is created using U-wire (U-MOT), but the magnetic field of such trap is highly deviated from the ideal quadrupole field. Therefore, volume of the trapping region is limited. We developed new wide-wire U-MOT (Fig. 2), which approximates quadrupole field much better.

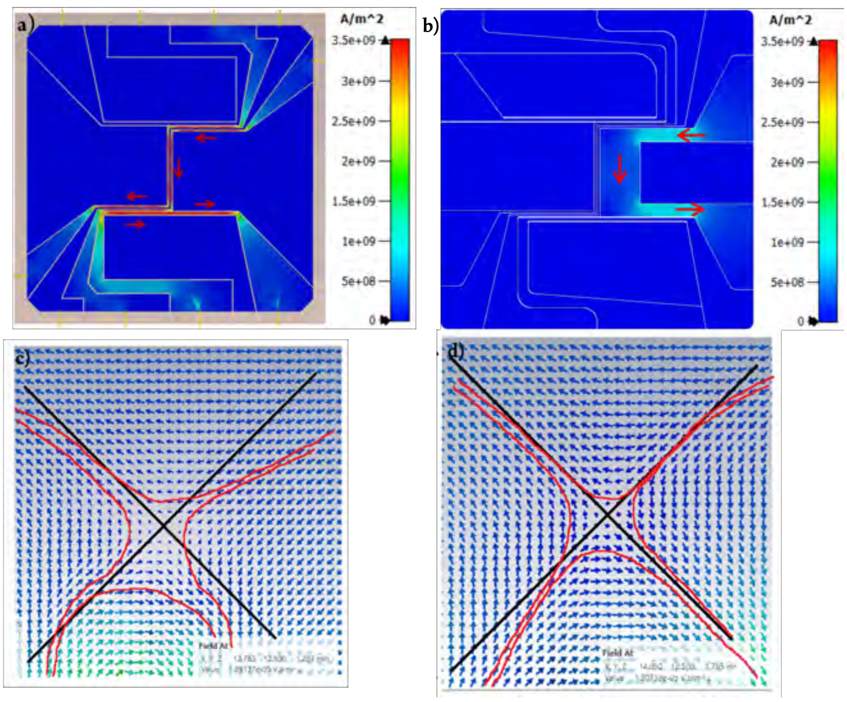


Figure 2: a, b - simulation of current distribution on the chip in narrow and wide traps respectively. c, d - magnetic field distribution in the plane perpendicular to narrow/wide wire

According to numerical simulations, such trap would trap 1.7 times more atoms than usual U-MOT on a chip.

# References

[1] *R. Geiger, A. Landragin, S. Merlet, and F. Pereira Dos Santos,* AVS Quantum Sci. **2**, 024702 (2020).

[2] *G. M. Tino,* Quantum Sci. Technol. , 024014 (2021).

[3] *V. Ménoret, P. Vermeulen, N. le Moigne, S. Bonvalot, P. Bouyer, A. Landragin, and B. Desruelle,* Sci. Rep. **8**, 12300 (2018).

[4] *D. K. Mao, X. B. Deng, H. Q. Luo, Y. Y. Xu, M. K. Zhou, X. C. Duan, and Z. K. Hu,* Rev. Sci. Instrum. **92**, 053202 (2021).

[5] *C. Janvier, V. Ménoret, B. Desruelle, S. Merlet, A. Landragin, and F. Pereira dos Santos*, Phys. Rev. A **105**, 022801 (2022).

[6] *C. L. Garrido Alzar,*, AVS Quantum Sci. **1**, 014702 (2019).

[7] *P. Gillot, O. Francis, A. Landragin, F. Pereira Dos Santos, and S. Merlet,*, Metrologia **51**, L15 (2014).

[8] *Y. Bidel, N. Zahzam, C. Blanchard, A. Bonnin, M. Cadoret, A. Bresson, D. Rouxel, and M. F. Lequentrec-Lalancette,* Nat. Commun. **9**, 627 (2018).

[9] *Y. Bidel, N. Zahzam, A. Bresson, C. Blanchard, M. Cadoret, A. V. Olesen, and R. Forsberg, J.*, Geodesy **94**, 20 (2020).

[10] *V. Singh, V. B. Tiwari, and S. R. Mishra,* Laser Phys. Lett. **17**, 035501 (2020).

[11] *S. A. Hopkins,* PhD Thesis (Open Univ., Milton Keynes, UK, 1996).

[12] *A. E. Afanasiev, A. S. Kalmykov, R. V. Kirtaev, A. A. Kortel, P. I. Skakunenko, D. V. Negrov, and V. I. Balykin,* Opt. Laser Technol. **148**, 107698 (2022).

[13] *Afanasiev, A.E., Bykova, D.V., Skakunenko, P.I. et al.* Jetp Lett. **115**, 509–517 (2022).

# Deep laser cooling of $^6$Li atoms in two-field configuration MOT

**Roman Ilenkov**[1,2], **Oleg Prudnikov** [1,2],
**Anna Kirpichnikova**[1]

[1] *Institute of Laser Physics SB RAS, Novosibirsk, Russia*
[2] *Novosibirsk State University, Novosibirsk, Russia*
*E-mail: `ilenkov.roman@gmail.com`

**Abstract**

Two field magnetooptical configuration for deep laser cooling of $^6$Li atoms was studded. The model takes into account the optical pumping to all hyperfine levels of D1 and D2 lines. We distinguish the most perspective light field configurations with both pumping fields assist to deep cooling of $^6$Li atoms in a magnetooptical trap.

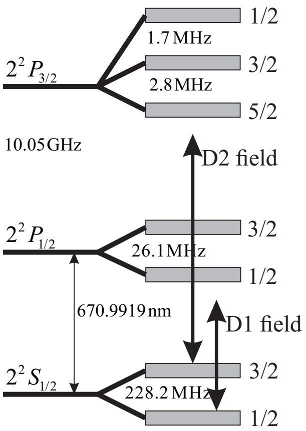


Figure 1: Level structure of $^6$Li atom.

Laser cooling of atoms is used for a wide range of scientific research: quantum sensors; to studding Bose condensates and Fermi gases; to create optical frequency standards. For these problems, the development of efficient methods for deep laser cooling of atoms are required. The complexity of the implementation of laser cooling of $^6$Li Fig. 1 lies in fact that the width of hyperfine splitting of energy sublevels is comparable to $\gamma$ - the natural linewidth that results to pumping both hyperfine sublevels of the ground state. Therefore, it is necessary to use another pump field to return the atoms to the cooling cycle. We consider two-frequency light field configuration where both fields have a dissipative effect on atoms, which make possible to achieve fast and efficient laser cooling of lithium atoms. The aim of this study is to find appropriate field configuration for deep cooling and trapping the atoms in MOT.

The results represent achieved kinetic energy of cooled atoms for various field configurations are represented on the Fig. 2. Here the parameter $U = 4\Omega^2|\delta|/3(\gamma^2/4 + \delta^2)$ represents saturation of the light fields determined by them intensity ($\Omega$ is Rabi frequency) and field detuning $\delta$.

It is shown that the field polarization and the depth of the optical D2 line play a decisive role in the laser cooling of $^6$Li atoms. To achieve the lowest temperatures $< \hbar\gamma/2$, it is necessary to use linear polarizations of the light field tuned to the D2 line. The intensity of the light field should be chosen to $U_{D2} < 30\hbar w_r$. The polarization of the field on the D1 line and its intensity mainly determine the size of the optimal cooling region.

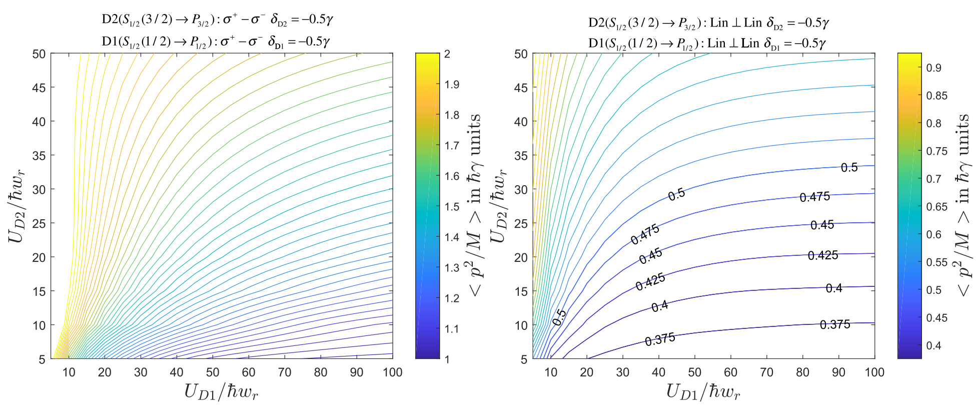


Figure 2: Kinetics energy of $^6$Li atoms for different polarization configurations of laser waves. Left - both fields $\sigma^+ - \sigma^-$, Right - both fields Lin⊥Lin, $\delta_{D2} = -0.5\gamma$,$\delta_{D1} = -0.5\gamma$,

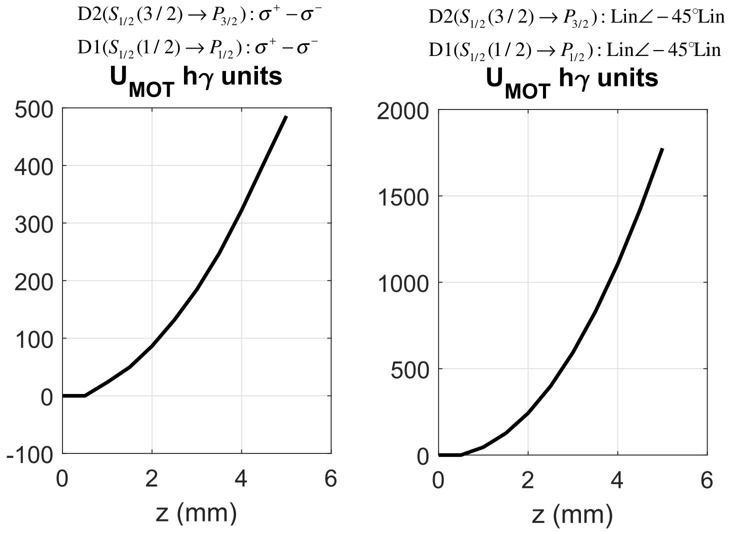


Figure 3: Deep of magneto-optical potential for different polarization configurations of laser waves. Left - both fields $\sigma^+ - \sigma^-$, Right - both fields Lin−45°Lin, $U_{D2} = 30\hbar w_r$, $\delta_{D2} = -0.5\gamma$, $U_{D1} = 50\hbar w_r$, $\delta_{D1} = -0.5\gamma$, dB/dz=6Gs/sm

In addition, calculations were made of the magneto-optical force arising in a magneto-optical trap formed by fields of various configurations Fig. 3. It is shown that using two fields of linear polarization located at an angle of -45 degrees, it is possible to create a magneto-optical potential with a depth $> 1500\gamma$. This becomes possible due to anomalous polarization contributions to the friction force [4].

The work of R.Ya. Ilenkov and A.A. Kirpichnikova was supported by grant from the President of the Russian Federation (MK-6295.2021.1.2). The work of O.N. Prudnikov was supported by RFBR 19-29-11014.

## References

[1] *Kirpichnikova A.A., Prudnikov O.N., Il'enkov R.Ya., Taichenachev A.V., Yudin V.I.,*, Laser cooling limits in fields with a polarisation gradient of atoms with different recoil energies. Quantum Electron. **50**, 939 (2020).

[2] *Riedmann M., Kelkar H., Wubbena T., Pape A., Kulosa A., Zipfel K., Fim D., Ruhmann S., Friebe J., Ertmer W., Rasel E.,*, Beating the density limit by continuously loading a dipole trap from millikelvin-hot magnesium atoms. Phys. Rev. A. **86**, 043416 (2012).

[3] *Hobson R., Bowden W., Vianello A., Hill I.R., Gill P.*, Midinfrared magneto-optical trap of metastable strontium for an optical lattice clock. Phys. Rev. A. **101**, 013420 (2020).

[4] *Prudnikov O. N., Taichenachev A. V., Tumaikin A. M., and Yudin V. I.*, New friction force due to spontaneous light pressure. JETP Letters **70**, 443 (1999).